2019-01-01

Thermal Characterization Of Abs/carbon Fiber, Abs/ Glass Fiber And Petg/glass Fiber Reinforced Composites Used In Large Area Additive Manufacturing

Fernando Adrian Rodriguez Lorenzana
University of Texas at El Paso

THERMAL CHARACTERIZATION OF ABS/CARBON FIBER, ABS/ GLASS FIBER AND PETG/GLASS FIBER REINFORCED COMPOSITES USED IN LARGE AREA ADDITIVE MANUFACTURING

FERNANDO ADRIAN RODRIGUEZ LORENZANA

Master's Program in Mechanical Engineering

APPROVED:

David Espalin, Ph.D., Chair

Yirong Lin, Ph.D.

Amit Lopes, Ph.D.

Stephen L. Crites, Jr., Ph.D.
Dean of the Graduate School

Dedication

This work is dedicated to my family and friends.

THERMAL CHARACTERIZATION OF ABS/CARBON FIBER, ABS/ GLASS FIBER AND PETG/GLASS FIBER REINFORCED COMPOSITES USED IN LARGE AREA ADDITIVE MANUFACTURING

by

FERNANDO ADRIAN RODRIGUEZ LORENZANA, B.S.M.E.

THESIS

Presented to the Faculty of the Graduate School of

The University of Texas at El Paso

in Partial Fulfillment

of the Requirements

for the Degree of

MASTER OF SCIENCE

Department of Mechanical Engineering

THE UNIVERSITY OF TEXAS AT EL PASO

December 2019

Acknowledgements

To begin with, I would like to extend my deepest appreciation to Dr. David Espalin. As my mentor and chair of my committee, he oversaw the progress of this work by me providing extensive guidance, encouragement and patience; not only that, Dr. Espalin inspired me to gradually improve at a professional level and challenge myself. I would also like to extend my deepest gratitude to my thesis members committee, Dr. Yirong Lin and Dr. Amid Lopes, for their direction, time and support. Also, I'm extremely grateful to the Mechanical Engineering Department from the University of Texas at El Paso for providing me financial support through the duration of my graduate studies, the W.M. Keck Center for 3D Innovation at the University of Texas at El Paso and Dr. Ryan Wicker, director of the W.M. Keck Center for 3D Innovation, for providing me the opportunity to conduct this research within the Keck Center.. I would also like to thank my friends at the laboratory for their guidance, company and for sharing their research experience with me: Eduardo Meraz, Xavier Jimenez, Kazi Billah, Christopher Minjares, Jose Coronel, Leonardo Gutierrez, and Emerson Armendariz. Lastly, I would like to thank my family for their unconditional love.

Abstract

Additive manufacturing has seen continuous advancements, such as the inclusion of large-area additive manufacturing extrusion systems. These systems precede small-scale 3D printing by means of research and technological development for the manufacturing of plastic and fiber industries. Big Area Additive Manufacturing (BAAM), a material extrusion process, is capable of 3D printing large parts using thermoplastic composites by adding fiber reinforcements. The incorporation of fibrous materials, carbon fiber (CF) or glass fiber (GF), is a common practice in which percentage nominal ratios of fiber reinforcement by weight are implemented to the polymer matrix. In general, this enables warpage reduction during printing, increases stiffness and provides thermal stability to the three-dimensional printed part. This work focused on the thermophysical changes, by thermogravimetry (TGA) and differential scanning calorimetry (DSC), of thermoplastic matrix composites reinforced with either glass or carbon fiber. Specifically, the composite materials contained a matrix of acrylonitrile-butadiene-styrene (ABS) filled (by weight) with 20% CF, 20% GF, or 40% GF. In addition, another thermoplastic composite material contained poly (ethylene terephthalate)-glycol (PETG) filled (by weight) with 30% GF. The materials were tested in pelletized form (i.e., as received by the material manufacturer and before processing with the BAAM machine) within a controlled temperature profile and a low conductive inert atmosphere, as prescribed by ASTM standards. As such, through thermal stability experimental studies (i.e., TGA), the material's one percentage weight loss as a result of exposure to elevated temperatures (the decomposition temperature) was determined. Through software analysis with Trios v4.5.1 and thermogravimetric profile observations, the step transition events were identified via mass loss. In the same manner, residual measurements at 750 °C (mass change plateau) allowed making observation about the manufacturer-specified filler reinforcement. The

inclusion of the derivative thermogravimetry peak temperature enable to report the maximum deflection point attained in the differential thermogravimetric (DTG)curve. In addition, the area under the DTG deflection allowed making observation as to the mass loss events. Thereafter, DSC studies at fixed heating and cooling scanning rates traced the glass transition events, and the endothermic and exothermic events.

Table of Contents

Dedication iii

Acknowledgements v

Abstract vi

Table of Contents viii

List of Tables A x

List of Tables B xi

List of Figures A xiii

List of Figures B xv

Chapter 1: Introduction 1

1.1 Background 1

1.2 Motivation 5

1.3 Objectives 6

1.4 Thesis Outline 7

Chapter 2: Literature Review 8

2.1 Polymers 8

2.2 Thermoplastics 15

2.3 Thermoplastic Polyesters 22

2.4 Thermal Analysis 25

2.5 Additive Manufacturing 32

Chapter 3: Methodologies 41

3.1 Thermogravimetric Analysis 43

3.2 Differential Scanning Calorimetry 47

Chapter 4: Results 52

4.1 Thermogravimetric and Derivative Thermogravimetric Analysis 52

4.2 Differential scanning calorimetry 58

Chapter 5: Discussion of TGA 69

5.1. ABS 20 (GF & CF) 69

5.2. ABS (40-GF & 20-GF) 73
5.3. ABS 20-GF (SABIC) & ABS 20-GF (Techmer) 76
Chapter 6: Discussion of DSC 79
6.1. ABS 20-CF 79
6.2. ABS 20-GF 80
6.3. ABS 40-GF 81
6.4. PETG 30-GF 82
6.5. ABS 20-GF (SABIC) 83
6.6. ABS Reinforced with GF and CF 84
6.7. ABS Filled with Varying Glass Fiber Reinforcement 85
Chapter 7: Conclusion 86
7.1. Conclusion 86
7.2. Recommendations 88
References 89
APPENDIX A 94
APPENDIX B 154
Vita 217

List of Tables A

Table A.1: The material's model and description for the thermal characterization of ABS and PETG..... 135
Table A.2: The material's description for ABS and PETG. 136
Table A.3 : The initial sample mass, major step transitions, minor step transitions and residual percentage for five engineering thermoplastics. 137
Table A.4: The initial sample mass initial mass prior thermal decomposition..... 138
Table A.5: The 1.0 % weight loss, decomposition temperature, for five engineering thermoplastics. 139
Table A.6: The residual percentage at 750 °C, fixed mass loss, for five engineering thermoplastics. 140
Table A.7: A single major step transitions for five engineering thermoplastics. 141
Table A.8: The maximum peak temperature for five engineering thermoplastics. 142
Table A.9: The area under the DTG maximum peak for five engineering thermoplastics. 143
Table A.10 The arithmetic mean values, TGA/DTG, for five engineering thermoplastics..... 144
Table A.11 The arithmetic mean values, TGA/DTG, for five engineering thermoplastics..... 145
Table A.12: The standard deviations, TGA/DTG, for five engineering thermoplastics..... 146
Table A.13:The standard deviations, TGA/DTG, for five engineering thermoplastics..... 147
Table A.14: The coefficient of variance, TGA/DTG, for five engineering thermoplastics..... 148
Table A.15: The coefficient of variance, TGA/DTG, for five engineering thermoplastics..... 149
Table A.16: The candidate temperatures for the DSC studies of five engineering thermoplastics. 150
Table A.17: The percentage changes from the comparison of ABS 20-GF and ABS 20-CF compounded by Techmer..... 151
Table A.18: The percentage improvements from the comparison of ABS 40-GF and ABS 20-GF compounded by Techmer..... 152
Table A.19: The percentage improvements from the comparison of ABS 20-GF (SABIC) and ABS 20-GF compounded by Techmer. 153

List of Tables B

Table B.1. The initial sample mass prior the DSC examination. 175
Table B.2. The average glass transition analysis of a set of three ABS 20-CF samples. Notice all the DSC analyses includes a replicate experiment. 176
Table B.3. The average endothermic peak thermal event analysis of a set of three ABS 20-CF sample. 177
Table B.4. The average exothermic peak thermal event analysis of a set of three ABS 20-CF samples. 178
Table B.5. The average glass transition analysis of a set of three ABS 20-GF samples. 179
Table B.6. The average endothermic peak thermal event analysis of a set of three ABS 20-GF samples. 180
Table B.7. The average exothermic peak thermal event analysis of a set of three ABS 20-GF samples. 181
Table B.8. The average glass transition analysis of a set of three ABS 40-GF samples. 182
Table B.9. The average endothermic peak thermal event analysis of a set of three ABS 40-GF samples. 183
Table B.10. The average exothermic peak thermal event analysis of a set of three ABS 40-GF samples. 184
Table B.11. The average glass transition analysis of a set of three PETG 30-GF samples. 185
Table B.12. The average exothermic peak thermal event analysis of a set of three PETG 30-GF samples. 186
Table B.13. The average endothermic peak thermal event analysis of a set of three PETG 30-GF samples. 187
Table B.14. The average glass transition analysis of a set of three ABS 20-GF (SABIC) samples. 188
Table B.15. The average endothermic peak thermal event analysis of a set of three ABS 20-GF (SABIC) samples. 189
Table B.16. The average exothermic peak thermal event analysis of a set of three ABS 20-GF (SABIC) samples. 190
Table B.17. The arithmetic mean values, heating up and cooling down DSC readings, for ABS 20-CF. 191
Table B.18 The arithmetic mean values, heating up and cooling down DSC readings, for ABS 20-GF. 192
Table B.19. The arithmetic mean values, heating up and cooling down DSC readings, for ABS 40-GF. 193
Table B.20. The arithmetic mean values, heating up and cooling down DSC readings, for PETG 30-GF. 194
Table B.21 The arithmetic mean values, heating up and cooling down DSC readings, for ABS 20-GF (SABIC). 195
Table B.22. The standard deviations, heating up and cooling down DSC readings, for ABS 20-CF. 196
Table B.23. The standard deviations, heating up and cooling down DSC readings, for ABS 20-GF. 197
Table B.24. The standard deviations, heating up and cooling down DSC readings, for ABS 40-GF. 198

Table B.25. The standard deviations, heating up and cooling down DSC readings, for PETG 30-GF. 199
Table B.26. The standard deviations, heating up and cooling down DSC readings, for ABS 20-GF (SABIC). 200
Table B.27. The coefficient of variation, heating up and cooling down DSC readings, for ABS 20-CF. 201
Table B.28. The coefficient of variation, heating up and cooling down DSC readings, for ABS 20-GF. 202
Table B.29. The coefficient of variation, heating up and cooling down DSC readings, for ABS 40-GF. 203
Table B.30. The coefficient of variation, heating up and cooling down DSC readings, for PETG 30-GF. 204
Table B.31. The coefficient of variation, heating up and cooling down DSC readings, for ABS 20-GF (SABIC). 205
Table B.32. The comparison between the initial to the secondary heating cycle for ABS 20-CF. 206
Table B.33. The comparison between the initial to the secondary heating cycle for ABS 20-GF. 207
Table B.34. The comparison between the initial to the secondary heating cycle for ABS 40-GF. 208
Table B.35. The comparison between the initial to the secondary heating cycle for PETG 30-GF. 209
Table B.36. The comparison between the initial to the secondary heating cycle for ABS 20-GF (SABIC). 210
Table B.37. The arithmetic mean of ABS 20-GF and ABS 20-CF for a set of three DSC replicate experiments after their secondary heating up and cooling down thermal events. 211
Table B.38. The arithmetic mean of ABS 40-GF and ABS 20-GF for a set of three DSC replicate experiments after their secondary heating up and cooling down thermal events. 212
Table B.39. The arithmetic mean of ABS 20-GF (SABIC) and ABS 20-GF (Techmer) for a set of three DSC replicate experiments after their secondary heating up and cooling down thermal events. 213
Table B.40. The summary indicating the percentage change in the secondary DSC analyses, when comparing ABS 20 wt. % GF to ABS 20 wt. % CF. 214
Table B.41. The summary indicating the percentage change in the secondary DSC analyses, when comparing ABS 40-GF to ABS 20-CF. 215
Table B.42. The summary indicating the percentage change in the second DSC analyses, when comparing ABS 20-GF (SABIC) to ABS 20-GF (Techmer). 216

List of Figures A

Figure A.1:The TGA readings obtained from three ABS 20-CF samples after heated to a temperature of 800 °C in nitrogen. 95
Figure A.2: The DTG readings obtained from three ABS 20-CF samples after heated to a temperature of 800 °C in nitrogen. 96
Figure A.3: The arithmetic averages for the 1 % percentage weight loss and residual analyses at 750 °C, obtained from three ABS 20-CF samples. 97
Figure A.4: The arithmetic averages for the maximum peak temperature analysis, obtained from the DTG curves of three ABS 20-CF samples. 98
Figure A.5: The TGA readings obtained from three ABS 20-GF samples after heated to a temperature of 800 °C in nitrogen. 99
Figure A.6: The DTG readings obtained from three ABS 20-GF samples after heated to a temperature of 800 °C in nitrogen. 100
Figure A.7: The arithmetic averages for the 1 % percentage weight loss and residual analyses at 750 °C, obtained from three ABS 20-GF samples. 101
Figure A.8: The arithmetic averages for the maximum peak temperature analysis, obtained from the DTG curves of three ABS 20-GF samples. 102
Figure A.9: The TGA readings obtained from three ABS 40-GF samples after heated to a temperature of 800 °C in nitrogen. 103
Figure A.10: The DTG readings obtained from three ABS 40-GF samples after heated to a temperature of 800 °C in nitrogen. 104
Figure A.11: The arithmetic averages for the 1 % percentage weight loss and residual analyses at 750 °C, obtained from three ABS 40-GF samples. 105
Figure A.12: DTG curves of ABS 40 wt. % GF arithmetic averages for the maximum peak temperature analysis. 106
Figure A.13: The TGA readings obtained from three ABS 20-GF samples, by SABIC, after heated to a temperature of 800 °C in nitrogen. 107
Figure A.14: The DTG readings obtained from three ABS 20-GF samples, by SABIC, after heated to a temperature of 800 °C in nitrogen. 108
Figure A.15: The arithmetic averages for the 1 % percentage weight loss and residual analyses at 750 °C, obtained from three ABS 20-GF samples by SABIC. 109
Figure A.16: The arithmetic averages for the maximum peak temperature analysis, obtained from the DTG curves of three ABS 20-GF samples by SABIC. 110
Figure A.17: The TGA readings obtained from three PETG 30-GF samples after heated to a temperature of 800 °C in nitrogen. 111
Figure A.18. The DTG readings obtained from three PETG 30-GF samples after heated to a temperature of 800 °C in nitrogen. 112
Figure A.19: The arithmetic averages for the 1 % percentage weight loss and residual analyses at 750 °C, obtained from three PETG 30-GF samples. 113
Figure A.20: The arithmetic averages for the maximum peak temperature analysis, obtained from the DTG curves of three PETG 30-GF samples. 114
Figure A.21: The inert thermal stability history of the first ABS 20-CF, TG/DTG curves, sample. Notice that all the retrieved Trios graphs in Appendix A are courtesy of Trios v.4.5.0. software package. 115
Figure A.22: The inert thermal stability history of the second ABS 20-CF sample. 116

Figure A.23: The inert thermal stability history of the third ABS 20-CF sample. 117
Figure A.24: The inert thermal stability history of the first ABS 20-GF sample. 118
Figure A.25: The inert thermal stability history of the second ABS 20-GF sample. 119
Figure A.26: The inert thermal stability history of the third ABS 20-GF sample. 120
Figure A.27: The inert thermal stability history of the first ABS 40-GF sample 121
Figure A.28: The inert thermal stability history of the second ABS 20-GF sample. 122
Figure A.29: The inert thermal stability history of the third ABS 40-GF sample. 123
Figure A.30: The inert thermal stability history of the first ABS 20-GF (SABIC) sample..... 124
Figure A.31: The inert thermal stability history of the second ABS 20-GF (SABIC) sample. .. 125
Figure A.32: The inert thermal stability history of the third ABS 20-GF (SABIC) sample. 126
Figure A.33: The inert thermal stability history of the first PETG 30-GF (SABIC) sample. 127
Figure A.34: The inert thermal stability history of the second PETG 30-GF (SABIC) sample. 128
Figure A.35: The inert thermal stability history of the third PETG 30-GF (SABIC) sample. ... 129
Figure A.36: The average decomposition temperature for a set of three replicate experiments per material investigated. This was stablished according to the 1 wt. % loss from the overall sample mass. There was not statistical difference among the results. Vertical error bars are illustrating the ± standard deviation. 130
Figure A. 37: The average weight loss for a set of three replicate experiments per material investigated. This analysis was stablished between the decomposition temperature up to a visible plateau region after the decomposition event. There was a relatively low statically difference among the results. Vertical error bars are illustrating the ± standard deviation. 131
Figure A. 38: The average maximum peak temperature for a set of three replicate experiments per material investigated. Notice it is shown a significant statistical difference among the results, please note the temperature scale range shown, 404 °C to 424 °C, in the y-axis. Vertical error bars are illustrating the ± standard deviation. 132
Figure A. 39: The average residue percent measured at 750 °C for a set of three replicate experiments per material investigated. There was not significant statistical difference among the results. Vertical error bars are illustrating the ± standard deviation. 133
Figure A. 40: The area under the DTG curve identifying the amount of decomposed material matrix for a set of three replicate for five engineering thermoplastics, ABS and PETG, respectively. There was not significant statistical difference among the results. Vertical error bars are illustrating the ± standard deviation. 134

List of Figures B

Figure B.1. The DSC curves, illustrating a heating up scan, red curve; in addition, a cooling down scan, blue curve, for the first sample. Please notice, Figure B.1 represents the initial experiment and Figure B.2 demonstrates the replicate experiment, both under the same processing parameters. 155
Figure B.2. The DSC curves, illustrating a heating up scan, red curve, and a cooling down scan, blue curve for the second sample. 156
Figure B.3. The DSC curves, illustrating a heating up scan, red curve, and a cooling down scan, blue curve for the third sample. 157
Figure B.4. The overlay for a set of three sample, notice the red curves represent the first sample, the blue curves illustrates the second sample and the green curve is attributed to the third sample. 158
Figure B.5. The DSC curves, illustrating a heating up scan, red curve; in addition, a cooling down scan, blue curve, for the first sample. Please notice, Figure B.1 represents the initial experiment and Figure B.2 demonstrates the replicate experiment, both under the same processing parameters. 159
Figure B.6. The DSC curves, illustrating a heating up scan, red curve, and a cooling down scan, blue curve for the second sample. 160
Figure B.7 The DSC curves, illustrating a heating up scan, red curve, and a cooling down scan, blue curve for the third sample. 161
Figure B.8. The overlay for a set of three sample, notice the red curves represent the first sample, the blue curves illustrates the second sample and the green curve is attributed to the third sample. 162
Figure B.9. The DSC curves, illustrating a heating up scan, red curve; in addition, a cooling down scan, blue curve, for the first sample. Please notice, Figure B.1 represents the initial experiment and Figure B.2 demonstrates the replicate experiment, both under the same processing parameters. 163
Figure B.10. The DSC curves, illustrating a heating up scan, red curve, and a cooling down scan, blue curve for the second sample. 164
Figure B.11. The DSC curves, illustrating a heating up scan, red curve, and a cooling down scan, blue curve for the third sample. 165
Figure B.12. The overlay for a set of three sample, notice the red curves represent the first sample, the blue curves illustrates the second sample and the green curve is attributed to the third sample. 166
Figure B.13. The DSC curves, illustrating a heating up scan, red curve; in addition, a cooling down scan, blue curve, for the first sample. Please notice, Figure B.1 represents the initial experiment and Figure B.2 demonstrates the replicate experiment, both under the same processing parameters. 167
Figure B.14. The DSC curves, illustrating a heating up scan, red curve, and a cooling down scan, blue curve for the second sample. 168
Figure B.15. The DSC curves, illustrating a heating up scan, red curve, and a cooling down scan, blue curve for the third sample. 169
Figure B.16. The overlay for a set of three sample, notice the red curves represent the first sample, the blue curves illustrates the second sample and the green curve is attributed to the third sample. 170

Figure B.17. The DSC curves, illustrating a heating up scan, red curve; in addition, a cooling down scan, blue curve, for the first sample. Please notice, Figure B.1 represents the initial experiment and Figure B.2 demonstrates the replicate experiment, both under the same processing parameters. 171
Figure B.18. DSC analyses displaying a heating up scan (red curve) and a cooling down scan (blue curve) Where figure B.1 represents the first experiment and figure B.2 represents is its replicate experiment under the same processing parameters..... 172
Figure B.19. DSC analyses displaying a heating up scan (red curve) and a cooling down scan (blue curve) Where figure B.1 represents the first experiment and figure B.2 represents is its replicate experiment under the same processing parameters..... 173
Figure B.20. The overlay for a set of three sample, notice the red curves represent the first sample, the blue curves illustrates the second sample and the green curve is attributed to the third sample. 174

Chapter 1: Introduction

1.1 BACKGROUND

Polymer, also referred as plastics and resin, is a noun that derives from the Greek language (*pulumeres*). Where, *polus* signifies a repeating unit and *meros* a basic unit. These repeating units are linked together forming networks (one-dimensional, two-dimensional or three-dimensional). Where the word plastic has multiple uses, for example, engineers can use it to describe a specific mechanical behavior in a material, such as plastic deformation and elastic deformation. In manufacturing, it is accepted to describe materials with the capability to be molded. Similarly, plastic, is a noun that derives from the Greek language (*plastikos*), it means to form or shape, and is used interchangeably with the word thermoplastic (Larson, 2015; "The Basics: Polymer Definition and Properties", n.d.). According to accepted terminology standards, a plastic is a material that contains as an essential ingredient one or more organic polymeric substances of large molecular weight, is solid in its finished state, and, at some stage in its manufacture or processing into finished articles, can be shaped by flow. Some examples of plastics are thermoplastics, thermosets and elastomers (ASTM D883-19c, 2019*).* In metals, the effect of temperature is reflected in the mechanical properties of the material; for example, the yield strength, tensile strength and modulus of elasticity decreases as the temperature increases. Conversely, metals/alloys may exhibit an increase in ductility as the temperature rises, and brittleness decays when the temperature is reduced. Similarly, in polymers, the temperature profile impacts the polymer-processing operations. From an extrusion standpoint, a rise in temperature induces an increment in ductility, this is advantageous to dispense the semi-molten or molten material. However, the glass transition temperature, in part, dictates the temperature processing parameters to work with polymers. In this sense, brittleness is equivalent to temperatures below the glass

transition temperature and ductility increases above the glass transition temperature. Generally, the glass transition temperature depends of the rate of cooling and the polymer molecular weight distribution (Askeland & Wright, 2015; Larson, 2015). According to accepted terminology standards, the glass transition temperature is the approximate midpoint of the temperature range over which the glass transition takes place. Alternatively, the glass transition is the reversible change in an amorphous polymer or in amorphous regions of a partially crystalline polymer from (or to) a viscous or rubbery condition to (or from) a hard and relatively brittle one. In the same manner, semicrystalline materials have a glass transition temperature, but it usually only affects the amorphous (non-crystalline) areas of the material (ASTM D883-19b, 2019; Larson, 2015).

To enable the formation of these networks (plastic molecules), a bond gets formed between atoms and small compounds. Essentially, these compounds can consist of carbon, hydrogen, nitrogen, and sometimes oxygen, just to name a few. These are bonded into a monomer (small molecule) or fewer units (oligomers) with the objective of creating larger molecules (chemically independent macromolecules); consequently, chains are formed through polymerization. Specifically, polymerization occurs when atoms are joined by covalent bonding (Askeland & Wright, 2015; Larson, 2015; "The Basics: Polymer Definition and Properties", n.d.). In terms of accepted terminology, polymerization is a chemical reaction in which the molecules of monomers are linked together to form polymers (e.g., polycondensation and polyaddition) (ASTM D883-19b, 2019). At a macromolecular level, molecular chains have an average molecular weight ranging from 10,000 to more than one million g/mol (Askeland & Wright, 2015). In manufacturing, polymers are processed through a wide variety of plastic processing technologies. This includes plastic tooling, plastic forming, vacuum forming, pressure forming, plastic welding, extrusion, plastic molding and injection molding, to name a few. As previously mentioned, polymers are one

class of materials often used in additive manufacturing (Larson, 2015). As categorized by the American Society for Testing and Materials Committee F42, additive manufacturing (AM) comprises seven process categories: vat photopolymerization, powder bed fusion, material extrusion, material jetting, binder jetting, sheet lamination and direct energy, respectively. Additionally, there were introduced materials categories; accordingly, metal powders, ceramic powders, photopolymer resins, polymer powders, metals rods and polymer filaments ("ASTM F42/ISO TC 261 Develops Additive Manufacturing Standards", n.d.). Additive manufacturing, also known as 3D printing, entered the commercial platform in the late 1980's. Technologies within AM are capable to produce parts directly from a computer-aided design (CAD) data; further, these are intended for low volume production and mass customization. Fused Deposition Modeling (FDM), for example, is a heated material extrusion additive manufacturing process, employs thermoplastic filaments as feedstock. This process heats up the material and induces a semi-molten state, where the system selectively deposits the material in a horizontal pattern through a nozzle into a build platform; consequently, it forms cross sections or layers. For instance, the build platform descends, and thermal fusion of each layer is accomplished (Espalin, 2012). . Thus, AM marks new possibilities in material testing and applications for the biomedical, automotive, pharmaceutical, and aerospace industry (Balderrama-Armendariz *et al.*, 2019).

In the opposite scenario, large scale systems are capable to build geometries of greater dimensions than a small-scale polymer 3D printer. Currently, Big Area Additive Manufacturing (BAAM), a large-scale Fused Filament Fabrication (FFF) system, takes the design constraints of small-scale 3D printers and employs a heated barrel and a single-screw for the extrusion of pelletized material through a nozzle (e.g., thermoplastic and thermoplastic-based composite materials). In fact, the implementation of a single-screw extruder allows higher deposition rates

and the use of lower cost materials. In part, the filler material helps to eliminate the use of an oven because thermal expansion effects on either side of the glass transition temperature are comparable. Thus, fiber reinforcements in composites materials, carbon fibers or glass fibers, are incorporated to the matrix material to mitigate warping and distortion. Therefore, BAAM machines enables faster and reduced cost capabilities in the 3D printing of large-scale parts. (Espalin, 2017; Roschli *et al.*, 2019). In the economic aspect, in 2011, the globally primary additive manufacturing market, China, noted a total revenue of approximately 1.71 billion (USD). Accordingly, 643 million for AM systems and materials, 642 million from the sale of parts produced by AM systems and 237 million for maintenance contracts, training, seminars, conferences, just to name a few. However, in 2010, the U.S became the second largest manufacturing nation in the world. When compared China to the U.S, the U.S is producing slightly less than China (Thomas, 2013).

1.2 MOTIVATION

Polymer are of great interest because they provide promising characteristics to manufacture products across different industries. Among their most important characteristics are their lightweight (e.g., as found in toys, frame structurers of space stations, nylon fibers, or bulletproof vests), density (e.g., lower when compared to the density of stones, concrete, steel, cooper, or aluminum.), strength, flexibility (e.g., as seen in soft drink bottles), low cost, their adaptability, their thermal resistance (e.g., home appliances as coffee pot handles, foam core of refrigerators and freezers, insulated cups, microwave cookware, thermal underwear), electric insultation (power cords and electrical outlets), and their optical properties. Further, polymers are used in the construction, furniture, electronics, communication, packaging, energy, health care, transportation, aeronautics, textiles, and sports and leisure industries. Accordingly, this work aims to explore the lack of thermomechanical data in the public landscape for thermoplastic matrix composite materials used in large-area additive manufacturing (“The Basics: Polymer Definition and Properties", n.d.; "Polymer Chemistry", n.d.)

1.3 OBJECTIVES

There are four thesis objectives and are listed as follow:

1. Incorporate thermal analysis methods to characterize carbon fiber and glass fiber reinforced acrylonitrile-butadiene-styrene (ABS) as per ASTM standards.
2. Assess glass fiber reinforced polyethylene terephthalate glycol (PETG) composites through thermal characterization as per ASTM standards.
3. Investigate the thermal stability of ABS and PETG, nitrogen-controlled atmosphere, at varying ratios of added fiber reinforcement.
4. Study the effects of two replicate DSC scanning cycles in a nitrogen-controlled atmosphere, heating and cooling, and evaluate the glass transition, exothermic and endothermic events.

1.4 THESIS OUTLINE

The present thesis document was divided in seven chapters. The succeeding chapters are presented as follows: Chapter 2 contains an overview to polymers, morphologies, thermoplastics, thermoplastic polyesters, filler reinforcements, thermogravimetry and differential scanning calorimetry. Chapter 3 introduces the materials and experimental methodologies to examine two matrix materials composites (i.e., ABS and PETG) by thermogravimetry and differential scanning calorimetry. Chapter 4 provides the results of thermal stability studies under nitrogen, and the effects of two replicate cycles, heating and cooling, by DSC for two distinct proprietary thermoplastics (ABS and PETG). Chapter 5 and Chapter 6 discusses the thermal characterization experimental results. Lastly, Chapter 7 provides conclusions and future recommendations.

Chapter 2: Literature Review

This chapter offers a brief description of polymers and thermoplastics, with special emphasis on the characteristics and application of two thermoplastics: ABS and PETG. Thereafter is a review of polymer thermal characterization in the context of thermogravimetry and differential scanning calorimetry. Lastly, the seven process classifications in additive manufacturing are described.

2.1 POLYMERS

Polymers are found in nature or are engineered to resolve specific needs. Deoxyribonucleic acid (DNA), ribonucleic acid (RNA), spider silk, hair, starch, and cellulose, are common molecular networks found in nature. In fact, polymers are chemical compounds (mixture of compounds) formed by a polymerization reaction. Other definitions include: compounds of high molecular weight derived either by the incorporation of many smaller molecules (e.g., polyethylene) or by condensation of smaller molecules (e.g., eliminating the presence of water or alcohol); a compound formed from two or more polymeric compounds; a product of polymerization; or a system of macromolecules (Larson, 2015; Gooch, 2007). Regarding accepted terminology standards, polymers are substance consisting of molecules characterized by the repetition (neglecting ends, branch junctions and other minor irregularities) of one or more types of monomeric units (ASTM D883-19b, 2019, 2019).

Polymer chains are compounded through interchain attraction, these collected chains (polymer matrix) are divided in two main categories, thermoplastics (linear polymers) and thermosets (thermosetting plastic materials). These classifications are generally considered to manufacture useful product with plastic materials. Strictly speaking, the differences in their chemistry, behavior, their processing and handling are imperative to design and manufacture

products. Thermoplastics are one-dimensional chains (molecules) capable to melt; engineered to be reformed through heating and cooling cycles. In this sense, a thermoplastic is capable of being repeatedly softened by heating and hardened by cooling through a temperature range characteristic of the plastic, and that in the softened state can be shaped by flow into articles by molding or extrusion for example. On the other hand, thermosets are designed as three-dimensional networks uncapable to melt once unified (e.g., epoxy resins). In fact, a reheating cycle causes the material degradation if temperatures are sufficiently high (Biron, 2018; Gooch, 2007; Kutz, 2017; Larson, 2015; "The Basics: Polymer Definition and Properties", n.d.). According to accepted terminology standards, a thermoset is plastic that, after having been cured by heat or other means, is substantially infusible and insoluble. Therefore, scientist and engineers are continuously developing polymer compounds with distinct and innovative characteristics (ASTM D883-19b, 2019).

As we have seen throughout history (e.g., Stone age, to the Bronze age, the Iron age, and the age of Steel), societies learned to discover and exploit new materials to create sophisticated tools. Egypt and Babylon civilizations learned to use eight classes of materials: metals, stones, woods, ceramics, glasses, skins, horns and fibers. Vestiges of natural plastics can be traced back to the book of *Genesis,* the book of *Exodus,* or in ancient Egypt mummies. As an example, mummies employed a cross-linking technique that was a pioneer in terms of the vulcanization of rubber and the production of thermosetting plastics. In the 19th century, mankind employed these materials to fabricate possessions, homes, tools, and furniture. Near the 20th and 21st century, rubbers and plastics were developed. In fact, the major growth period of the plastic industry started in the 1930's, and in early stages of the twentieth century, natural rubbers were utilized (BPF, "British Plastics Federation: A History of Plastics", n.d.; Gilbert, 2017; Kutz, 2017).

The year 1909 marked the start of the age of synthetic plastics and the discovery of synthetic phenolformaldehyde resin (PF). In 1909 and 1910, Bakelite became the first synthetic manufactured plastic and Rayon the first manufactured polymeric fiber (Gilbert, 2017; "The Basics: Polymer Definition and Properties", n.d.). While in the 1930-1940, polystyrene (PS), poly (vinyl chloride) (PVC), polyolefins, and PMMA (acrylic) were developed from ethylene. Polyethylene (PE), an electrical insulator and a chemically resistant material, was discovered in 1933. In addition, this year was marked with the first synthesis of PMMA, wherein it was employed to produce aircraft glazing. Throughout the 1940's and 1950's, polyethylene and polystyrene were produced in large tonnages and at low cost. Nonetheless, it was not until 1945-1955 when there were achieved improvements in the quality of existing plastics materials. These continuous efforts allowed the introduction of high-impact polystyrene as a commercial plastic, and acrylonitrile-butadiene-styrene (ABS) as a terpolymer (Gilbert, 2017).

In1941, polyethylene terephthalate (PET) was used as a fiber; nevertheless, PET was not employed to produce beverage bottles until 1957. The 1970's and 1980's were known for the development of high-performance thermoplastics, these to endure temperature of approximately 200 °C. Examples of high-performance thermoplastics included polyetherether ketone (PEEK), polyphenyl sulfide (PPS), polyether sulfone (PES) and novel liquid crystals polymers. In 1900, polyhydroxybutryate became the first biodegradable plastic; meanwhile, the twenty-first century consisted of improvements to existing plastics. This was accomplished by changes in their production methods, blending and copolymerization, and through use of additives, particularly fillers and flame retardants. In addition, the 20th century marked the pathway to increase awareness of health and safety issues, sustainability, and recycling of polymer (Gilbert, 2017).

After World War I, the petrochemical industry was founded and solvents were produced from olefins (waste products of cracking); likewise, this industry branch contributed during World War II in the production of ethylene dichloride, vinyl chloride, ethylene glycol, ethylene oxide, and styrene. Today, petroleum is the main feedstock for the polymer industry; and ethylene, a commercial product from steam cracking, has become one of the most important products in the petrochemical industry. In fact, bio-based renewable sources are of great interest to produce polymers, since fossil fuels such as petroleum will not last forever (Gilbert, 2017).

In 2019, according to the *New York Times*, more than a million tons of plastic will be produced by one of the largest active construction projects in the United States; however, as concern grows about plastic debris in the oceans and recycling continues to falter in the United States, the production of new plastic is booming. A *Royal Dutch Shell's* fabric will create pellets to manufacture phone cases, auto parts and food packaging; in fact, more than a dozen are being built or have been proposed around the world by petrochemical companies. Further, studies have observed plastic fibers in places such as the stomachs of sperm whales, in tap water and in table salt. Based in this previous example, it can be noted that the plastic industry comes with advantages and disadvantages (Corkery, "A Giant Factory Rises to Make a Product Filling Up the World: Plastic", 2019). Thermoplastic materials are classified in three categories. This includes commodity thermoplastics, engineering thermoplastics, and advance engineering thermoplastics (AETP: specialty, advanced, or ultrapolymers). As the plastics industry experienced a fast growth phase, engineering thermoplastics (ETPs) were adopted by the markets once dominated by metals. In comparison the metals, ETPs offer advantages as corrosion resistance, transparency, lightness, self-lubrication and economy in fabrication. In general, engineering thermoplastics owe this accelerated expansion to the adoption from the electrical/electronic and automotive markets. In the

economic context, ETP are regarded as the fastest growing segment in the plastic industry. For example, the global consumption of ETP in 2012 was approximately 19.6 million metric tons and it is estimated it will reach 29.1 million metric tons by 2020. Further, commodity thermoplastics are known as the highest volume of usage (1 million tons per annuum on global scale). Whereas, engineering thermoplastics are distinguished as a high-performance segment of synthetic plastics materials. When properly formulated, ETP are implemented to fabricate mechanical functionals parts. This means, these parts can prevail if they are subjected to mechanical stress, impact, flexure, vibrations, sliding friction, extreme temperatures, or hostile environments, just to name a few. Advance engineering thermoplastics constitute the top position in the plastic performance pyramid. Compared to ETPs and commodity thermoplastics, AETPs have unmatched thermal, mechanical and chemical properties (Gilbert, 2017).

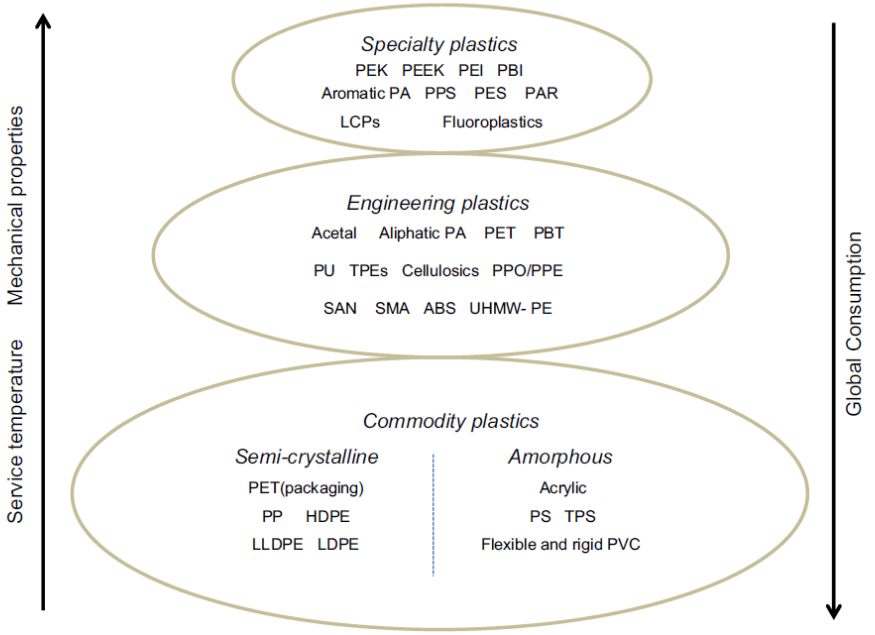

Figure 2.1.1: Classification of thermoplastics. By courtesy of *Applied plastics engineering handbook: Processing materials*, M. Kutz, 2017, United Kingdom: Elsevier.

These three primary classifications, commodity thermoplastics, ETP and AETP, are developed when long chains of atoms are bounded forming a backbone chain. Eventually, different compounds can be bonded to form distinct backbones. Polymer have diverse morphologies and their molecular response to different conditions is important. The molecular arrangement of polymers is divided in three morphologies: amorphous, crystalline and semi-crystalline. An amorphous state refers to molecules without a regular order and their polymer chains are not capable to arrange themselves (e.g., random/haphazard manner). In contrast, a crystalline molecular arrangement consists of molecules organized in distinct patterns, where their molecules are oriented in a regular, repeating pattern (ASTM D883-19c, 2019; Gilbert, 2017; Larson, 2017).

Crystallinity, a thermal phenomenon, is a process triggered by factors such as the wall thicknesses of a part, nucleating agents in the material, or the heat transfer dynamics. Additionally, crystallinity is the regular arrangement of the atoms of a solid in space. Contrarily, the melting temperature entails the breaks down of the crystalline structure and involves a molecular change, an amorphous state, respectively. In other words, at a given pressure, the temperature at which a crystalline solid undergoes a phase transition to the isotopic state when heat is added (ASTM E1142-15, 2015; Larson, 2015). This melting temperature is a reversible and predictable event in crystalline structures. On the other hand, amorphous materials, lack of a distinct melting temperature. Amorphous polymers can be manufactured to be transparent (e.g., food wraps, plastic windows and headlight lenses); whereas, crystalline polymers may be designed to be translucent and opaque. The degree of translucence or opaqueness of the polymer resembles crystallinity (Larson, 2015; “The Basics: Polymer Definition and Properties", n.d.). Additionally, manufacturers can inflict amorphous morphologies by controlling the polymerization process and quenching the molten polymers. Moreover, amorphous morphologies in thermoplastic extrusion

do not exhibit a sharp change in the specific volume nor in the coefficient of thermal expansion during cooling. Whereas, crystalline polymers show a sharp specific volume change during cooling and experience a rise in coefficient of thermal expansion (Espalin, 2017; Larson, 2015; “The Basics: Polymer Definition and Properties", n.d.)

To enable further improvements on plastic materials, polymer manufacturers can introduce physically additive, such as fillers, antiaging additives, colorants, plasticizers and softeners, lubricants and flow promoters, impact modifiers, flame retardants and blowing agents. The use of additives liquid or powder form, or in the shape of small solid particles enables changes on a physical level, such as changes in viscosity, strength or stiffness of the material, electrical properties, and it may impact the chemistry of the base resin. In fact, compounding, also known as the most common method of modification, employs a great variety of additives. As an example, processing aids, fillers, reinforcements, and performance modifiers are well suited as additives. In fact, additives are known for altering the bulk properties of a polymer (Gilbert, 2017; Larson, 2015). The purpose of processing aids is to modify the viscous properties, such as enhancing flowability and homogeneity. Processing aids can also induce modifications to their cooling and solidification process. Fillers enable to replace some of the volume of the resin with filler materials, such as low-cost generic items (e.g., talc), mica, glass beads, glass microspheres, or glass fibers. Additionally, fillers allow manufacturers to adjust the density of a final part. However, when comparing filled resin and reinforced resin, filled resins typically does not exhibit chemical bonds between the filler and the polymer chain, and often are stiffer than an unfilled resin. Reinforced resins, on the other hand, when compared to filled resin, have a significant effect on the chemical bonds between the additive and the polymer chains, this by increasing the strength and stiffness of the material. Typical fiber-reinforcing agents include glass fiber, carbon fiber, and aramid fiber.

Lastly, performance modifiers such as stabilizers, tougheners, lubricants, pigments and dyes are devoted to improving the resistance to UV degradation, exposure to heat, or improve impact resistance, just to name a few. In this present work, a brief description of thermoplastic is introduced in the next subsection, since this experimental research was related to thermoplastic (Larson, 2015).

2.2 THERMOPLASTICS

According to accepted terminology standards, a thermoplastic is capable of being repeatedly softened by heating and hardened by cooling through a temperature range characteristic of the plastic, and that in the softened state can be shaped by flow into articles by molding or extrusion (ASTM D883-19b, 2019). Composites are formed when there are incorporated reinforcement (additives) in the form of short, long, or continuous fibers into the thermoplastic. In general, thermoplastics are limited by their sensitivity to environmental parameters and mechanical loadings; parameters such as temperature, moisture, deleterious solids, liquids, gases and chemical products condition the performance and life of the plastic. In fact, studying the thermomechanical behavior of engineering thermoplastics enables to predict the immediate physical and long-term effects cause by thermal exposure. Immediate physical effects are such that the decline of the mechanical properties, physical properties, and changes in dimensional stability (Biron, 2018; Larson 2015).

In fact, the glass transition temperature dictates the reversible change in an amorphous material or in amorphous regions of a partially crystalline material, from (or to) a viscous or rubbery condition to (or from) a hard and relatively brittle one (ASTM E1142-15, 2015). The thermophysical property is of great interest to the polymer's industry. In which the glass transition

temperature is used to describe the thermal history of amorphous polymers. Where the glass transition temperature enables to describe the kinetic energy of the molecules; accordingly, the molecular short-range vibrations and rotations initiate as the temperature is increased (Menczel & Prime, 2009). However, this phenomenon is restricted if the polymer still resembles a glasslike structure. Note that as the temperature raises, the polymer no longer resembles a glasslike structure; consequently, this temperature is defined as the glass transition temperature (Tg). Beyond the temperature glass transition, a loss of elasticity is experienced and a flowable liquid is produced. In summary, at a molecular level, the glass transition temperature entails long-range molecular motion, rotational freedom and segmental motion of the molecular chains. Where these segmental motions indicate an increase of free volume; accordingly, an increase of specific volume (Espalin 2012, Espalin 2017).

Despite this thesis focus on engineering thermoplastics, it is the author's opinion that a brief background of thermoset is of benefit to the reader. As such, a brief description on thermosets is given. A thermoset is divided in three types, formaldehyde resins, epoxies, and unsaturated polyesters, respectively. Thermosets before hardening are independent macromolecules like that of thermoplastics. Following a hardening event, thermosets achieve a 3D structure by chemical cross-linking produced after or during the processing (Biron, 2018). These chemical reactions are triggered by heat, oxygen, UV light, a reagent material, or a catalyst. Hence, links created between the chains of the thermosets limit their mobility and possibilities relative displacements (Larson, 2015). As reported by accepted standards, a thermoset is a plastic that, after having been cured by heat or other means, is substantially infusible and insoluble (ASTM D883-19b, 2019). In fact, thermosets are susceptible to infusibility, this means the degradation by heat without reaching a liquid state; thus, improving some aspects of fire behavior. Yet another example of their advantages includes, modulus retention as temperature is increased, and better general creep behavior. On the other hand, thermosets require prolonged time for the chemical reaction to reach cross-linking, their processing is difficult to monitor, and some thermoset may release gases (e.g., water vapor). Ultimately, thermosets are known due to their irreversible conversion process (Biron, 2018). Thermoset applications can include paints, lacquers, varnishes, adhesives (e.g., epoxy), caulks, and all kinds of rubbery stuff (Larson, 2015). The following sections are dedicated to a single thermoplastic, acrylonitrile-butadiene-styrene (ABS), respectively. The acronym (ABS) entails the following monomer compositions: acrylonitrile, butadiene and styrene. Subsection 2.2.2 through subsection 2.2.3 presents an overview to these monomers with focus on their characteristics and hazards. Thereafter, subsection 2.2.4 describes the properties from ABS as a thermoplastic.

2.2.1 Acrylonitrile

Acrylonitrile, also known as 2-propenenitrile, acrylic acid nitrile, acrylon, among other terms, is a colorless and volatile liquid with a pungent odor; also, distinguished as a flammable and a water-soluble liquid at room temperature. In the plastic industry, acrylonitrile has been devoted to produce rubber, resins, elastomers, synthetic fibers. Currently, acrylon has been used to manufacture carbon fibers, which are used in aircrafts, defense and aerospace industries (National Center for Biotechnology Information., "Acrylonitrile", 2004). When freed to the environment, acrylonitrile is soluble in water (75.1 g./liter at 25.0 °C); and it can transfer to the soil and sediment. Further, it is miscible with most organic solvents. In addition, acrylonitrile has a molecular mass of about 53.1 g/mol, a melting point temperature of -30.6 °C, boiling point temperature 145.0 °C, flash point temperature -1.0 °C, autoignition temperature 481.0 °C and a relative density in the range of 0.80 (International Programme on Chemical Safety INCHEM, 2001). After exposure to acrylonitrile, it is distinguished for promptly be absorbed by all routes of exposure; however, it has a minor occurrence to accumulate in any organ. This chemical can lead to a variety of biological effects. (such as irritate the mucous membranes, causes headache, nausea, dizziness, impaired judgment, difficulty breathing, limb weakness, cyanosis, convulsions and collapse.). Usually, acrylonitrile is excreted in the urine within the first twenty-four to forty-eight hours. Ultimately, this monomer may polymerize spontaneously and violently (such as in the presence of concentrated caustic acid, on exposure to visible light, or in the presence of concentrated alkali) (Long *et al.*, 2002).

2.2.2 Butadiene

Butadiene, also known as 1, 3-butadiene, divinyl, buta-1,3-diene, among other names, is a synthetic colorless gas and insoluble in water (0.735 g/liter at 25 °C); whereas, it is soluble in ethanol, ether, acetone and benzene. This monomer is characterized mainly to manufacture other polymers, copolymers and as an intermediate in the production of other industrial chemicals.

Specifically, 1, 3-butadiene is used to manufacture tires, car sealants, epoxy resins, lubricating oils, hoses, drive belts, adhesives, and paint, just to mention a few. However, butadiene, has some drawbacks, upon heating may cause acrid fumes and turns flammable. In fact, divinyl oxidizes in the presence of air and forms explosive peroxides. In addition, inhalation is known as the primary channel to butadiene exposure. After acute exposure to butadiene, it causes irritation of the eyes, nasal passages and throat; henceforth, high butadiene concentrations augment the possibilities to induce headache, fatigue, a decline in blood pressure and pulse rate. While the central nervous system may become compromised or prompt an unconscious state in humans (Hughes *et al.*, 2001; National Center for Biotechnology Information., "1,3-Butadiene", 2005). Butadiene, a human carcinogen and possibly genotoxic, is a major product of the petrochemical industry, which it is employed to produce synthetic rubbers. In the context of economics, it is expected that butadiene experiences a growth about 3 % through the end of this decade. In fact, the buta-1,3-diene global demand is anticipated to exceed 9 million metric tons. Steam cracking (e.g., olefin plants), a petrochemical process, accounts for the 95% of the global butadiene production. This principal industrial method employs feedstock (such as ethane, propane, butane, naphtha, condensate or gas oil). Where this process is driven by feeding the feedstock into a pyrolysis furnace. After being driven into a furnace, the feedstock is exposed to steam at a temperature range of 790-830 ºC. Ultimately, olefin plants go through a series of process to produce crude butadiene. There are two typical olefin plants, the light gas crackers pyrolysis plants (e.g., ethane and propane) and heavy liquid crackers (e.g., naphtha, condensates or gas oils), where in average an ethane cracker is capable to produce 2 lb. of butadiene per 100 lb. of ethylene. On the other hand, a naphtha cracker can achieve close to 16 lb. per 100 lb. of ethylene. In this fashion, the resulting collected crude butadiene by the olefin plants can be typically up to 40% and 50% (White, 2017). Among the butadiene physical properties are, the molecular mass (54.1 g/mol), melting point temperature -109.0 °C, boiling point temperature -4.4 °C, flash point temperature -76.0 °C and relative density 0.60 (International Programme on Chemical Safety INCHEM, 2017).

2.2.3 Styrene

Styrene, also known as ethenylbenzene, vinylbenzene, among other terms, is a colorless liquid and is insoluble in water (less dense than water). This monomer evaporates effortlessly, and it can be released to the environment by facilities manipulating this chemical. For example, this monomer is released through automobile exhausts, or the combustion of products (such as cigarettes smoke), just to name a few. In the plastic industry, styrene has been devoted to fabricating packaging materials, insulation materials (e.g., polystyrene plastics and resins), liquid toners for photocopiers (such as styrene copolymers), fiberglass reinforcement material and plastic pipes (e.g., copolymers as styrene-acrylonitrile). However, styrene, has some disadvantages and it can unleash potential health hazards for humans (Rosemond *et al.*, 2010). For example, it can be inhale (in its vapor phase) and absorbed through our skin (acute exposure); moreover, styrene at 100 ppm (parts per million) causes irritation to eyes, nose, throat and lungs. Also, it is recognized for removing the protective oils from the skin and inflict dermatitis (skin rash), dryness, redness, flaking, and cracking of the skin at prolonged exposure. Yet another example of hazards due to exposure to high levels of styrene includes headache, dizziness, lightheadedness, and passing out. Likewise, extreme overexposure through inhalation (e.g., closed spaces) could result in a pulmonary edema. Repeated exposure to lower levels of styrene may induce problems in concentration, memory, balance and learning ability, and it can cause confusion and slowed reflexes. Furthermore, there is limited evidence to demonstrate that styrene causes cancer on animals (California Department of Public Health, 1990; New Jersey Department of Health, 2011). Lastly, styrene has an approximate molecular mass of 104.2 g/mol, melting point -30.6 °C, boiling point 145.0 °C, flash point 31.0 °C, relative density 0.91 and a solubility in water of (0.03 g/liter at 20 °C) (International Programme on Chemical Safety INCHEM, 2006; National Center for Biotechnology Information., "Styrene", 2004).

2.2.4 Acrylonitrile-butadiene-styrene (ABS)

Acrylonitrile-butadiene-styrene, an amorphous material, is often classified as a terpolymer or triblock copolymer. It has a petrochemical origin and it is typically denoted by a low melting point at around 105 °C (Espalin, 2012; Ahmad, Gopinath, & Dutta, 2019). In the 1940's, after the invention of styrene-acrylonitrile (SAN), a copolymer, and continuous advancements in polymeric materials, it enabled the introduction of butadiene as a third monomer into SAN. As such, ABS matrix material was consolidated and became available in 1950 (McKeen, 2014). However, this polymer has a dispersed phase of butadiene, an intermediate phase of SAN (styrene-acrylonitrile) grafted to the butadiene, and a continuous phase of SAN. The commercial ABS constitution is approximately 65 wt. % SAN and 35 wt. % acrylonitrile-butadiene. Additionally, it should be noted that ABS is distinguished by its rubber concentration; for example, ABS resin has higher rubber content when compared to high impact-polystyrene resin (HIPS). In fact, the butadiene content determines the polymer's toughness level. Where butadiene can be found in two configurations, 1,4-*trans* and 1,4-*cis*, accordingly. However, 1,4-*trans* butadiene is used in most of commercially ABS grades. The typical monomeric composition in commercial ABS resin is: (20 % - 30.0 %) acrylonitrile, (5.0 % - 35.0 %) butadiene and (35.0 % - 75.0 %) styrene (Scheirs, 2002). Typically, ABS is used to manufacture medical devices (such as in cartilage tissue engineering), cosmetics and vehicle components, just to name a few. In addition, ASTM D4673 provides a standard classification system for ABS material and ABS alloys. In which ABS materials (e.g., intended for injection molding and extrusion) are grouped rather than rigidly classified. These groups are subdivided by class and grades. More specifically, in the case of reinforced ABS/alloys, ABS is given a designation grade in the context of its materials properties. The tensile properties as per ASTM D638–14, flexural properties as per ASTM D790-17, impact

properties as per ASTM D256–10 and ISO 179-1:2010, softening temperature (D1525-17e1) and deflection temperature under flexural load as per ASTM D648–18 are among the most adopted examinations for ABS/alloys (ASTM D4673–02, 2002). In general, ABS resin is well adopted by the commercial industry due to its high impact resistance, strength, toughness, thermal stability, dimensional stability and processability. Further, these monomers as a triblock copolymer produce beneficial effects on heat tolerance (provided by the acrylonitrile monomer), robust impact strength (provided by the butadiene), and rigidity (provided by the styrene) (Ahmad, Gopinath, & Dutta, 2019; Zhang et al., 2018). Mainly, polybutadiene regards as the weakest component in ABS in the context of thermal oxidation. In fact, acrylonitrile-butadiene-styrene is susceptible to degradation, and presents difficulties to densify at high concentrations of rubber content. Lastly, this hygroscopic thermoplastic has the disadvantages to absorb up to 0.3% moisture in 24 h (Kutz, 2017; McKeen, 2014 McKeen, 2014).

2.3 THERMOPLASTIC POLYESTERS

Thermoplastics polyester (TP polyester), also known as linear polyesters or saturated polyesters, are polymerized through condensation polymerization (step grow polymerization) (McKeen, 2014). This method is in which monomers are linked together by the splitting off water or other simple molecules. TP polyester have esters functional groups (– COO –) adhered to the growing polymer main chain. Where the ester link dictates the properties of the polymer. For example, esters as polar groups are responsible of the high-frequency electrical insulation properties, molecular chain flexibility and the interchain attraction. Below the glass transition temperature (Tg), their electrical insulation influence is lower. Additionally, these sites are vulnerable to hydrolytic degradability; consequently, inflicting chain scissions. In general, linear polyester are placed in three categories: aliphatic, partly aromatic, and aromatic. Aliphatic polyesters are those produced from aliphatic dicarboxylic acids (esters) and aliphatic diols, have low melting points and are susceptible to hydrolysis. Whereas, partly aromatic polyesters are

known for being formed with aromatic dicarboxylic acids and aliphatic diols. Furthermore, aromatic polyesters have all ester linkages adhered to aromatic rings (Gilbert, 2017). In fact, partially aromatics polyesters (e.g., homopolyesters and copolyesters) are among the most consumed thermoplastic polyesters by the industry. Examples of homopolyesters are: polycyclohexylenedi methylene terephthalate (PCT), poly (ethylene naphthalate) (PEN), and poly(trimethylene) terephthalate (PTT), poly (ethylene terephthalate) PET (PETP or PETE). Where, PET is found in two morphologies (amorphous and crystalline form). The amorphous PET is abbreviated as (APET) and the crystalline form as (CPET). Semicrystalline PET, a transparent material, has good strength, ductility, stiffness and harness. Whereas, amorphous PET, an opaque and white material, has good ductility and shows a decline in stiffness and hardness. Examples of copolyesters are: PETG (CHDM-modified PET), PCTG (glycol-modified PCT), and PCTA (dibasic-acid-modified PCT) (Gilbert, 2017; McKeen, 2014).

2.3.1 Poly (ethylene terephthalate)-glycol (PETG)

PETG, also known as polyethylene terephthalateco-1, 4-cylclohexylenedimethylene terephthalate and poly (ethylene terephthalate)-glycol, is a copolyester recognized for being a non-crystalizing amorphous copolymer Also, it is used in high volume and consumer applications (e.g., films, fibers, and food containers); further, it can be polymerized through condensation polymerization by incorporating more than one glycol and dibasic acid. In the context of applications involving large thermoformed parts, it can retain the properties of an amorphous PET and endure crystallization. Both thermoplastics, PET and PETG, are miscible at all concentrations (Dupaix, 2003; Dupaix, 2017; Gilbert, 2017).

2.4 THERMAL ANALYSIS

Thermal analysis (TA) are measuring techniques noted for identifying the material thermal response (e.g., through heating, cooling or held isothermally); therefore, TA aims to relate the temperate and the material specific physical properties. Measurement and analysis techniques include thermogravimetric analysis (TGA), differential scanning calorimetry (DSC), thermomechanical analysis (TMA), dynamic mechanical analysis (DMA), dielectric analysis (DEA) and micro/nano thermal analysis (μ /n – TA). These are among the most popular TA techniques. This subsection provides insight into two thermal analysis techniques, TGA and DSC, since these are the emphasis of this work (Menczel & Prime, 2009).

2.4.1 Thermogravimetric analysis

Thermogravimetric analysis, TGA, is a technique in which the mass of a substance is measured as a function of temperature or time, while the substance is subjected to a controlled-temperature program in a specified atmosphere (ASTM E473-18, 2018). Commercial thermogravimetry analyzers, are capable to withstand temperature programs ranging, for example, from ambient temperature to 1000 °C. In general, the purging gas flowing through the balance can be an inert atmosphere (e.g., nitrogen, argon or helium), an oxidative atmosphere (air or oxygen) or a forming gas atmosphere. Air, nitrogen and argon are known as low-conductivity gases, and helium is a high-conductive gas. In addition, the heating scanning rates are classified as slow, constant, and fast. Fast heating rates starting at 20 °C/min are helpful to build survey analysis, constant heating rates are about 5 °C/min to 20 °C/min, and slow scanning rates enable polymer scientists to analyze the overlapping thermal events from TG curves. TGA is capable to retrieve information as the volatile content, the onset of thermal decomposition, inorganic filler content, volatility of additives, or define kinetic analysis through isothermal runs, just to name a few.

Among the experimental variables in thermogravimetric experimentation are noted: the sample to thermocouple distance, sample mass (the specimen should be small enough to prevent heat transfer, and large enough to be representative), sample particle size, sample packing density, controlling the size and geometry of the sample, the flow of the purging gas (should be fast as possible to facilitate the removal of volatiles; however, it must not cause disruption in the thermal stability studies), and heating rate (keeping in mind that faster heating rates yield higher decomposition temperatures). In addition, TG curves are used to quantify the mass loss from the polymer or measure the mass gain (e.g., this can be observed at slow scanning rates in oxidizing atmospheres prior decomposition). Moreover, the mass loss rates are not only dependent of the formation of volatile products but also their diffusion to the surface where mass loss occurs. The TGA temperature programs are selected in relation to the research interest. For example, a low limit temperature is adequate to examine solvents, moisture evaporation or phenolic cure (100°C–300°C), an intermediate limit temperature is intended for most polymer decomposition (500°C–600°C) and high limit temperatures to determine filler content and for thermally stable polymers (650°C–1000°C). The derivative thermogravimetry (DTG) profile, is known to provide the maximum rate of mass loss and developed DTG peak contains information relative to a separate thermal event (Menczel, 2009; Scheirs, 2000). Ultimately, ASTM E-2550 describes the assessment of material thermal stability through the determination of the temperature at which the materials start to decompose or react and the extent of the mass change using thermogravimetry.

2.4.2 TGA- Acrylonitrile-butadiene-styrene

ABS have been broadly studied by scientists. For example, (Suzuki & Wilkie, 1995) examined the thermal stability and performed infrared spectroscopy studies on acrylonitrile-butadiene-styrene (ABS), polystyrene, polybutadiene, polyacrylonitrile (PAN), and styrene-acrylonitrile (SAN) copolymer. Where, ABS contained 15.0 wt.% acrylonitrile, 40.0 wt.% butadiene, and 45 wt.% styrene, respectively. In addition, PAN contained 25.6 % acrylonitrile. The specimen's mass was approximately 40 mg. and it employed a heating rate that was about 20 °C/min. ABS experimental studies, under an inert atmosphere, purged at approximately 30-50 cc/min, showed a single degradation step transition in the TG profile. Additionally, the residual analysis measured at 600 °C, yielded approximately 4.0 %. According to the authors, the initial decomposition was noted at 340 °C, which corresponds to the formation of the butadiene monomer (demonstrated by the infrared spectrum of the gases evolved from ABS). Moreover, aromatics were identified around 350 °C. This corresponded to the evolution of butadiene. Following the formation of aromatics, due to an increment in the temperature profile, it was noted that styrene played a major role. In fact, the intensities from the C-H bands, butadiene and styrene, were about the same at 420 °C. Further, increasing the temperature produced a decline in the intensity from the aromatics, whereas, the butadiene intensity was maintained. In particular, the acrylonitrile evolution initiated at 400 °C and finalized at approximately 450 °C. Also, since commercial ABS contains an intermediate phase of SAN. It is important to discuss SAN decomposition. The authors noted a single degradation step transition which initiated at 370 °C and finalized at 530 °C. There were not identified residual traces. (Yang, Castilleja, Barrera, & Lozano, 2004), published studies on ABS filled with single-walled carbon nanotube (SWNT). These studies were carried out under air and nitrogen, both purged at 25 ml./min and at heating rate of about 10 °C/min. The specimens

were approximately (5.0-10.0 mg.). The temperature program was conducted from room temperature to 1000 °C. Consequently, two degradation step transitions were identified for pure ABS, under static air. As far as thermal stability, the first degradation step was observed through 180 °C to 480 °C. In addition, a second degradation transition was noted through 480 °C to 620 °C. In fact, the authors acknowledge it exists a variability in their results when compared to other works published on TGA. Therefore, these variations reported through different publication are prevalent due to the polymer matrix compounding parameters and testing parameters, including: the molecular weight, ABS component ratios, sample weight, sample volume, heating rate and purging gases, just to name a few. Ultimately, these variations define the actual degradation of ABS. Additionally, ABS degradation is described by the authors as a radical process, where the butadiene rich-domains are the most vulnerable sites for degradation. A two-step process was noted for pure ABS under nitrogen, where the first step showed the major weight loss. (Yang, M., 2000) studied ABS resin, under nitrogen gas, purged at 40 ml/min with varying heating rates of (5, 10. 20, and 40 °C/min), and specimen that were approximately 60.0 mg. These TGA examinations aimed to determine the thermal decomposition kinetics parameters on ABS. For instance, the authors concluded that ABS resin, in nitrogen, degraded in one-step process. (Hitachi High-Tech Science Corporation [APA], 1995), performed thermogravimetry studies on ABS resin under a nitrogen atmosphere. Where a heating rate of 20 °C/min, a steady flow rate about 200 ml./min, and a specimen weighing 10 mg were utilized, accordingly. The authors found one degradation step decomposition through 350 °C to 500 °C; further, it was shown the specimen were almost completely decomposed at 500 °C. Whereas, quasi-isothermal thermogravimetric studies on ABS resin demonstrated two-stage decomposition events. This corresponded to the

styrene and butadiene components. In fact, this was confirmed through FTIR analysis of decomposition gas.

2.4.3 TGA- Poly (Ethylene Terephthalate)-Glycol

(Ranade, Thellen, & Ratto, 2005) performed thermogravimetry studies on neat amorphous PETG and PETG nanocomposites, montmorillonite layered silicates at two distinct concentrations, tested under a nitrogen atmosphere with heating rates at 10.0 °C/min. Also, it employed a controlled temperature profile in the range of 30.0 °C to 900 °C; however, the nitrogen flow rate and the specimen's weight were not reported. As a result, both PETG nanocomposites reported two decomposition step transitions. Lastly, the authors reported a weight loss of 4.0 % at 418.0 °C for the neat PETG. In addition, (Paszkiewicz, *et al.*, 2019) the authors carried out TGA examinations on PETG. Likewise, PETG based nanocomposites were studied, reinforced with multiwalled carbon nanotube, graphene nanoplatelet, and nanosized carbon black nanofillers. These under dry synthetic air (N2:O2 = 80:20 vol %), heating rates of 10.0 °C/min, and employed a controlled temperature of 20.0 °C to 700 °C. The thermo-oxidative thermograms demonstrated two degradation step transitions. The authors reported a mass loss of 5.0 % at 376.0 °C for the neat PETG. In addition, the first degradation step transition, 375.0 °C to 465.0 °C, accounted approximately 82.0 % of the total original mass. Moreover, the second step ,495.0 °C to 550.0 °C, demonstrated the char oxidation for the PETG polymer hybrid nanocomposites. (Paszkiewicz, et al., 2017) examined the thermal stability of PETG and PETG-block-PTMO (poly (tetramethylene oxide)) copolymers, under air (N2:O2 = 80:20 vol %) and under an argon atmosphere. The testing parameters comprised heating rates of 10.0 °C/min and a temperature profile of 20.0 °C to 700 °C. Thermo-oxidative studies, resulted in two degradation steps for neat PETG. Accordingly, the first step transition was reported around 350.0 °C to 470.0 °C, and the secondary step at 500.0 °C to 570 °C. PETG-block-PTMO analysis, on the contrary, yielded three degradation steps. The first step transition was reported around 254.0 °C to 350.0 °C, the secondary step around 350.0 °C to

460 °C, and the third stage at about 480.0 °C to 560 °C. Consequently, the authors concluded the initial and secondary steps corresponded to the decomposition of flexible and rigid segments. In fact, this means as the temperature is increased, the flexible segments are susceptible to the attack of oxygen molecules (typical in poly(etherester) block copolymers).

2.4.4 Differential scanning calorimetry

The differential scanning calorimetry studies, originated from the pharmaceutical and polymer material industries, has been used in research settings, as a technique in which the heat flow difference into a substance and a reference material is measured as a function of temperature technique in which the heat flow difference into a substance and a reference material is measured as a function of temperature (ASTM E473-18, 2018; Cordella *et al.*, 2002). A DSC temperature-programed scan, heating, cooling or isothermally, is capable to cause some structural modifications or decompositions (Menczel, 2009). More specifically in the case of DSC, it is possible to retrieve information, such as the heat capacity, melting temperature, crystallization temperature, heat of fusion, heat of reaction, fast purity determination. Additionally, it can indicate the mechanical and thermal history of polymers, the kinetic evaluation of chemical reactions, or the glass transition temperature (Menczel, 2009; Scheirs, 2000). Temperature regards as the most important quantity in differential scanning calorimetry. In fact, temperature represents the average kinetic energy of the system. Whereas, heating rate is the most relevant parameter in DSC experimentation. More specifically, it indicates how fast the specimens are heated up or cooled down. As an example, fast heating rates are responsible of large temperature gradients within the sample, which originates a decline in temperature resolution. Similarly, large specimens turn into thermal reservoirs, thus, this introduces broadening in the thermal transitions and induces thermal lag. The DSC heating rates are selected in relation to the focus of research. For example: purity determination employs heating rates of (1 °C /min); however, most polymer examinations utilize heating rates of (10 °C /min). In the same manner, cooling rates influence the crystallinity from the polymers; in fact, the crystallization temperature and glass transition temperature change drastically due to the selected cooling rate (e.g., the samples may become quenched). That is, the sample avoids the crystallization and it is transferred to the glassy state (Menczel, 2009).

2.5 ADDITIVE MANUFACTURING

Additive manufacturing (AM), a revolutionizing manufacturing technique and computer-based technology, also known as 3D printing, offers design freedom, such as the creation of complex geometric models for product development. Additionally, it allows to build parts with desirable mechanical properties (Love, et al., 2014; Neff, Trapuzzano, & Crane, 2018). Where recent developments in AM, accuracy, functionality and materials properties, catapulted into testing, tooling and manufacturing (Espalin 2012). Typically, AM machines operate with a resolution of a few tens of a micron; however, the accuracy is different along different orthogonal axes. As an example, when compared to the two axes in the build plane, the vertical build axis (layer thickness) exhibits higher resolution. Additive manufacturing are those processes accomplished with a three-dimensional Computer-Aided Design system, 3D CAD, in which a 3D problem is break up into a series of finite 2D cross-sections with a nominal thickness. This technology selectively adds material layer by layer, where each layer is derived from CAD data. Example of CAD applications include aid in the geometric, electrical, thermal, dynamic, and static behavior of new designs. Yet another example of benefits includes to implement changes easily and cheaply. In general, all major commercialized AM machines use a layer-based approach; however, these systems differ by 1) the material that can be used, 2) how the layers are created and 3) the layers bonding process (Gibson, Rosen, & Stucker, 2016). In fact, AM has enabled the use polymeric materials, waxes, paper laminates, composites, metals and ceramics; however, as with many manufacturing technologies, parts are susceptible to flaws. Voids and anisotropy, such as is commonly the case with some AM parts, may be caused due to processing parameters, part orientation or design input (Gibson, Rosen, & Stucker, 2016). On the contrary, recent advancements as the inclusion of fiber reinforcement into the polymer matrix, carbon fibers (CF's), can increase the strength and stiffness of the final product. Yet another advantage of fiber reinforcement includes the changes of the coefficient of thermal expansion (CTE) and thermal conductivity of a polymer AM final part. In this fashion, the residual stresses caused by thermal

gradients in the parts during manufacturing are decreased; consequently, parts distortion are reduced (e.g.; warp and curls). Ultimately, these technological efforts are now being be adopted by large-area additive manufacturing; hence, parts now can exceed 2 m in length without significant distortion (Love, et al., 2014). Another aspect to be consider is the classification scheme in additive manufacturing, according to development and adoption of ASTM/ISO standard terminology, AM is classified in seven process categories. vat photopolymerization, powder bed fusion, material extrusion, material jetting, binder jetting, sheet lamination and direct energy deposition, respectively (Gibson, Rosen, & Stucker, 2016). This to avoid anomalies where dissimilar processes are grouped together; consequently, it brings the possibility to compare the similarities, benefits, drawbacks, and processing characteristics of the seven process categories.

2.5.1 Vat Photopolymerization

In vat photopolymerization AM processes, also known as VP technologies, complex structures can be created with excellent accuracy, high-resolution and surface finish; in which this is achieved by processes that utilize a liquid photopolymer, as such as liquid, radiation-curable resins, or photopolymers, that is contained in a vat and processed by selectively delivering energy to cure specific regions of a part cross-section (Aduba, et al., 2019; Espalin, 2017). In general, photopolymers react to various types of radiation, in which is used gamma rays, X-rays, electron beams, UV and sometimes visible light, which facilitates a chemical reaction, cross-linking, and it is follow by a solidification process. However, UV and visible light are the most prevalent in commercial systems (Gibson, Rosen, & Stucker, 2016). The vat photopolymerization technology uses a variety of materials including polymers, composites, and ceramics (Espalin, 2017). Additionally, VP technologies has two primary configurations, vector scan (point-wise) and mask projection (layer-wise). Vector scan is a process analogous to commercial stereography (SL) machines; whereas, mask projection entails to irradiate entire layers at one time. Both configurations are required to apply a new layer of resin (recoating). Alternatively,

photopolymerization can be accomplished by a two-photon approach, a high-resolution point-by-point approach, in which photopolymerization occurs at the intersection of two scanning laser beams. This configuration permits to fabricate parts below the resin surface; hence, recoating is unnecessary. In fact, vector scan and two-photon are processes in which scanning laser beams are employed. Mask projection, on the other hand, employs a large radiation beam that is patterned by Digital Micromirror Device™ (DMD). In general, VP photopolymers are cross-linked; this means these materials do not melt and are less susceptible to creep and stress relaxation. Thermoplastic polymers, on the other hand, have linear or branched molecular structures, that allows them to melt and solidify repeatedly. With respect to commercially available today SL resins, these are composed by acrylate and epoxides (hybrid resins). When acrylate is incorporated into the epoxy resin, the acrylate is in charge to provide strength to the build part, reduce distortion and decrease the brittleness of the epoxy parts. Examples of vat photopolymers components includes, photoinitiators, reactive diluents, flexibilizers, stabilizers, and liquid monomers. The first step of photopolymerization requires the photoinitiators to undergo a chemical transformation, this means a polymer chains are built. Subsequently, a cross-linking process is started. Essentially, photopolymer chemistry can be placed in two categories: free-radical photopolymerization (e.g., acrylate) or cationic photopolymerization (e.g., epoxy and vinylether). Additionally, VP processes offers flexibility, as such is different machine configurations and size scales. Other advantages are the variety of light source (such as lasers, lamps and LEDs) and different pattern generators (such as scanning galvanometers or DMDs). Whereas, when compared to the quality of injection molded thermoplastics, SL materials exhibit lower impact strength and durability (such as the degradation of mechanical properties over time) (Gibson, Rosen, & Stucker, 2016).

2.5.2 Powder Bed Fusion

The powder bed fusion (PBF) process, initially commercialized as selective laser sintering (SLS), employs thermal energy for inducing fusion between the powder particles, four different fusion mechanisms (such as solid-state sintering, chemically induced binding, liquid-phase sintering (LPS), and full melting), this to construct three-dimensional objects (Gibson, Rosen, & Stucker, 2016). This is accomplished by energy sources like lasers, electron beams, coils and infrared energy (Espalin, 2017). In general, PBF technologies are classified in polymer laser sintering (pLS) machines and metal laser sintering (mLS) machines. In fact, this technology enables to work with a broad range of materials that can be melted and re-solidified. For example, polymers, metals, ceramics, and composites, respectively. In fact, this subsection is focused on thermoplastics, and as such a brief description of polymer laser sintering is offered (Gibson, Rosen, & Stucker, 2016). The basic principle of this process is to fuse thin layers of powder and evenly spread powder in a layer across a building area, an enclosed chamber surrounded with inert gas (nitrogen or argon); accordingly, this to decrease the oxidation, prevent the degradation of the powder material and remove the condensate that is produced by melting the powder (Brandt, 2017; Gibson, Rosen, & Stucker, 2016). This is followed by selectively directing a carbon dioxide melting beam onto the powder to build slice cross sections. Thus, it indexes down as each layer is completed and new powder is spread over the build area (Gibson, Rosen, & Stucker, 2016). Typically, thermoplastics materials have the advantage of having low melting temperatures and low thermal conductivities. However, the polymer powder material must be maintained at high temperatures below the melting point or the glass transition temperature. Thermosets, on the contrary, are not intended to be processed by PBF. More specifically, semi-crystalline materials are used with pLS machines because, when compared to amorphous polymers, they exhibit distinct melting points, leading to reliability. Amorphous polymers, on the other hand, sinter into highly porous shapes and do not have defined solidify features. Crystalline polymers, contrarily, are susceptible to greater shrinkage, curling and distortion when compared to amorphous materials;

consequently, it is required a uniform temperature control. Examples of polymers that have been processed using pLS includes polyamides (nylon), flame-retardant polyamides, polystyrene-based materials, elastomeric thermoplastic, polyaryletherketone (PAEK/PEEK), biocompatible and biodegradable polymers (such as polycaprolactone (PCL), polylactide (PLA), and poly-L-lactide (PLLA)). Also, metals, if the material can get welded, are good candidates for powder bed fusion processes. Examples of the most commonly used metals in mLS includes stainless and tool steels, titanium and its alloys, nickel-base alloys, aluminum alloys and cobalt-chrome (Gibson, Rosen, & Stucker, 2016).

2.5.3 Material Extrusion

Extrusion based systems, known as the most popular AM technology, operates by liquefying a large range of bulk materials, such as pellets, powders, granules or continuous filaments, through thermal or chemical changes to induce solidification (Gibson, Rosen, & Stucker, 2016). For example, thermal processing, enable the use of temperature for controlling the material state to convert the solid plastic to a flowable molten extrudate (Espalin, 2017). Strictly speaking, the molten material contained in a reservoir, in semisolid state, flows out through a tractor-feed system (e.g. extrusion nozzle). Methods employed to initialize a propelling process include pressure, gravity, screws and plungers. After being driven out the FDM system, the material initializes a bonding process with the adjacent material prior solidification. Ultimately, this technology builds complex geometrical structures by selectively utilizing supports structures. As an example, when using polymer-based additive manufacturing processes, the resulting parts constructed using FDM are among the strongest. On the contrary, chemical changes involves curing agents, residual solvents or reactions with air, this to fully permit a bonding process to occur after the material is dispended. However, the plastic materials inside the chamber must be monitored since some polymers degrade and therefore gradually generate residual content on the chamber. Fused deposition modeling (FDM), produced and developed by *Stratasys*, regarded as

the most common extrusion-based AM technology, is characterized for having low-cost, small-scale to large-scale and sophisticated machines, with build envelopes ranging from (5” x 5” x 5”) to (36” x 24”x 36”), just to name a few (Gibson, Rosen, & Stucker, 2016). However, FDM technologies has some disadvantages as build speed, accuracy and the material density. Examples of material extrusion include dispensing thermoplastics, food and conductive inks (Espalin, 2017; Gibson, Rosen, & Stucker, 2016). Another discussed FDM thermoplastic material extrusion process, is large area additive manufacturing, in which parts are built by extruding materials in layers using thermoplastic materials, metal, concrete, or construction materials (Espalin, 2017). Big Area Additive Manufacturing is an example of large-scale AM, the basic principle of this process is to employ a single-screw extruder to melt pellet feedstock and extrude thermoplastic and thermoplastic-based composite materials; thus, when using a single-screw extruder, it enables higher deposition rates and the use of less expensive materials (Roschli *et al.*, 2019). In fact, the composite materials are typically reinforced with carbon fiber (CF) or glass to mitigate warping and distortion. Since, warping and delamination due to thermal stresses remain as an impediment to the adoption of large-scale AM. Additionally, BAAM machines, with a build volume of (20” × 8” x 6”) and throughput of approximately 100 lb./hr., employ a tamping mechanism to control and reduce the void content between the deposited beds (Compton *et al.*, 2017; Espalin, 2017; Roschli, et al., 2019).

2.5.4 Material Jetting

Material jetting (MJ) is an AM process that deposits material, such as waxy polymers, acrylic photopolymers and it has also been experimented with polymer, ceramics and metal, from a printer head to a build platform or print over previously dispensed material. However, only waxes and photopolymers are commercially available (Espalin, 2017; Gibson, Rosen, & Stucker, 2016). When using material jetting, these droplet formation methods is constrained by a printable viscosity threshold, approximately of 20–40 centipoise in respect to the printing temperature. In

fact, the two primary mechanisms for droplet generation are the continuous mode (CS) and drop-on-demand (DOD) mode. In general, the DOD mode are individual pressure pulses generated at specified times by thermal, electrostatic, piezoelectric, acoustic, or other actuators. However, the most common practice in the DOD printing industry is in the context of thermal (bubble-jet) and piezoelectric actuator technologies. Where the DOD mode has the capability of depositing droplets of 25–120 μm at a rate of 0–2,000 drops per second. Typical companies that manufacturer DOD printer heads include *Hewlett-Packard*, *Canon*, *Dimatix*, *Konica-Minolta*, just to name a few. Whereas, the continuous mode employs steady pressure to impulse the fluid reservoir; accordingly, the material is pressurized and dispensed by a nozzle. Moreover, the material deposition is break into droplets, Plateau–Rayleigh instability, and inflict a consistent breakup through vibrations, perturbations or by modulating the jet at a fixed frequency. Consequently, the particles destination is precisely directed by a deflection field. Ultimately, the basic principle of this process is to liquefy the solid material into a viscous fluid. Typical common practices include the use of heat, solvents or low viscosity components. Further advancements in polymer inkjet technologies, has enabled the production of macro three- dimensional structures. Drawbacks of material jetting when compared to vat photopolymerization and material extrusion includes a decline in part accuracy for the printing of large parts. In general, MJ process are used at low cost, high speeds and enabled scalability. Further, advancements have enabled to print parts with multiple materials. In general, material jetting technologies are currently used in numerous application areas, such as electronic packaging, optics and additive manufacturing (Gibson, Rosen, & Stucker, 2016).

2.5.5 Binder Jetting

Binder jetting (BJ), invented at MIT, are those processes that entails the deposition of small quantities of liquid-bonding agent (binder droplets), approximately 60 μm in diameter, into a powder bed to fabricate a part. Consequently, this deposition, through piezo-electric inkjet printer heads, offers the formation of spherical agglomerations, such as binder liquid and powder particles,

in which a bonding process is initialized with the previously printed layer. Additionally, post-processing, infiltration or sintering are applied to the printed part to strengthen and induce other mechanical properties. Further, the BJ additive manufacturing process has been used, both in industry and research settings, with a variety of applications in a range of materials including plastics, glass, ceramics, metals, foundry sand, glass/ceramic composite, and metal/ceramic composites. In fact, MJ processes are known for being significantly cheaper when compared to powder bed and direct energy deposition processes. Further, this technology was adopted by *ExOne* for printing fine grains of metals and use this approach to 3D printing of large sand objects. In the same manner, BJ technologies has been licensed for the development of 3D printing medication (Gibson, Rosen, & Stucker, 2016; Zhang & Jung, 2018).

2.5.6 Sheet Lamination

Sheet lamination (SL), a partially subtractive process and known as laminated object manufacturing (LOM), are those technologies with a construction principle that selectively cuts the outer contours of the part; additionally, the material sheets are stacked and form bonding sheets of materials to build three dimensional objects. SL process can employ four bonding mechanisms, such as gluing or adhesive bonding, thermal bonding, clamping and ultrasonic welding. Examples of materials that have been processed with SL techniques include plastics, metals, ceramics, and paper (Espalin, 2017; Gibson, Rosen, & Stucker, 2016).

2.5.7 Direct Energy Deposition

Direct energy deposition (DED) is a process in which the creation of parts requires melting feedstock material, such as powders or wires; therefore, DED consist of directing a heat source, a laser, electro-beam, discharge arc and plasma, as the material is being deposited into a substrate melt pool to build intricate 3D-shapes; however, it is primarily referred as a metal deposition technology incorporating the characteristics of powder bed fusion and material extrusion

techniques. The DED process has been used with a diversity of materials including polymers, ceramics and metal matrix composites. Also, DED machines differentiate from one to another by their laser power, laser spot size, laser type, powder delivery method, inert gas delivery method and feedback control scheme. In summary, direct energy deposition involves the deposition, melting and deposition of powder materials to produce fully dense parts; whereas, DED is limited by slow build speeds, poor surface finish and surface finish (Ahmad, Gopinath, & Dutta, 2019; Gibson, Rosen, & Stucker, 2016).

Chapter 3: Methodologies

This chapter introduces the materials and provides the experimental steps used to accomplish the thermal analysis of the following thermoplastic composites: ABS with three varying percentage nominal ratios of fiber reinforcement by weight percentage (20 CF, 20 GF, 40 GF, and 20 GF compounded by Techmer) and PETG (30 GF). Therefore, this present work reports two based composites in pellet form for this thesis, ABS and PETG. The next subsections in this chapter describes the temperature-controlled thermal characterization techniques used for: 1) thermogravimetric analysis (TGA) and 2) differential scanning calorimetry (DSC). The materials were acquired, tested and studied at the laboratory facilities of the W.M. Keck Center for 3D innovation. In addition, Table A.1 summarizes the material used through these studies, their general description, product number, and lot number. Then, Table A.2 briefs in the context of the matrix material and the amount of fiber reinforcements by weight percentage (wt.%). For this thesis, materials from two companies were used: Techmer PM Polymer Modifiers (Clinton, TN, USA) and SABIC Americas Inc. (Houston, Texas, USA). Additionally, one ABS matrix fiber-reinforced composite by SABIC was chosen to further these comparisons. The selected engineering polymers (by Techmer PM Polymer Modifiers) examined throughout this research were as follow:

1) ABS 20-CF: this polymer composite with 20% by weight carbon fiber reinforcement is formulated to target systems in large area additive manufacturing. Furthermore, this material aims to improve the dimensional stability, reduce warping and decrease distortion on 3D printed products as explained by the manufacturer.

2) 2) ABS 20 GF: this ABS matrix and glass fiber filler reinforcement (20% by wt.) are compounded to be implemented in additive manufacturing for general printing equipment.
3) ABS 40 GF: this ABS polymer composite is filled with 40% by wt. and is fabricated for general use (e.g. automotive electronics, business equipment or injection molding systems).
4) PETG 30 GF: this composite contained polyethylene terephthalate glycol as the matrix and was filled with 30% wt. glass fibers. It is known as a printing optimized engineering thermoplastic specialized for general applications in additive manufacturing.
5) ABS 20 GF: this composite was the only product acquired from a different polymer manufacturer. Provided by SABIC, this is an engineering thermoplastic intended to improve processability, reduce warping effects and enrich the print surface quality. Like Techmer PM's composite, this composite contains ABS as the matrix and is reinforced with 20% by wt. glass fibers.

3.1 THERMOGRAVIMETRIC ANALYSIS

The present section informs how the analyses were accomplished in the context of thermogravimetry. Each sample examination was based in the procedure parameters indicated by ASTM-E-2550-17. (ASTM E2550 - 07, 2007). Furthermore, all these engineering thermoplastic samples that came in pelletized form, were prepared to match the sample mass recommendations given by the TGA manufacturer. However, the sample shapes were not studied prior to their examination nor how their geometry could have impacted the present work. Mostly, the samples carried an irregular shape representative of plastic pellets during their thermal analysis. This means their height and width were not obtained. A total of 15 TGA/DTG tests were conducted and evaluated in a controlled nitrogen atmosphere with a thermogravimetric analyzer equipment.

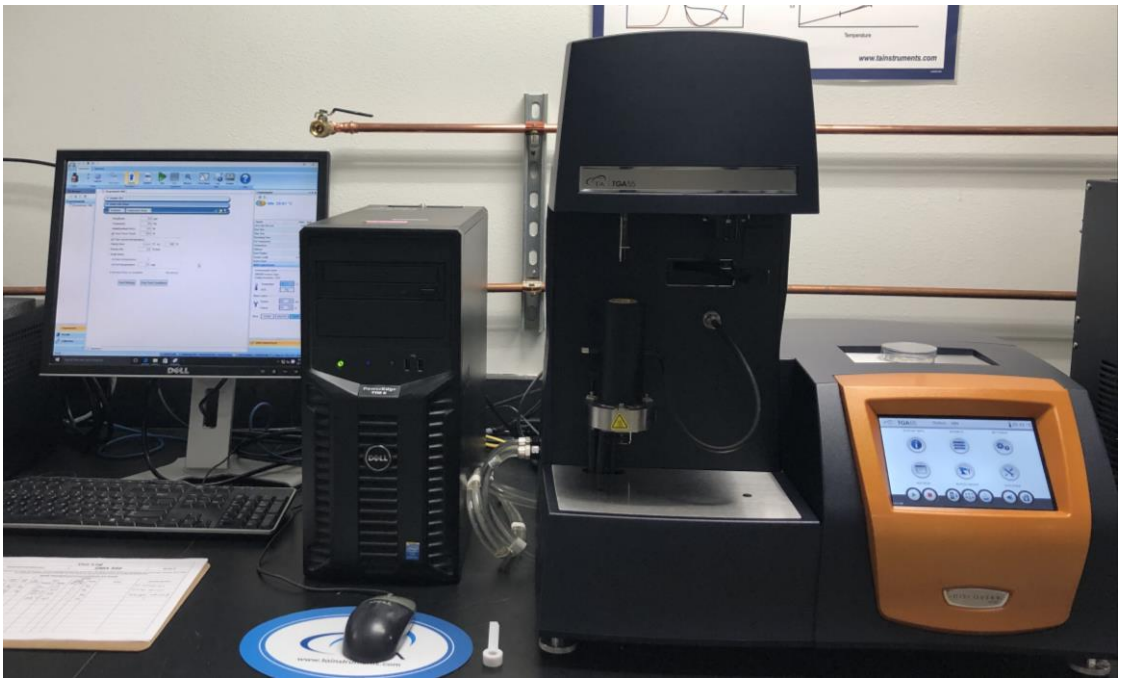

Figure 3.1.1: Thermogravimetric equipment (TGA 55, TA Instruments).

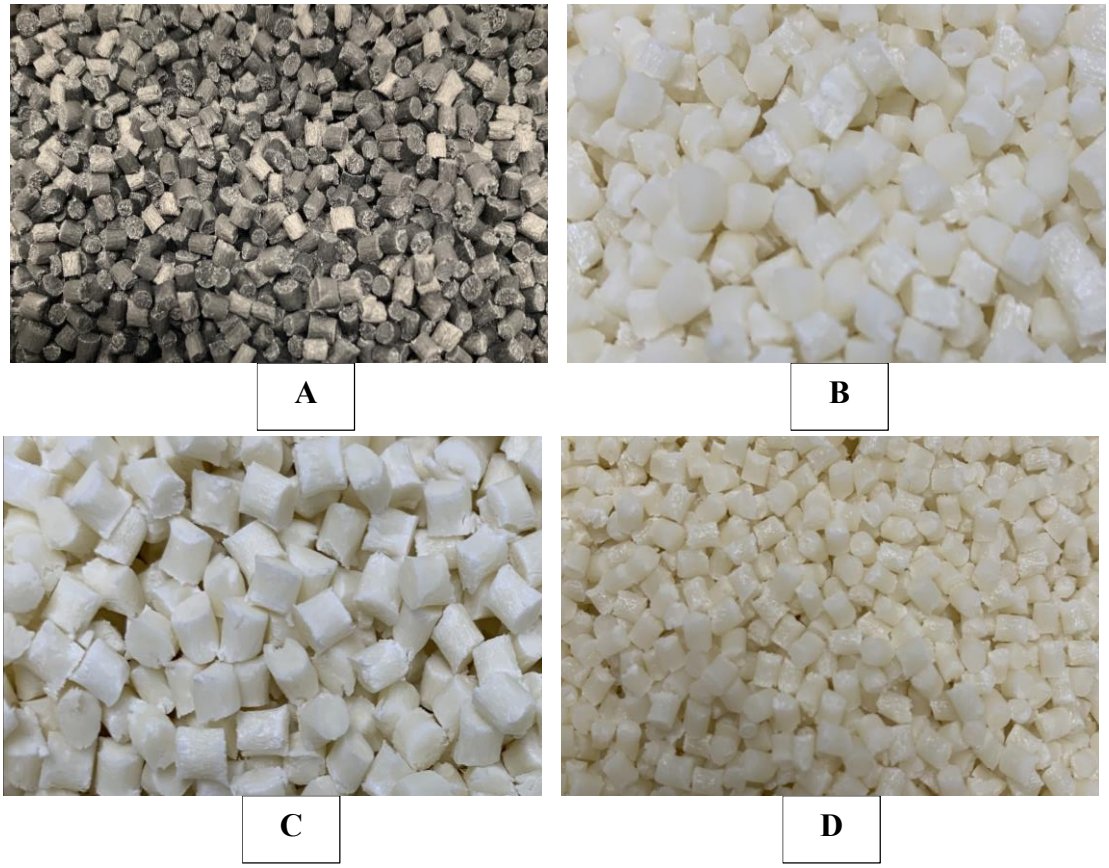

Figure 3.1.2: ABS in pelletized form: A) 20 wt.% CF provided by Techmer, B) 20 wt.% GF by Techmer, C) 40 wt.% CF by Techmer and D) 20 wt.% CF formulated by SABIC

Where a TGA 55 Discovery Series (TA Instruments, United States of America, New Castle, DE.) test equipment was used to conduct the thermal decomposition of these polymer matrix composite materials. For the thermogravimetric analysis, no prior heat treatment nor conditioning procedure was used to eliminate the moister content from the pelletized materials. The objective of the testing was to understand the effects of thermal decomposition of ABS and PETG composites. The separate materials were kept at room temperature (23°C) and stored in sealed plastic bags and tested in a nitrogen environment to better control variables like exposure to contaminants that can affect standard deviation and variability.

Additionally, this research did not consider the physical aging (of amorphous polymers) from the pelletized material. The author realizes that there are aging factors which might implicate a source of error in this experimental research, but aging was not considered. At first, a total of 15 already prepared samples were individually pre-weighted and deposited into a high temperature sample pan from TA Instruments. The container was positioned on a hanging wire of the TGA machine. The pan was then positioned by its own automated loader equipment onto a precise balance mechanism. The open pan container was enclosed in a heating chamber made of alumina ceramic (wire-wound furnace). This enabled to surround the test materials with a controlled atmosphere and heat input. To control the heat input, the temperature rise was measured with the machine's integrated thermocouples. A platinum container (Platinum – HT) with a capacity of 100 μL was selected to accommodate the material. In addition, the TGA equipment station located at the W.M. Keck Center for 3D Innovation is shown connected to a desktop system in Figure 3.1.1.

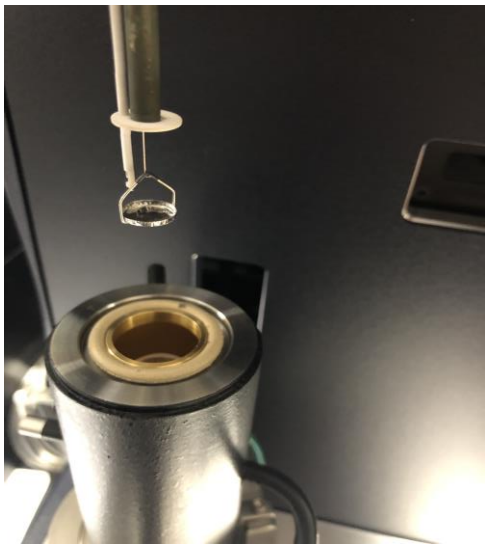

Figure 3.1.3: Sample placed over a Platinum HT pan.

This container was chosen due to its reusability, its capability to withstand elevated temperatures profiles (up to 1000 °C) and represented a viable option attributed to its cleanliness when the appropriate cleaning protocols are follow as indicated by the manufacturer. The material samples were taken from pelletized material as seen in Figure 3.1.2, and were sampled by cutting the pellets to get smaller mass quantities as seen in Figure 3.1.3. Initial mass measurement for all the experimental tests, their sample standard deviations and corresponding coefficient of variance. In this research, three replicate experiments were performed per material and one heating cycle was used. In terms of testing parameters, the thermoplastic samples were thermally decomposed in a nitrogen atmosphere. Further, these tests were monitored with a nitrogen flow rate that was steadily purged. These were subjected to a balance flow rate of 40 mL/min and a sample flow rate of 60 mL/min. Scanning rates under this controlled inert atmosphere consisted to ramp the heat transfer with a heating rate of 10 °C/min. Furthermore, the control temperature was programmed to initialize the measurements once the heating chamber attained a temperature of 25 °C. Eventually, the analyses finalized once an upper limit temperature of 800°C was reached. The acquired data was processed with the software package V.4.5.0, property of TA Instruments. Most notably, this research targeted to determine the decomposition temperatures from the thermograms, quantify the degradations steps by weight percentage, determine residual percentage at 750 °C, and offers to measure the maximum peak temperatures from the DTG curves. Mean values and standard deviation were determined as well. Lastly, the area under the DTG exothermic peak was explored. These exothermic events were processed with the analyzing tool (peak integration from the y vs x). The following parameters were selected:

- baseline type: linear
- onset type: inflection
- divide peak function: activated (type: 3 equal x regions).

3.2 DIFFERENTIAL SCANNING CALORIMETRY

This section describes how the analyses were accomplished in the context of differential scanning calorimetry (DSC). A total of 15 DSC thermal characterization tests were conducted and evaluated in a controlled nitrogen atmosphere using a DSC 250 (TA Instruments, United States of America, New Castle, DE) (Figure 3.2.1). Each sample examination was based in the procedure parameters indicated by ASTM E1356–08 (ASTM Standard E1356-08, 2008). Like subsection 3.1, Table B.1 provides the initial mass measurement for all the experimental tests, their sample standard deviations and corresponding coefficient of variance. Eventually, pre-weighing intended to decrease the overall data dispersion. Given the specimen pans used in the DSC machine, the pelletized thermoplastic composite material ranged in mass from 2.0 to 2.40 mg. The author realizes the specimen masses departed from the recommendation (5.0 to 20.0 mg) given in ASTM E1356 – 08. The approach used in this work accommodated less mass due to the volume capacity from to the encapsulations (avoid overlapping from the specimen with the aluminum lid). The DSC tests used aluminum sample pans (T_{zero} series from TA Instruments) to encapsulate the material; therefore, the specimens were placed in-between T_{zero} aluminum pans and aluminum lids. The pans containing the thermoplastic composite material were hermetically sealed when pressed with a DSC sample encapsulation press.

In terms of testing parameters, the analyses consisted of two replicate cycles in which each contained a heating and cooling scan. The DSC scans studied the heat flux from the system to each sample and tracked their thermal events. Thermogravimetry studies in section 3.1 helped to determine the 1 wt. % loss for each thermoplastic composite; therefore, the decomposition temperatures were used to limit the DSC controlled temperatures and avoid contamination of the DSC machine from volatized thermoplastic. The decomposition temperatures are summarized in Table A.16. In addition, the generated DSC thermal curves, courtesy of Trios software v.4.5.0, highlighted the thermal transition in two morphologies: amorphous and crystalline, respectively. The DSC replicate curves enabled comparisons in the thermal histories and estimated the thermal events in the DSC curves

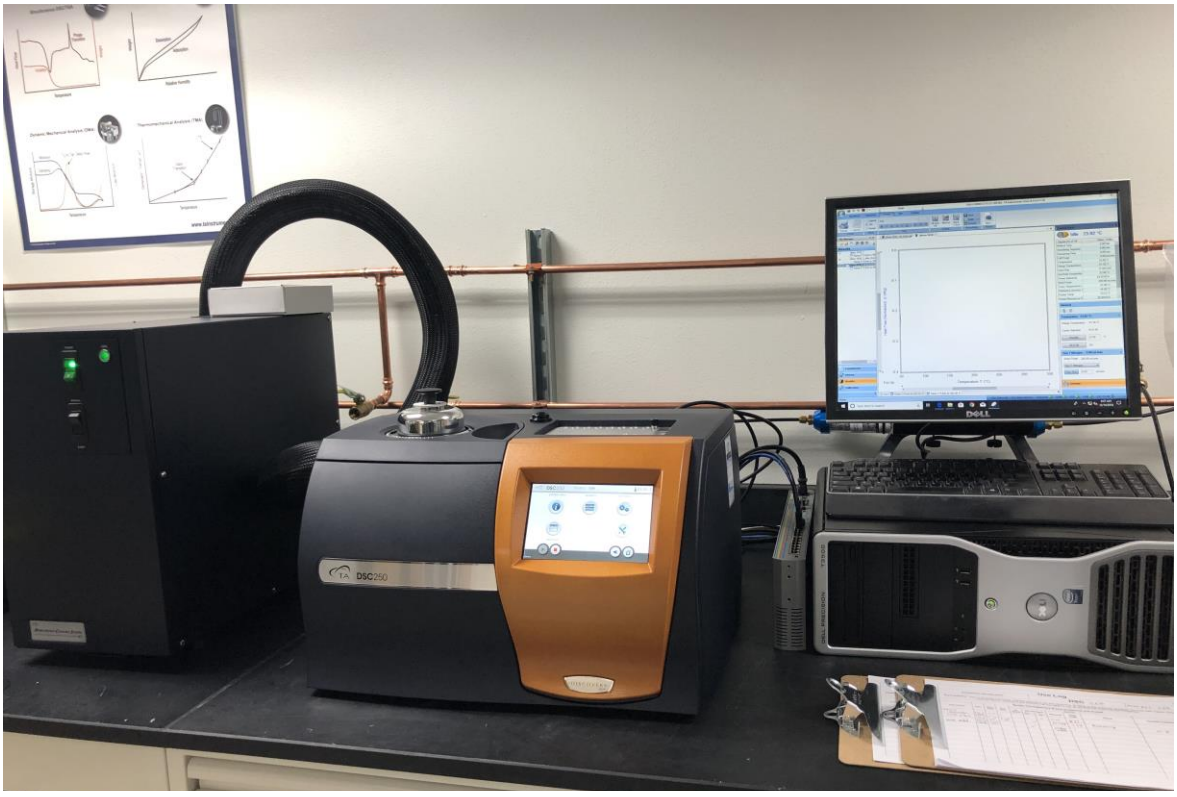

Figure 3.2.1. Differential scanning calorimetry equipment (DSC 250, TA Instruments).

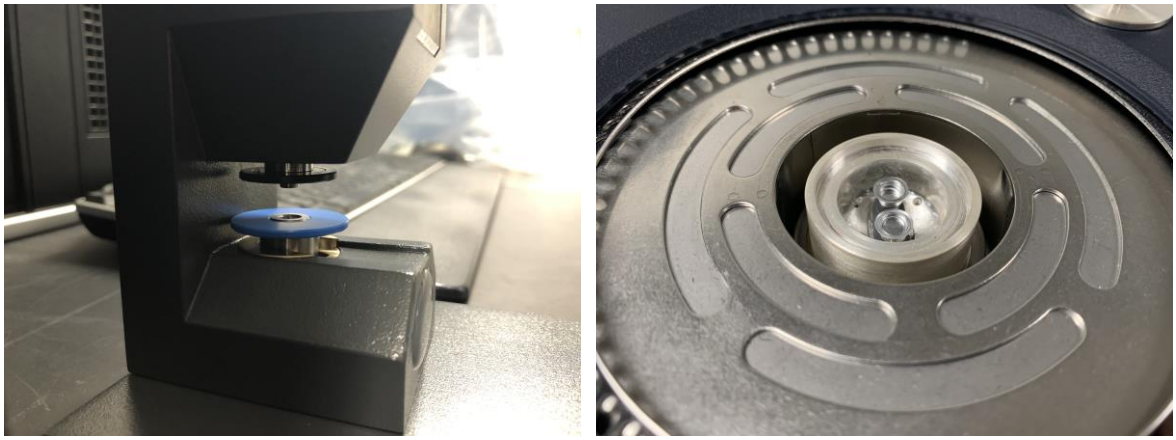

A B

Figure 3.2.2. Where figure A represents the sample encapsulation press, and where figure B represents a typical encapsulated sample and an empty reference pan sitting in the cell module.

In this research, the separate materials were kept at room temperature (23°C) and stored in sealed plastic bags. Test temperatures started at 25 °C and increased at a rate of 10 °C/min until reaching the final target temperature, which were limited to a temperature 40 °C below the 1 wt. % loss temperature as determined from TGA. This approach prevented contaminants to accumulate and impact the performance of the DSC equipment. The final target temperatures studied in a nitrogen atmosphere were as followed:

- ABS 20-CF: 220 °C
- ABS 20-GF: 220 °C
- ABS 40-GF: 227 °C
- PETG 30-GF: 340 °C
- ABS 20-GF (SABIC): 255 °C

After reaching the target upper temperature, the DSC equipment held the upper temperature prior to initializing the cooling events. Thus, the samples were maintained in thermal equilibrium at that specific final target temperature. Afterwards, the DSC instrument proceeded to monitor the samples during the cooling down thermal transitions. This employed a fixed scanning rate of 20 °C/min to cooled down the samples 25 °C. In addition, a nitrogen atmosphere was purged with a recommended base purge flow of 300 mL/min and with a volumetric flow rate for the cell purge of 50 mL/min. Next, the samples were maintained in thermal equilibrium inside the DSC cell module at a temperature of 25 °C. Subsequently, the testing parameters were followed identically to study their duplicate DSC profiles. The elapsed time between the two cycles was not considered. Note that these replicate cycles were not pre-programmed as a series of runs. These were manually configured as two single runs by the operator to achieve better control in the data recollection. Thus, the experimental procedures in this present section were carried out in the following custom segments.

1. Initial temperature 25 °C,
2. Ramp 10 °C/min to the designated final target temperature,
3. Equilibrate (final target temperature),
4. Ramp 20 °C/min to 25 °C,
5. Save the results.
6. Time lapse to create a second run sequence with the exact testing parameters.
7. Initialize the second run sequence and save the results.

Most notably, this research targeted to determine the glass transition temperature, and explored: the midpoint point temperatures, the onset temperatures, the change in specific heat and energy change. Lastly, this section explored the exothermic and endothermic events in the DSC studies; therefore, these analyses covered the peak temperatures, the onset temperatures, heat per mole and enthalpies from these thermal transitions.

However, the author realizes the omission to study the geometry from the specimens (thickness and length), the exclusion to eliminate the moister content from the samples, nor consider the physical aging (of amorphous polymers). This might implicate a source of error in this experimental research. The author realizes that there are moisture absorption factors, aging factors, deviations in the thermal events attributed to annealing which might implicate a source of error in this experimental research.

Chapter 4: Results

This chapter provides and discusses the thermogravimetric analysis (TGA) and derivative thermogravimetric results obtained for ABS and PETG. For each polymer, three samples were tested under a nitrogen atmosphere and following the guidelines set by ASTM 2550-17. Additionally, differential scanning calorimetry (DSC) studies were conducted with a control inert atmosphere (nitrogen). DSC consisted of two replicate cycles in which each contained a heating and cooling scan. Similarly, the DSC analysis was recorded in groups of three samples. Each sample was tested following the guidelines from ASTM E1356-08.

4.1 Thermogravimetric and Derivative Thermogravimetric Analysis

Throughout the following subsections, the arithmetic mean, sample standard deviation and coefficient of variance were provided for each set of three specimens. This aimed to estimate the dispersion of the collected data based on three specimens per material. Thus, this present work can function as a reference to build in the future interlaboratory studies (ILS) for thermal characterization. Additionally, this data will allow to determine and exhibit the precision and bias in future studies. This can be achieved by following the guidelines from ASTM-E691 (Heyes, 2018). Appendix A discloses all the raw data accompanied with TGA/DTA figures and tables. The body text summarizes the findings from this research. Table A.10 highlights the arithmetic mean from the TG/DTG studies. Lastly, Table A.12 summarizes the coefficient of variance for these results. Further details regarding the thermal analysis made with the Trios software are available from Figure A.21 through Figure A.35.

4.1.1 ABS 20-CF (Techmer)

Results for a set of three specimens with replicate testing parameters are shown Figure A.1, where region A corresponds to the initialization of the controlled heating program; consequently, the thermogram baseline underwent trough gradual mass losses. This was ascribed to the

controlled temperature program and one percent decomposition of the total material matrix (measured in weight percentage in the TG thermal curve). The decomposition temperature (1 wt.% loss) was reported at an average temperature of~259 °C ($\sigma \approx 4.40$, CV ≈ 1.70) and the measurements for the initial sample mass showed. ~3.30 mg. ($\sigma \approx 0.20$, CV ≈ 4.50). After that, region B exhibited a sudden decline in mass. The ABS 20-CF thermograms revealed a one-step decomposition during which 75 wt. % ($\sigma \approx .70$, CV ≈ .90) was lost. These measurements were initiated from the decomposition temperature (~259 °C) until a constant mass was observed (plateau region). This approach allowed to approximate the decline in mass as displayed in region B. This calculation indicated the loss of the ABS constituents from the composite matrix. It is point out, no complex decomposition thermal events occurred in these thermograms (additional step transitions). Once the decomposition step was finalized, a measurement of ~22 wt. % ($\sigma \approx 1.10$, CV ≈ 4.70) residue occurred after heating to 750 °C. This remaining residue weight percentage corresponds to the carbon fiber reinforcement added to polymer matrix composite as shown in region C. The reasoning behind selecting 750 °C is the samples did not experience subsequent mass losses. Thus, thermal stability was achieved. The residual weight (22 %) closely matched to the manufacturer-specified filler reinforcement (20 %) added to the ABS resin. In addition, Figure A.3 provides a TG visual reference for the mean value.

Results for a set of three specimens with replicate testing parameters are shown Figure A.2; furthermore, a maximum peak temperature was determined at ~416 °C ($\sigma \approx 1.0$, CV ≈ .20) around region D. This led to examine the maximum rate of degradation attained in the decomposition step transition. In addition, Figure A.4 provides a DTG visual reference for the mean value for this thermal event. The approximate mass loss has been validated in the DTG profile; therefore, the area from the DTG peak integration was close to ~73 ($\sigma \approx 1.20$, CV ≈ 1.70). It is evident the DTG peak integration (73 %) closely matched to the one-step decomposition (75 %). Lastly, further details regarding the thermal analysis made with the Trios software are available from Figure A.21 through Figure A.23.

4.1.2 ABS 20-GF (Techmer)

The resulting TG curves from testing three specimens of ABS 20-GF (as received from Techmer) with equal experimental procedures are shown in Figure A.5, where region A constituted one percent decomposition of the total material matrix; in fact, the 1 % weight loss was observed at a temperature of ~260 °C ($\sigma \approx 4.30$, CV ≈ 1.60). With regards to the average initial sample mass, mass measurements showed. ~3.80 mg. ($\sigma \approx 0.20$, CV ≈ 5.80). Then, region B exhibited a sudden decline in mass; accordingly, the TG curve revealed a single decomposition event (or one step). This decreasing trend was measured at the decomposition temperature (~260 °C) until a constant mass was observed (plateau region); that is, immediately after the weight loss event. Wherein the weight loss was ~76 wt. % ($\sigma \approx .60$, CV ≈ 0.80). It is point out, there were not additional step transitions in the ABS resin decomposition; moreover, there was noted a residual percentage measurement of ~23 wt. % ($\sigma \approx 0.70$, CV ≈ 3.0) in region C at 750 °C. This temperature range was chosen because ABS was no longer susceptible to mass losses. The residual weight (23 %) closely matched to the manufacturer-specified filler reinforcement (20 %) added to polymer. In addition, (Figure A.7) contains a visual representation of the averages from all three tests at the 1 % weight loss decomposition location and at the residual mass at 750 °C.

The resulting DTG curves from testing three specimens of ABS 20-GF (as received from Techmer) with equal experimental procedures are shown in Figure A.6, where region D exhibit a single dW/dT peak noted at ~413 °C ($\sigma \approx 0.40$, CV ≈ 0.10) (maximum peak temperature); therefore, the maximum rate of degradation was identified. In addition, (Figure A.8) illustrates the average captured at the maximum peak temperature from the DTG curves. The approximate mass loss has been verified in the DTG profile; therefore, the area under the maximum peak event was explored. As a result, the area from the DTG peak integration was about ~74 ($\sigma \approx 0.50$, CV ≈ 0.60). The DTG peak integration (74 %) closely matched to the single decomposition weight loss (76%). Lastly, further details regarding the thermal analysis made with the Trios software are available from Figure A.24 through Figure A.26.

4.1.3 ABS 40-GF (Techmer)

Figure A.9 shows the TG curves created from testing three specimens of ABS 40-GF using identical experimental procedure. In similar fashion to ABS 20-GF, the development of gradual mass loss and deviation in the thermogram baseline was shown in region A; as result, the decomposition temperature (1 wt.% loss) was measured at ~267 °C ($\sigma \approx 1.50$, CV ≈ 0.60). The arithmetic means for the initial sample mass was~4.00 mg. ($\sigma \approx 0.10$, CV ≈ 2.80). In addition, region B depicts a sudden decline in mass. As with the ABS 20-GF, this material experienced one transition (mass loss) due to decomposition; therefore, this unchanged trend was measured from the decomposition temperature (~267 °C) until a plateau region was observed immediately after the event. This event was noted by the weight loss of ~58 wt. % ($\sigma \approx 1.20$, CV ≈ 2.10). Again, the TGA curve did not experience complex decomposition events. After reaching the maximum test temperature of 750 °C, the residual weight percentage was ~40 wt. % ($\sigma \approx 0.80$, CV ≈ 2.0) matching the manufacturer-specified reinforcement percentage of 40% as shown in region C. In addition, Figure A.11 shows the TGA average curve.

Curves generated from the DTG analysis (Figure A.10) reflected one maximum peak (dW/dT peak) of~416 °C ($\sigma \approx 0.60$, CV ≈ 0.20) as detected in region D; hence, this was associated to the maximum rate of degradation attained in one-step decomposition. The approximate mass loss has been verified in the DTG profile; therefore, the area under the maximum peak region was studied. As a result, the area from the DTG peak integration was roughly ~56 ($\sigma \approx 1.10$, CV ≈ 2.0). It is evident the DTG peak integration (56 %) closely matched to the single decomposition weight loss (58%). Furthermore, Figure A.12 DTG shows the average curve. Lastly, further details regarding the thermal analysis made with the Trios software are available from Figure A.27 through Figure A.29.

4.1.4 ABS 20-GF (SABIC)

Acquired TG data from testing three specimens of ABS 20-GF compounded by SABIC can be found in Figure A.13; namely, the decomposition temperature after a 1 % weight loss was recorded at ~295 °C ($\sigma \approx 5.20$, CV ≈ 1.70) as presented in region A. As with the ABS 20-GF, a total of ~75 wt. % ($\sigma \approx 0.80$, CV ≈ 1.10) weight loss was attributed to one decomposition event as depicted in region B.; therefore, this decreasing trend was measured at the decomposition temperature (~295 °C) until a constant mass was observed (plateau region); that is, immediately after the weight loss event. Once more, the TGA curve did not experience complex decomposition events. In addition, the corresponding average initial sample mass was ~3.60 mg. ($\sigma \approx 0.10$, CV ≈ 2.20) and residue percentage at 750 °C was found to be ~22 wt. % ($\sigma \approx 0.70$, CV ≈ 3.0), nominally higher than the manufacturer-specified value of 20 %; further, this residue percentage analysis was depicted in region C. The plot showing the TG arithmetic means was shown in Figure A.15.

The DTG results showed a single maximum peak temperature at ~413 °C ($\sigma \approx 1.40$, CV ≈ 0.30) as demonstrated in region D; as a result, this was associated to the maximum rate of degradation attained in one-step decomposition (Figure A.14). The approximate mass loss has been validated in the DTG profile; therefore, the area from the DTG peak integration was roughly ~74 ($\sigma \approx 1.0$, CV ≈ 1.40). It is evident the DTG peak integration (74 %) closely matched to the single decomposition weight loss (75 %). The plot showing the DTG arithmetic means is shown in Figure A.16. Lastly, further details regarding the thermal analysis made with the Trios software are available from Figure A.30 through Figure A.32.

4.1.5 PETG 30-GF

Results from the TG analysis of three specimens of PETG 30-GF can be found in Figure A.17. These identified the decomposition temperature after 1 % weight loss at ~361 °C ($\sigma \approx 2.70$, CV ≈ 0.70) in region A, the measured average initial specimen mass was 3.60 mg. ($\sigma \approx 0.20$, CV ≈ 5.90) and a total of ~65 wt. % ($\sigma \approx 1.40$, CV ≈ 2.0). In region B, the measurements were initiated from the decomposition temperature (361 °C) until a constant mass was observed immediately after the event. Again, the TGA curve did not experience complex decomposition events. After reaching the final test temperature of 750 °C in region C, the residual weight percentage was noted as ~30 wt. % ($\sigma \approx 1.40$, CV ≈ 4.60), matching the manufacturer-specified value of 30 %. The reasoning behind selecting 750 °C is the samples did not experience subsequent mass losses in this region. As shown in Figure A.19, the collected data was used to plot the TGA average results. Figure A.18 displays the DTG curves showing the single maximum peak temperature at ~419 °C ($\sigma \approx 2.50$, CV ≈ 0.60) in region D. That is, the maximum rate of degradation attained in the decomposition step transition. As shown in Figure A.20, the collected data was used to plot the TGA average results. The approximate mass loss throughout the decomposition step transition can be observed in the DTG profile; therefore, the area under the dW/dT peak was explored. As a result, the area from the DTG peak integration was about~64 ($\sigma \approx 1.40$, CV ≈ 2.20). Lastly, further details regarding the thermal analysis made with the Trios software are available from Figure A.33 through Figure A.35.

4.2 DIFFERENTIAL SCANNING CALORIMETRY

Throughout the following exhibited information, the arithmetic mean, sample standard deviation and coefficient of variance were provided for the 15 replicates experiments for the heating up and cooling down thermal events seen in the differential scanning calorimetry curves. This aimed to estimate the dispersion of the collected data based on three samples per material investigated. The precision and bias analyses for DSC were not explored for this thesis. However, this can be achieved by following the guidelines from ASTM-E691 (Heyes, 2018). Appendix B discloses all the raw data accompanied with DSC figures and tables summarizing the findings from the thermal events studied in this present section. (Table B.17 through Table B.31) highlights the arithmetic means, standard deviations and coefficient of variance from the DSC heating up and cooling down studies. A complete disclosure of the standard deviations and coefficient of variance for the thermal events are available from (Table B.1 through Table B.16). Further details regarding the thermal analysis made with the Trios software are available from (Figure B.1 through Figure B.20).

4.2.1 ABS 20-CF (Techmer)

First Calorimetric Study

ABS 20-CF samples were continuously tracked throughout a controlled heating cycle in a steadily purged environment (nitrogen) for one set of three specimen. The DSC thermograms can be observed in (Figure B.1 through Figure B.3); therefore, there were collected the means for a single glass transition event (region A) and an endothermic event (region B) under a heating examination from 25 °C to 220 °C. The measurements for the initial sample mass showed. ~2.20 mg. ($\sigma \approx 0.04$, $CV \approx 1.80$).

First, the glass transition event enabled to examine the onset temperature, the midpoint temperature, the change in specific heats and the change in energy (measured in milliwatts), consequently, these were the approximate experimental results: 102.0 °C (σ ≈ 1.80, CV ≈ 1.80), 105.0 °C (σ ≈ 2.10, CV ≈ 2.0), 0.20 J/g·°C (σ ≈ 0.02, CV ≈10.0), 0.10 mW (σ ≈ 0.01, CV ≈ 11.30), respectively. In addition, the endothermic event allowed to evaluate the onset temperature, the peak temperature, their heat per mole and the enthalpy analysis, therefore, the estimated results under heating scanning rates (10 °C /min) were: 129.0 °C (σ ≈ 0.80, CV ≈ 0.60), 139.0 °C (σ ≈ 0.40, CV ≈ 0.30), 72.40 J/mol (σ ≈ 2.90, CV ≈3.90) and 1.40 J/g (σ ≈ 0.10, CV ≈ 4.20), correspondingly.

Succeeding the heating cycle, the ABS 20 wt. % CF material was equilibrated to 220.0 °C and the specimen's temperature were descended to ~25 °C upon scanning rates by (20 °C /min); as a result, there were collected the means for the exothermic reaction. The exothermic signal can be observed in the DSC curve in region C in the context of cooling. Further, the exothermic event allowed to evaluate the onset temperature, the peak temperature, their heat per mole and the enthalpy analysis, therefore, the estimated results were: 125.0 °C (σ ≈ 0.10, CV ≈ .10), 121.0 °C (σ ≈ 0.30, CV ≈ 0.20), 90.40 J/mol (σ ≈ 6.0, CV ≈ 7.0) and 1.80 J/g (σ ≈ 0.10, CV ≈ 6.70).

Secondary Calorimetric Study

Preceding the cooling down cycle, a subsequent DSC analysis was carried out to provide information about the sample's thermal history and study the thermal response to the secondary heating and cooling cycle (tracking the changes in the thermal events); accordingly, the presence from the previous phase transitions reappeared in this series of experiments; therefore, there were collected the means for the glass transition event (region A') and an endothermic event (region B') upon a replicate heating up examination.

Initially, the glass transition event enabled to examine the onset temperature, the midpoint temperature, the change in specific heats and the change in energy; consequently, these were the

approximate experimental results: 103.0 °C (σ ≈ 0.20, CV ≈ 0.20), 106.0 °C (σ ≈ 0.10, CV ≈ 0.10), 0.10 J/g·°C (σ ≈ 0.01, CV ≈2.10) and 0.10 mW (σ ≈ 0.004, CV ≈ 4.40), respectively. In addition, the endothermic event allowed to evaluate the onset temperature, the peak temperature, their heat per mole and the enthalpy analysis, thus, the quantified results under heating scanning rates for a replicate examination were: 131.0 °C (σ ≈ 0.30, CV ≈ 0.20), 140.0 °C (σ ≈ 0.10, CV ≈ 0.04), 76.50 J/mol (σ ≈ 6.80, CV ≈8.90) and 1.50 J/g (σ ≈ 0.10, CV ≈ 8.60), correspondingly.

Lastly, the secondary cooling down cycle was marked by an exothermic event (region C'); likewise, the DSC instrument delivered experimental calculation for the peak temperature, the onset temperature, their heat per mole and the enthalpy analysis; hence, these were the approximate experimental results: 124.0 °C (σ ≈ 0.10, CV ≈ 0.10), 120.0 °C (σ ≈ 0.40, CV ≈ 0.30), 84.70 J/mol (σ ≈ 7.10, CV ≈8.30) and 1.70 J/g (σ ≈ 0.10, CV ≈ 8.30).In addition, Figure B.4 provides a DSC visual reference for the three samples.

4.2.2 ABS 20-GF (Techmer)

First Calorimetric Study

ABS 20 wt. % GF materials were continuously examined upon a controlled heating cycle for one set of three specimen. The DSC curve are facilitated in (Figure B.5 through Figure B.7); accordingly, there were collected the means for a glass transition event (region A) and an endothermic event (region B) under a heating examination from 25 °C to 220 °C. With regards to the average initial sample mass, mass measurements showed. ~2.0 mg. ($\sigma \approx 0.10$, CV ≈ 4.40).

At the beginning, the glass transition event enabled to examine the onset temperature, the midpoint temperature, the change in specific heats and the change in energy; therefore, these were the approximate experimental results: 103.0 °C ($\sigma \approx 2.0$, CV ≈ 2.0), 105.0 °C ($\sigma \approx 1.50$, CV ≈ 1.40), 0.30 J/g·°C ($\sigma \approx 0.10$, CV ≈19.40) and 0.10 mW ($\sigma \approx 0.02$, CV ≈ 20.0), respectively. Additionally, the endothermic event allowed to evaluate the onset temperature, the peak temperature, their heat per mole and the enthalpy analysis, therefore, the predicted results under heating scanning rates (10 °C /min) were: 130.0 °C ($\sigma \approx 1.50$, CV ≈ 1.10), 138.0 °C ($\sigma \approx 0.40$, CV ≈ 0.30), 54.0 J/mol ($\sigma \approx 6.20$, CV 11.40) and 1.0 J/g ($\sigma \approx 0.02$, CV ≈ 2.0), correspondingly.

Succeeding the heating cycle, the ABS 20 wt. % GF specimens were equilibrated to 220.0 °C and cooled down the specimens to 25 °C under controlled scanning rates (20 °C /min); as a result, there were collected the means for the exothermic reaction. The exothermic signal can be observed in the DSC curve in region C in the context of cooling; for instance, the exothermic event allowed to evaluate the onset temperature, the peak temperature, their heat per mole and the enthalpy analysis. The estimated results were: 123.0 °C ($\sigma \approx 0.30$, CV ≈ 0.20), 119.0 °C ($\sigma \approx 0.50$, CV ≈ 0.40), 76.0 J/mol ($\sigma \approx 14.80$, CV ≈ 19.50) and 1.50 J/g ($\sigma \approx 0.30$, CV ≈ 19.20).

Secondary Calorimetric Study

A subsequent DSC analysis carried out a secondary heating and cooling cycle tracking the changes in the thermal events; therefore, these were employed to collect the means for the glass transition event (region A') and an endothermic event (region B') upon a replicate heating up examination. Initially, the glass transition event enabled to examine the onset temperature, the midpoint temperature, the change in specific heats and the change in energy; consequently, these were the approximate experimental results: 103.0 °C ($\sigma \approx 0.90$, CV ≈ 0.90), 106.0 °C ($\sigma \approx 0.60$, CV ≈ 0.60), 0.30 J/g·°C ($\sigma \approx 0.010$, CV ≈4.60) and 0.80 mW ($\sigma \approx 0.010$, CV ≈ 0.80), respectively. However, the subsequent heating cycle was not different from the initial cycle. Similarly, the endothermic event served to evaluate the onset temperature, the peak temperature, their heat per mole and the enthalpy analysis, thus, the quantified results under heating scanning rates for a replicate examination were: 131.0 °C ($\sigma \approx 0.30$, CV ≈ 0.20), 139.0 °C ($\sigma \approx 0.40$, CV ≈ 0.30), 69.0 J/mol ($\sigma \approx 1.50$, CV ≈ 2.20) and 1.40 J/g ($\sigma \approx 0.03$, CV ≈ 2.20), correspondingly.

Finally, the second DSC cooling curve was marked by an exothermic event (region C'); certainly, the DSC instrument delivered experimental calculation for the peak temperature, the onset temperature, their heat per mole and the enthalpy analysis; hence, these were the approximate experimental results: 123.0 °C ($\sigma \approx 0.20$, CV ≈ 0.10), 118.0 °C ($\sigma \approx 0.80$, CV ≈ 0.70), 67.20 J/mol ($\sigma \approx 10.40$, CV ≈ 15.60) and 1.30 J/g ($\sigma \approx 0.20$, CV ≈ 15.0). In addition, Figure B.8 provides a DSC visual reference for the three samples.

4.2.3 ABS 40-GF (Techmer)

First Calorimetric Study

ABS 40 wt. % GF materials were continuously examined upon a controlled heating cycle for one set of three specimen. The DSC curves were provided in (Figure B.9 through Figure B.11); accordingly, there were collected the means for a glass transition event (region A) and an endothermic event (region B) under a heating examination from 25 °C to 227 °C. With regards to the average initial sample mass, mass measurements showed about 2.20 mg. ($\sigma \approx 0.03$, CV ≈ 1.40).

At the beginning, the glass transition event enabled to examine the onset temperature, the midpoint temperature, the change in specific heats and the change in energy; therefore, these were the approximate experimental results: 102.0 °C ($\sigma \approx 0.50$, CV ≈ 0.50), 106.0 °C ($\sigma \approx 0.20$, CV ≈ 0.20), 0.15 J/g·°C ($\sigma \approx 0.01$, CV ≈6.90) and 0.10 mW ($\sigma \approx 0.004$, CV ≈ 8.0), respectively. Additionally, the endothermic event allowed to evaluate the onset temperature, the peak temperature, their heat per mole and the enthalpy analysis, therefore, the predicted results under heating scanning rates (10 °C /min) were: 128.0 °C ($\sigma \approx 0.80$, CV ≈ 0.60), 138.0 °C ($\sigma \approx 0.20$, CV ≈ 0.20), 59.0 J/mol ($\sigma \approx 5.80$, CV ≈ 9.90) and 1.20 J/g ($\sigma \approx 0.10$, CV 9.40), correspondingly.

Succeeding the heating cycle, the ABS 40 wt. % GF specimens were equilibrated to 227.0 °C and cooled down to 25 °C by scanning rates (20 °C /min); that is, there were collected the means for the exothermic reaction. Further, the exothermic event can be observed in the DSC cooling profile in region C; for instance, the exothermic event allowed to evaluate the onset temperature, the peak temperature, their heat per mole and the enthalpy analysis. The estimated results were: 125.0 °C ($\sigma \approx 0.02$, CV ≈ 0.01), 120.0 °C ($\sigma \approx 0.04$, CV ≈ 0.03), 61.0 J/mol ($\sigma \approx 8.30$, CV ≈ 13.60) and 1.20 J/g ($\sigma \approx 0.20$, CV ≈ 13.10).

Secondary Calorimetric Study

A secondary heating and a secondary cooling cycle tracked the changes from DSC curves; therefore, the glass transition event (region A') and an endothermic event (region B') were studied. Initially, the assignment of the glass transition analysis functioned to analyze the onset temperature, the midpoint temperature, the change in specific heats and the change in energy; consequently, these were the retrieved experimental results: 103.0 °C ($\sigma \approx 0.80$, CV ≈ 0.70), 106.0 °C ($\sigma \approx 0.50$, CV ≈ 0.50), 0.20 J/g·°C ($\sigma \approx 0.010$, CV ≈7.30) and 0.60 mW ($\sigma \approx 0.010$, CV ≈ 8.30), respectively. Similarly, region B' (endothermic event) served to evaluate the onset temperature, the peak temperature, their heat per mole and the enthalpy analysis, thus, the quantified results under heating scanning rates for a replicate examination were: 130.0 °C ($\sigma \approx 0.70$, CV ≈ 0.50), 140.0 °C ($\sigma \approx 0.40$, CV ≈ 0.30), 60.0 J/mol ($\sigma \approx 6.50$, CV ≈ 10.80) and 1.20 J/g ($\sigma \approx 0.10$, CV ≈10.90), correspondingly.

Once more, the secondary cooling down curve revealed an exothermic event (region C'); certainly, the DSC analysis delivered the experimental calculation for the peak temperature, the onset temperature, their heat per mole and the enthalpy analysis; hence, these were the approximate experimental results: 125.0 °C ($\sigma \approx 0.30$, CV ≈ 0.20), 120.0 °C ($\sigma \approx 0.10$, CV ≈ 0.10), 56.0 J/mol ($\sigma \approx 5.60$, CV ≈ 10.0) and 1.10 J/g ($\sigma \approx 0.10$, CV ≈ 9.80). In addition, Figure B.12 provides a DSC visual reference for the three samples.

4.2.4 ABS 20-GF (SABIC)

First Calorimetric Study

ABS 20 wt. % GF (SABIC) specimens were continuously examined under a controlled heating cycle for one set of three specimen using identical experimental procedures. The DSC curves are presented in (Figure B.13 through Figure B.15). In similar fashion to ABS 40 wt. % GF there were collected the means for the glass transition event (region A) and an exothermic event (region B) under a heating examination from 25 °C to 255 °C. With regards to the average initial sample mass, mass measurements showed about 2.40 mg. ($\sigma \approx 0.10$, CV ≈ 3.70).

Initially, the glass transition event enabled to examine the onset temperature, the midpoint temperature, the change in specific heats and the change in energy; therefore, these were the approximate experimental results: 106.0 °C ($\sigma \approx 0.70$, CV ≈ 0.70), 109.0 °C ($\sigma \approx 0.60$, CV ≈ 0.60), 0.20 J/g·°C ($\sigma \approx 0.010$, CV ≈5.0) and 0.10 mW ($\sigma \approx 0.010$, CV ≈ 6.0), respectively. Moreover, the development of an exothermic event allowed to evaluate the onset temperature, the peak temperature, their heat per mole and the enthalpy analysis, consequently, the predicted results under heating scanning rates (10 °C /min) were:

Succeeding the heating cycle, the ABS 20 wt. % GF (SABIC) specimens were equilibrated to 255.0 °C and cooled down to 25 °C by scanning rates (20 °C /min); that is, there were collected the means for an endothermic event upon cooling. Further, the endothermic event can be found in the DSC cooling profile in region C; for instance, the exothermic event allowed to evaluate the onset temperature, the peak temperature, their heat per mole and the enthalpy analysis. The approximate results were: 240.0 °C ($\sigma \approx 0.10$, CV ≈ 0.02), 233.0 °C ($\sigma \approx 0.10$, CV ≈ 0.04), 46.30 J/mol ($\sigma \approx 1.80$, CV ≈ 3.80) and 0.90 J/g ($\sigma \approx 0.03$, CV ≈ 3.30).

Secondary Calorimetric Study

The secondary heating up studies by DSC found one glass transition event (region A') and an exothermic event (region B'); therefore, the assignment of the glass transition analysis functioned to analyze the onset temperature, the midpoint temperature, the change in specific heats and the change in energy. These were the retrieved experimental results: 106.0 °C ($\sigma \approx 0.30$, CV ≈ 0.30), 109.0 °C ($\sigma \approx 0.30$, CV ≈ 0.30), 0.20 J/g·°C ($\sigma \approx 0.010$, CV $\approx$2.90) and 0.10 mW ($\sigma \approx$ 0.010, CV ≈ 8.30), respectively. Furthermore, region B' (exothermic event) served to report the onset temperature, the peak temperature, their heat per mole and the enthalpy analysis, thus, the quantified results upon heating scanning rates for a secondary examination were: 231.0 °C ($\sigma \approx$ 0.10, CV ≈ 0.02), 237.0 °C ($\sigma \approx 0.10$, CV ≈ 0.10), 48.0 J/mol ($\sigma \approx 5.20$, CV ≈ 10.80) and 1.0 J/g ($\sigma \approx 0.10$, CV $\approx$10.50), correspondingly.

Lastly, the secondary cooling down curve experienced an exothermic event as depicted in region C'; thus, the corresponding peak temperature, the onset temperature, their heat per mole and the enthalpy analysis were noted at: 239.0 °C ($\sigma \approx 0.30$, CV ≈ 0.10), 233.0 °C ($\sigma \approx 0.02$, CV ≈ 0.010), 44.90 J/mol ($\sigma \approx 1.30$, CV ≈ 3.0) and 0.90 J/g ($\sigma \approx 0.02$, CV ≈ 2.20). In addition, Figure B.16 provides a DSC visual reference for the three samples.

4.2.5 PETG 30-GF

First Calorimetric Study

DSC curves for PETG 30-GF are presented in (Figure B.17 through Figure B.19). In similar fashion to PETG 30-GF there were collected the means for the glass transition event (region A) and an exothermic event (region B) upon a heating examination from 25 °C to 340 °C. In addition, the measured average initial specimen mass was 2.20 mg. ($\sigma \approx 0.10$, CV ≈ 2.80). Region A (glass transition event) enabled to examine the onset temperature, the midpoint temperature, the change in specific heats and the change in energy; therefore, these were the approximate experimental results: 75.10 °C ($\sigma \approx 0.10$, CV ≈ 0.10), 77.50 °C ($\sigma \approx 0.50$, CV ≈ 0.60), 0.25 J/g·°C ($\sigma \approx 0.02$, CV ≈8.10) and 0.10 mW ($\sigma \approx 0.010$, CV ≈ 12.50), respectively. Moreover, the collected DSC curve depicted an exothermic event which enabled to measure the onset temperature, the peak temperature, their heat per mole and the enthalpy analysis. Consequently, the results were measured at: ~231.0 °C ($\sigma \approx 0.10$, CV ≈ 0.10), ~237.0 °C ($\sigma \approx 0.04$, CV ≈ 0.01), ~54.50 J/mol ($\sigma \approx 5.30$, CV ≈ 9.80), ~1.10 J/g ($\sigma \approx 0.10$, CV ≈ 9.30)

After the heating cycle, the PETG 30-GF specimens were equilibrated to 340.0 °C and cooled down to 25 °C at (20 °C /min); that is, there were collected the means for an endothermic event under cooling. The endothermic signal can be found in the DSC cooling profile in region C; for instance, the exothermic event allowed to evaluate the onset temperature, the peak temperature, their heat per mole and the enthalpy analysis. The approximate results were: 240.0 °C ($\sigma \approx 0.30$, CV ≈ 0.10), 233.0 °C ($\sigma \approx 0.10$, CV ≈ 0.03), 56.20 J/mol ($\sigma \approx 2.40$, CV ≈ 4.20) and 1.10 J/g ($\sigma \approx$ 0.04, CV ≈ 3.60).

Secondary Calorimetric Study

The replicate heating cycle demonstrated one glass transition event (region A') and an exothermic event (region B'); therefore, the assignment of the glass transition analysis functioned to analyze the onset temperature, the midpoint temperature, the change in specific heats and the change in energy. These were the retrieved experimental results: 74.0 °C ($\sigma \approx 0.20$, CV ≈ 0.20), 77.0 °C ($\sigma \approx 0.04$, CV ≈ 0.10), 0.20 J/g·°C ($\sigma \approx 0.010$, CV ≈4.30) and 0.10 mW ($\sigma \approx 0.002$, CV ≈ 0.002), respectively.

Furthermore, region B' exhibited an exothermic event which lead to quantify the onset temperature, the peak temperature, their heat per mole and their enthalpy; thus, the quantified results for a replicate examination were: 231.0 °C ($\sigma \approx 0.30$, CV ≈ 0.10), 237.0 °C ($\sigma \approx 0.20$, CV ≈ 0.10), 50.90 J/mol ($\sigma \approx 15.30$, CV ≈ 30.0) and 1.0 J/g ($\sigma \approx 0.30$, CV ≈29.70), correspondingly.

Ultimately, the secondary cooling down curve marked an exothermic event as depicted in region C'; thus, the corresponding peak temperature, the onset temperature, their heat per mole and the enthalpy analysis were noted at: 239.0 °C ($\sigma \approx 0.30$, CV ≈ 0.10), 233.0 °C ($\sigma \approx 0.10$, CV ≈ 0.04), 54.0 J/mol ($\sigma \approx 2.40$, CV ≈ 4.50) and 1.0 J/g ($\sigma \approx 0.10$, CV ≈ 4.0). In addition, Figure B.20 provides a DSC visual reference for the three samples.

Chapter 5: Discussion of TGA

This chapter was designed to compare the improvements or decline in thermal stability (in the context of percentage change) of thermoplastics that possessed identical material matrix; therefore, the ABS TG/DTG thermal curves and mean thermal events were plotted in one single figure (section 5.1 through section 5.3).

5.1. ABS 20 (GF & CF)

5.1.1 Decomposition Temperature (1 wt.% loss)

When comparing ABS 20-GF to ABS 20-CF, a minor increase in 1 % weight loss was noted. The ABS 20-GF material experienced a moderate restrain in ABS matrix thermal decomposition; consequently, the 1 wt.% loss in nitrogen shifted 2.0 °C higher (representing a 0.70% increase in thermal degradation temperature). Therefore, the addition of glass fibers functioned to increases the thermal degradation temperature due to the heat distortion temperature was below the glass transition temperature. In addition, it was visually perceived by comparing the thermograms for ABS 20-GF to ABS 20-CF that there were no anomalies attributed to decomposition in nitrogen (Figure 5.1.1); certainly, the material matrix decomposition was nearly identical (compounded by Techmer). This indicates the absence of complex chemical decomposition in the context of thermal characterization by thermogravimetry.

5.1.2 Step Decomposition Thermal Event

When comparing ABS 20-GF to ABS 20-CF, a minor decrease in the one-step decomposition was perceived; accordingly, the ABS 20-CF undergo a lower decline in weight loss; therefore, the degradation step in nitrogen was 2.0 wt. % higher (representing a 1.20% increase in weight percentage conserved).

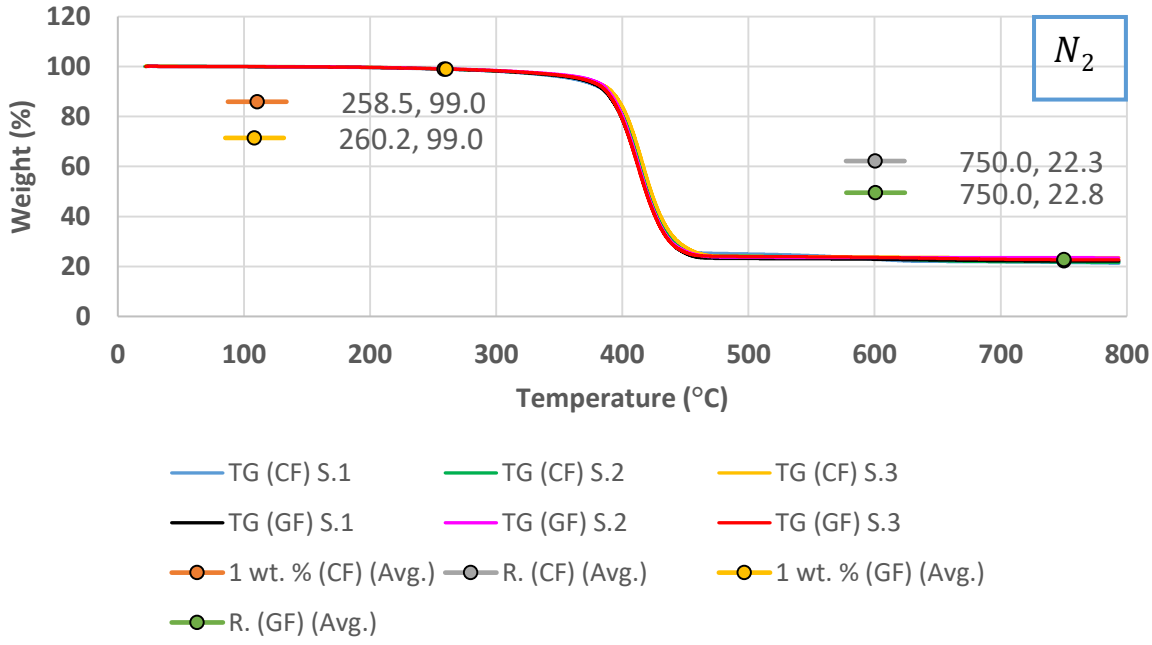

Figure 5.1.1: The TGA comparison between the ABS 20-GF and ABS 20-CF examination.

5.1.3 Residue Percentage at 750 °C

The residual percentage measurement at 750 °C probed a small improvement for ABS 20-GF (Figure 5.1.1) when compared to ABS 20-CF. Accordingly, ABS 20-GF was similar to ABS 20-CF after the one-step decomposition. In fact, ABS 20-GF when compared to ABS 20-CF did not have a notable effect to impede the continuous mass loss throughout the TG thermal characterization as studied in subsection 5.1.2. However, the mass conserved at 750 °C was slightly higher (0.50 wt.% higher). In terms of percentage, the glass fiber addition contributed in an approximate enhancement of 2.20 %. In addition, visual and analytical comparison of the plateau region at 750 °C confirmed the residue percentage for both materials closely matched to the manufacturer-specified filler reinforcement (20 %) added to polymer.

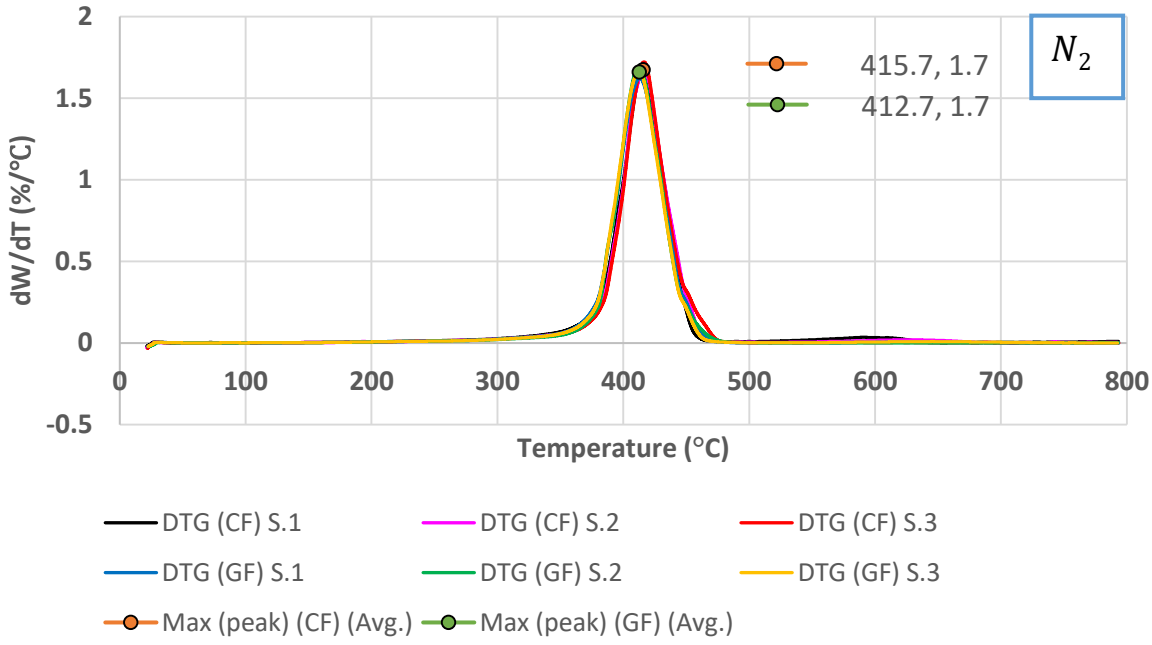

Figure 5.1.2: DTG curves were overlaid to compare the mean values from ABS 20 (GF to CF).

5.1.4 DTG Maximum Peak Temperature

Given the maximum peak temperatures, a low improvement was found for ABS 20-CF when compared to ABS 20-GF (Figure 5.1.2); therefore, the higher rate of degradation for ABS 20-CF shifted to a moderate higher temperature. In fact, ABS 20-GF did not have a notable effect to reduce the rate of degradation ascribed from the one-step decomposition; consequently, ABS 20-GF shown a decrease in thermal stability to endure thermal decomposition in nitrogen (3.0 °C lower). In terms of percentage, the glass fiber reinforcement reduced the thermal stability in the context of the maximum peak temperature by 0.70 %. The integration of this analysis corresponds to the upper limit of mass loss from the engineering thermoplastic. In addition, analytical comparison of DTG profiles showed the area under the dW/dT peak to be analogous to first degradation step transition from the TGA; in fact, this thermal analysis demonstrated the amount of matter lost in the decomposition step transition. The detection of the area under the DTG

maximum peak demonstrated a slight improvement for ABS 20-GF; therefore, ABS 20-GF managed to impede the continuous mass loss more than ABS 20-GF (1.30 higher area beneath the dW/dT curve). In terms of percentage, the glass fiber reinforcement contributed in a small enhancement of mass conserved (1.70 %). Lastly, by visually comparing the DTG curves for ABS 20-GF to ABS 20-CF led to the conclusion the DTG profiles were similar.

5.2. ABS (40-GF & 20-GF)

5.2.1 Decomposition Temperature (1 wt.% loss)

When comparing ABS 40-GF to ABS 20-GF, a minor increase in 1 % weight loss was noted. The ABS 40-GF material experienced a moderate restrain in ABS matrix thermal decomposition; consequently, the 1 wt.% loss in nitrogen shifted 7.0 °C higher (representing a 2.70% increase in thermal degradation temperature). In addition, it was visually perceived by comparing the thermograms for ABS 40-GF to ABS 20-GF that there were no anomalies attributed to decomposition in nitrogen (Figure 5.2.1); certainly, the material matrix decomposition was nearly identical (compounded by Techmer). This indicates the absence of complex chemical decomposition in the context of thermal characterization by thermogravimetry.

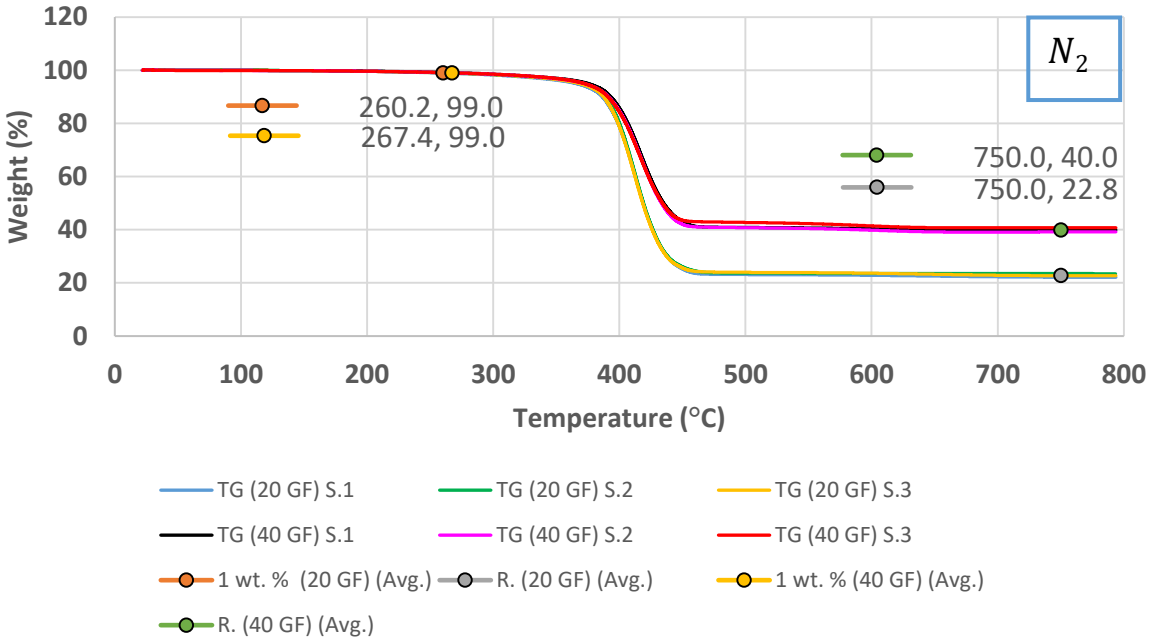

Figure 5.2.1: The TGA comparison between the ABS 40-GF and ABS 20-GF examination.

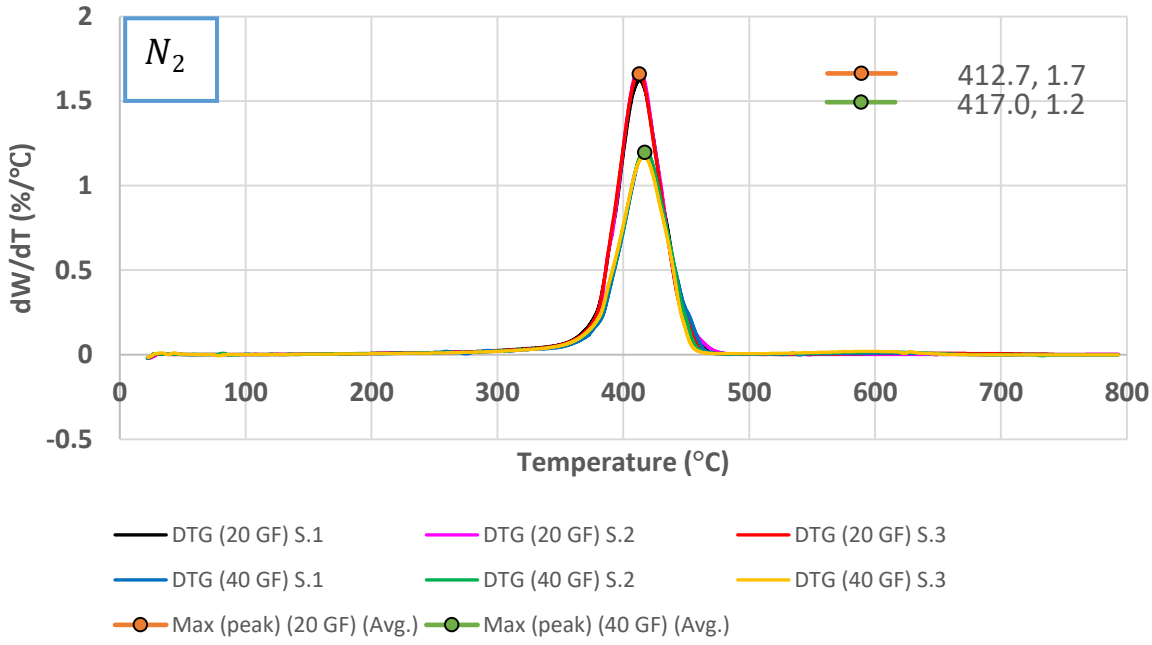

Figure 5.2.2: TG curves were overlaid to compare the mean values from ABS 40-GF to ABS 20-GF.

5.2.2 TG Step Thermal Decomposition

When comparing ABS 40-GF to ABS 20-GF, a higher decrease in the one-step decomposition was perceived; accordingly, the ABS 40-GF undergo a lower decline in weight loss; therefore, the degradation step in nitrogen was 18.0 wt. % lower (representing a 31.40% increase in the conversation of weight percentage). In addition, it was visually perceived by comparing the thermograms for ABS 40-GF to ABS 20-GF that the ABS 40-GF TG profile shifted to a lower weight percentage range (the weight loss was smaller).

5.2.3 Residual Percentage at 750 ° C

The residual percentage measurement at 750 °C probed a high improvement for ABS 40-GF (Figure 5.2.1) when compared to ABS 20-GF. Accordingly, ABS 40-GF was not like ABS 20-GF after the one-step decomposition. In fact, ABS 40-GF when compared to ABS 20-GF did have a notable effect to impede the continuous mass loss throughout the TG thermal characterization. Therefore, the mass conserved at 750 °C was increased (17.20 wt.% higher). In terms of percentage, the 40 wt. % glass fiber addition contributed in an approximate enhancement of 75.40 %. In addition, visual and analytical comparison of the plateau region at 750 °C confirmed the residue percentage for both materials closely matched to the manufacturer-specified filler reinforcement (40 %) added to polymer.

5.2.4 DTG Maximum Peak Temperature

Given the maximum peak temperatures, a modest improvement was found for ABS 40-GF when compared to ABS 20-GF (Figure 5.2.2); therefore, the higher rate of degradation for ABS 40 wt. % GF shifted to a moderate higher temperature. In fact, ABS 20-GF did not have a notable effect to reduce the rate of degradation ascribed from the one-step decomposition; consequently, ABS 20-GF shown a decrease in thermal stability to endure thermal decomposition in nitrogen (4.0 °C lower). In terms of percentage, the glass fiber reinforcement reduced the thermal stability in the context of the maximum peak temperature by 0.90 %. In addition, analytical comparison of DTG profiles showed the area under the dW/dT peak and demonstrated a higher improvement for ABS 40-GF; therefore, ABS 40-GF managed to impede the continuous mass loss more than ABS 20-GF (18.0 higher area beneath the dW/dT curve). In terms of percentage, the glass fiber reinforcement contributed in a higher enhancement of mass conserved (32.20 %). Finally, it was visually perceived by comparing the DTG profile for ABS 40-GF to ABS 20-GF that the ABS 40-GF maximum peak shifted to a higher temperature range and the DTG peak height was shorter.

5.3. ABS 20-GF (SABIC) & ABS 20-GF (TECHMER)

5.3.1 Decomposition Temperature (1 wt.% loss)

When comparing ABS 20-GF (SABIC) to ABS 20-GF (Techmer), a minor increase in 1 % weight loss was noted. The ABS 20-GF (SABIC) material experienced a moderate restrain in ABS matrix thermal decomposition; consequently, the 1 wt.% loss in nitrogen shifted 35.0 °C higher (representing a 13.50% increase in thermal degradation temperature). In addition, it was visually perceived by comparing the thermograms for ABS 20-GF (SABIC) to ABS 20-GF (Techmer) that there were no anomalies attributed to decomposition in nitrogen; certainly, the material matrix decomposition was nearly identical. This indicates the absence of complex chemical decomposition in the context of thermal characterization by thermogravimetry.

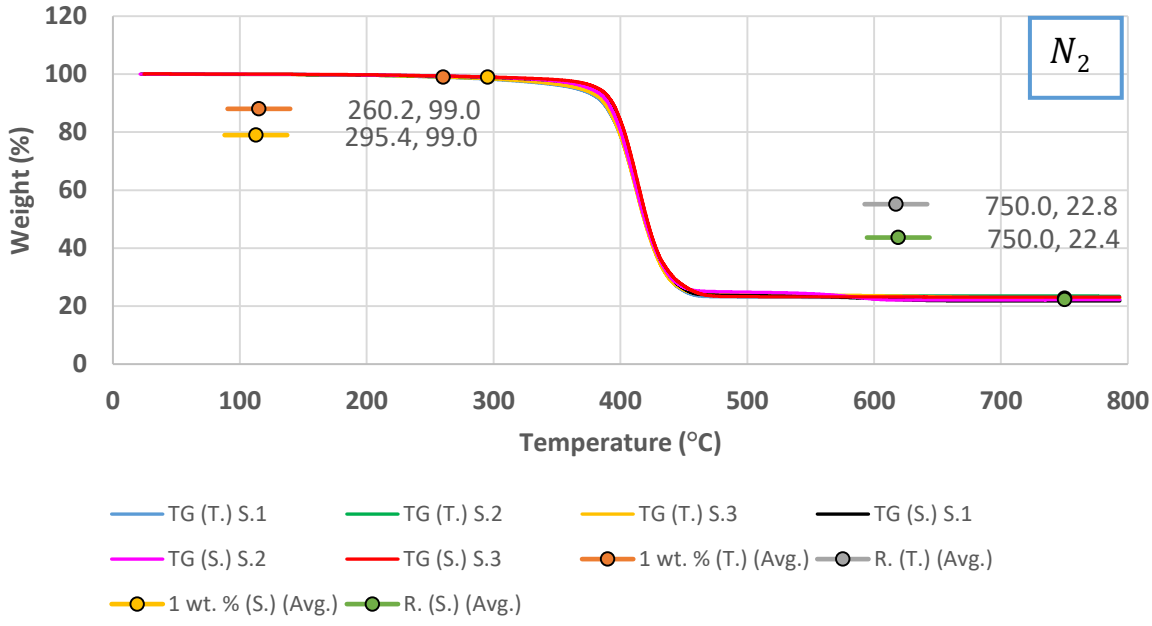

Figure 5.3.1: The TGA comparison between the ABS 20-GF (SABIC) and ABS 20-GF (Techmer) examination.

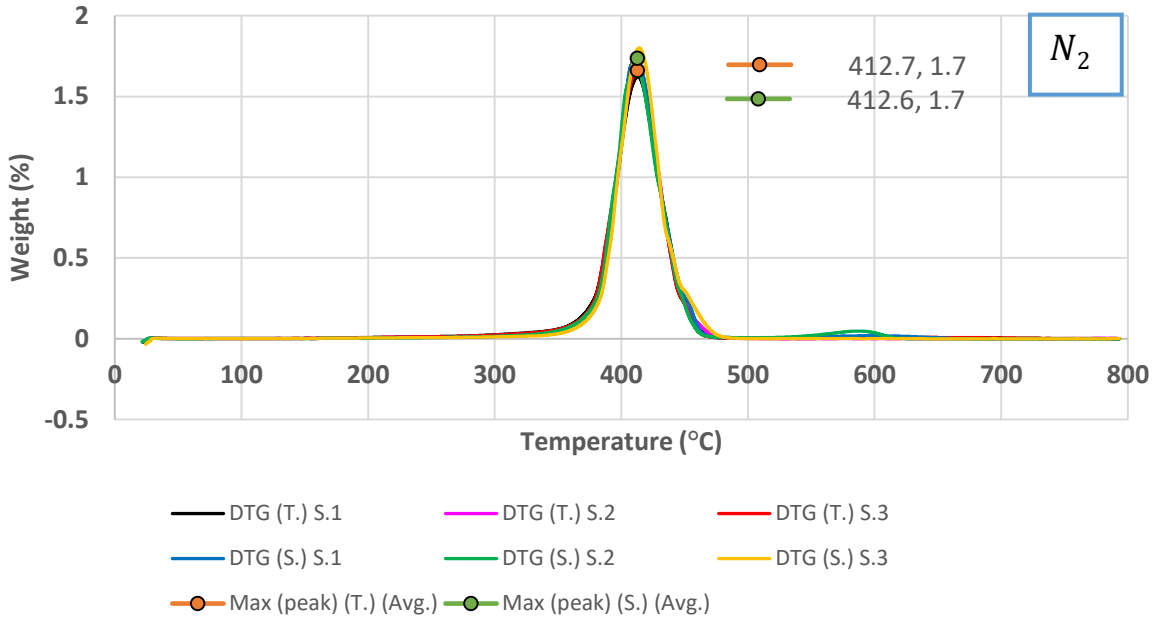

Figure 5.3.2: DTG curves were overlaid to compare the mean values from ABS 20 wt. % GF (SABIC) to ABS 20 WT. % GF (Techmer).

5.3.2 TG Step Thermal Decomposition and Residual Percentage at 750 ° C

When comparing ABS 20-GF (SABIC) to ABS 20-GF (Techmer), a similar decrease in the one-step decomposition was noted; accordingly, both materials experienced a decline in weight loss (~75 wt. % loss). Likewise, the mass conserved for a residual percentage measurement at 750 °C for both materials was (~22 wt. % conserved). Thus, their material matrix decomposition in nitrogen was nearly identical. In addition, visual and analytical comparison of the plateau region at 750 °C confirmed the residue percentage for both materials almost matched to the manufacturer-specified filler reinforcement (20 %) added to polymer.

5.3.3 DTG Maximum Peak Temperature

Given the maximum peak temperatures at 413 °C, there were not found improvements for 20-GF (SABIC) nor ABS 20-GF (Techmer) (Figure 5.3.2); therefore, the higher rate of degradation respect to temperature do not change. In addition, visual comparison of DTG profiles showed the area under the dW/dT peak to overlapped. Thus, 20-GF (SABIC) and ABS 20-GF (Techmer) managed to impede the approximate same amount of mass loss of (74 % area beneath the dW/dT curve).

Chapter 6: Discussion of DSC

This chapter was designed to compare in the context of the percentage change for thermal events encountered in two replicate cycles in which each contained a heating and cooling (section 6.1 through section 6.4). Additionally, section 6.5 was designed to compare ABS 20 wt. % GF to ABS 20 wt. % CF. Finally, section 6.6 compares ABS at varying percentage nominal ratios by weight (as received from the manufacturer) of glass fibers incorporated to the thermoplastic matrix.

6.1. ABS 20-CF

Glass Transition Event

The replicate midpoint glass transition temperature, onset temperature, change in specific heats analysis, and change in power increased by 1.0 °C, 1.0 °C, and by less than 0.10 J/g·°C and 0.10 mW, this when compared to the first heating DSC cycle for ABS 20-CF. This represented about 0.90 %, 0.90 %, 20.0 %, and a 13.0 % rise, this when compared to the first heating DSC cycle.

Endothermic Event

The secondary endothermic peak temperature, onset temperature, heat per mole analysis, and enthalpy analysis increased by less than 1.0 °C, by 1.0 °C, 4.10 J/mol, and 0.10 J/g, this when compared to the first heating DSC cycle for ABS 20-CF. This represented about 0.40 %, 1.10 %, 5.70 %, and 5.60 % rise, respectively. This when compared to the first heating DSC cycle.

Exothermic Event

The replicate exothermic peak temperature, onset temperature, heat per mole analysis, and enthalpy analysis decreased by 1.0 °C, less than 1.0 °C, 5.80 J/mol, and 0.10 J/g, this when compared to the first cooling DSC cycle for ABS 20-CF. This represented about 0.50 %, 0.30 %, 6.90 %, and 6.50 % decline, respectively. This when compared to the first cooling DSC cycle.

6.2. ABS 20-GF

Glass Transition Event

The replicate midpoint glass transition temperature and change in power increased by 1.0 °C and 1.0 mW, this when compared to the first heating DSC cycle for ABS 20-GF. This represented a 1.20 % and 700.0 % rise, this when compared to the first heating DSC cycle. There were not identified changes in the onset temperature. In addition, the specific heats decreased about 0.10 J/g·°C. This represented a 20.0 % decline, this when compared to the first heating DSC cycle.

Endothermic Event

The secondary endothermic peak temperature, onset temperature, heat per mole analysis, and enthalpy analysis increased by 1.0 °C, 1.0 °C, 15.20 J/mol, and 0.40 J/g, this when compared to the first heating DSC cycle for ABS 20-GF. This represented about 0.80 %, 0.90 %, 28.20 and 38.0 % rise, this when compared to the first heating DSC cycle

Exothermic Event

The replicate exothermic peak temperature, heat per mole and enthalpy analysis decreased by 1.0 °C, 8.80 J/mol and 0.20 J/g, this when compared to the first cooling DSC cycle for ABS 20-GF. This represented about 0.70 %, 11.50 % and 11.30 % decline. There were not identified changes in the onset temperature.

6.3. ABS 40-GF

Glass Transition Event

The replicate midpoint glass transition temperature, onset temperature and heat capacity increased by 1.0 °C, 1.0 °C and by less than 0.10 J/g·°C, this when compared to the first heating DSC cycle for ABS 40-GF. This represented about 0.80 %, 0.80 % and 31.70 % rise, this when compared to the first heating DSC cycle. There were not identified changes in the change in power.

Endothermic Event

The secondary endothermic peak temperature, onset temperature and the heat per mole analysis increased by 1.0 °C, 1.0 °C, and 1.40 J/mol, this when compared to the first heating DSC cycle for ABS 40-GF. This represented about 1.0 %, 1.0 %, and 2.50 % rise, this when compared to the first heating DSC cycle. There were not identified changes in the change in power.

Exothermic Event

The replicate heat per mole and enthalpy analysis decreased by 5.10 J/mol and 0.10 J/g, this when compared to the first cooling DSC cycle for ABS 40-GF. This represented about 8.30 % and 8.2 0 % decline. There were not identified changes in the exothermic peak and onset temperature.

6.4. PETG 30-GF

Glass Transition Event

The replicate onset temperature increased by 1.0 °C and the heat capacity decreased by less than 0.10 J/g·°C, this when compared to the first heating DSC cycle for PETG 30-GF. This represented a 1.10 % rise and 6.50 % decline, respectively. There were not identified changes in the midpoint glass transition temperature nor for the change in power.

Exothermic Event

The secondary heat per mole and enthalpy analysis increased by 4.0 J/mol and 0.10 J/g, this when compared to the first heating DSC cycle for PETG 30-GF. This represented about a 6.60 % and 6.50 % decline, this when compared to the first heating DSC cycle. There were not identified changes in the in the exothermic peak temperature nor in the onset temperature

Endothermic Event

The replicate heat per mole and enthalpy analysis decreased by 2.20 J/mol and less than 0.10 J/g, this when compared to the first cooling DSC cycle for PETG 30-GF. This represented an 3.80 % and 3.60 % decline. There were not identified changes in the endothermic peak and onset temperature.

6.5. ABS 20-GF (SABIC)

Glass Transition Event

There were not identified changes in the replicate midpoint glass transition temperature, onset temperature, heat capacity nor the change in power analyses.

Endothermic Event

The secondary heat per mole and enthalpy analysis increased by 0.60 J/mol and by less than 0.10 J/g, this when compared to the first heating DSC cycle for ABS 20-GF by SABIC. This represented about a 1.40 % and less than 1.0 % rise, this when compared to the first heating DSC cycle. There were not identified changes in the in the endothermic peak nor in the onset temperature

Exothermic Event

The replicate heat per mole and enthalpy analysis decreased by 1.40 J/mol and by less than 0.10 J/g, this when compared to the first cooling DSC cycle for ABS 20-GF by SABIC. This represented an 3.10 % and 3.80 % decline. There were not identified changes in the exothermic peak and onset temperature.

6.6. ABS REINFORCED WITH GF AND CF

Glass Transition Event

When comparing the replicates analysis for ABS 20-GF to ABS 20-CF, the replicate midpoint glass transition temperature nor the heat capacity changed. However, the ABS 20-GF material shifted 1.0 °C higher (representing a 0.50 % increase in the onset glass transition temperature). Additionally, ABS 20-GF material increased by 0.70 mW (representing a 789.0 % rise in the change of power to allow the molecular translations).

Endothermic Event

There were not identified changes in replicate analyses for the endothermic peak temperature, the onset temperature nor in the enthalpy analysis by comparing ABS 20-GF to ABS 20-CF. On the other hand, ABS 20-GF noted a change in the heat per mole analysis by 7.0 J/mol. This represented a 10.0 % decline in the heat input to inflict an endothermic event.

Exothermic Event

There were not identified changes in replicate analyses for the onset temperature, this by comparing ABS 20-GF to ABS 20-CF. The secondary exothermic event for ABS 20-GF exhibited a decline in the peak temperature of 2.0 °C and this represented a decrease of 1.80 %, if compared to the secondary analyses for ABS 20-CF. Further, the heat per mole analysis noted a reduction of 17.50 J/mol °C and this signified a 10.0 % decrease of heat released to inflict an exothermic event, this if compared to the secondary analyses for ABS 20-CF

6.7. ABS Filled with Varying Glass Fiber Reinforcement

Glass Transition Event

When comparing the replicates analysis for ABS 40-GF to ABS 20-GF, the midpoint glass transition temperature nor the onset glass transition temperature changed. Whereas, the ABS 40-GF material changed by 0.10 J/g·°C (exhibiting 26.50 % decrease in the heat capacity). Accordingly, the ABS 40-GF material changed by 0.70 mW (representing a 92.5 % decline in the change in power to originate the rearrangement of the polymer matrix segments).

Endothermic Event

There were not perceived changes in replicate analyses for the endothermic peak temperature, this by comparing ABS 40-GF to ABS 20-GF; whereas, the ABS 40-GF material descended by 1.0 °C (representing a 0.70 % decrease in the onset temperature), and the heat per mole analysis changed by 9.10 J/mol (representing a 13.20 % decrease in the absorbed heat to inflict the endotherm). Moreover, ABS 40-GF decreased by 0.20 J/g (representing a 13.80 % decline in the enthalpy upon heating), if compared to ABS 20-GF.

Exothermic Event

The secondary exothermic event for ABS 40-GF exhibited a change in the peak temperature and the onset temperature of 2.0 °C,\ this represented an increase of 1.10 %, if compared to the secondary analyses for ABS 20-GF. Further, the heat per mole analysis noted a reduction of 11.0 J/mol °C and this signified a 16.40 % decrease of heat released to inflict an exothermic event, if compared to the secondary analyses for ABS 20-CF. Ultimately, ABS 40-GF material decreased by 0.20 J/g (representing a 16.40 % decline in the enthalpy), when evaluated against ABS 20-GF.

Chapter 7: Conclusion

7.1. CONCLUSION

Big Area Additive Manufacturing (BAAM) machines, a large area thermoplastic extrusion AM system, offers higher extrusion rates and printing speeds when compared to traditional thermoplastic 3D printers. This emerging technology required the analysis of the thermomechanical properties of composite thermoplastics. This to guide the initial set of BAAM process parameters. Where these parameters have a significant effect on the fabrication of large carbon and glass fiber reinforced parts. This present work aimed to investigate the lack of thermomechanical data in the public landscape of materials in large area AM. The implementation of thermal analyses, thermogravimetry (TGA) and differential scanning calorimetry (DSC), allowed the user to comprehend the molecular interaction of two distinct proprietary engineering polymers composites. Such as, the thermal stability and thermophysical properties for developing best printing parameters. This thesis presented the use of TGA studies to compare the thermal stability, in nitrogen, of acrylonitrile butadiene styrene samples, in pelletized form, containing carbon fiber (CF) and varying glass fiber (GF) reinforcement by weight percentage (20 CF, 20 GF and 40 GF). The obtained one percent decomposition temperatures of ABS material ranged from (259.0 °C to 267.0 °C). Specifically, ABS 40-GF, compounded by Techmer, had a one percent weight loss at a temperature of 267.0 °C. This represented a 2.70% increase (7.0 °C higher) in thermal degradation temperature, when compared ABS 40-GF to ABS 20-GF (267.0°C versus 260.0°C). Proprietary ABS 20-GF, compounded by SABIC, experienced a one percent decomposition temperature of 295.0 °C. It was also experimentally determined the degradation temperature of poly (ethylene terephthalate)–glycol (PETG), a thermoplastics polyester, containing glass fiber reinforcement (PETG 30-GF), reaching a temperature of at least 361.0 °C. When considering the decomposition step transition events in the TGA profiles, ABS and PETG, it was visually determined a single step transition. The approximate measured weight percentage loss of ABS material ranged from (75.0 wt.% to 58.0 wt.%). Particularly, ABS 40-GF, had a weight

percentage loss of 58.0 wt.%. This represented a 31.40% increase in the conservation of weight percentage, when compared ABS 40-GF to ABS 20-GF (58.0 wt.% versus 76.0 wt.%). Whereas, PETG 30-GF experienced weight percentage loss of 65.0 wt.%. For the residual percentage analyses, a plateau region at 750 °C, based on observations of thermal stability in the TGA curve (were the polymer was no longer susceptible to mass losses), was established to examine the manufacturer-specified filler reinforcement, ABS and PETG, where the remaining residue weight percentage ranged from 22.0 wt.% to 40.0 wt.%. Derivative thermogravimetric data was used to validate the approximate weight loss. As such, the unit less area under the DTG peak integration, ABS and PETG, ranged from 74.0 % to 56.0 %. Therefore, it was shown that the DTG peak integration closely matched to the one-step decomposition weight loss data. Further, DTG information led to examine the maximum rate of degradation attained in the decomposition step transition. When considering the DSC studies of two replicate cycles, in which each contained a heating and cooling scan, it was experimentally determined the glass transition temperature (Tg), the endothermic and exothermic thermal events. For example, the first heating up cycle of ABS material, containing carbon fiber (CF) and varying glass fiber (GF) reinforcement by weight percentage (20 CF, 20 GF and 40 GF), reach midpoint glass transition temperatures of 105.0 °C; however, the secondary heating profile, the ABS materials reached midpoint glass transition temperatures of 107.0 °C. Proprietary ABS 20-GF, compounded by SABIC, experienced in the first heating up cycle midpoint glass transition temperatures of 109.0 °C; whereas, when evaluating the secondary heating DSC curve, the midpoint glass transition temperatures does not increased. Additionally, the initial heating up cycle presented an endothermic thermal event, 20 CF, 20 GF and 40 GF, where the endothermic onset temperature of ABS material ranged from (128.0 °C to 130.0 °C). When compared the secondary and first heating DSC data (131.0°C versus 129.0°C), the midpoint glass transition temperature of ABS material does not demonstrate a substantial increase. Similarly, ABS 20-GF by SABIC, when contrasted the secondary and first heating curves, the endothermic onset temperature does not demonstrate a substantial increase (231.0 °C versus 231.5 °C). In the examination of the first and secondary cooling down plots, the obtained exothermic onset temperature of ABS material, 20 CF,

20 GF and 40 GF, ranged from (123.0 °C to 125.0 °C). Likewise, regarding ABS 20 wt.% GF (SABIC), when compared the initial and secondary cooling down cycles (239.20°C versus 239.0°C °C), the exothermic onset temperature does not demonstrate a major change. PETG 30-GF, on the contrary, achieved a midpoint glass transition temperature of up to 78.0°C as compared to 77.0°C for a replicate heating cycle. In addition, the first and replicate heating profiles presented an exothermic thermal event, where PETG 30-GF reached onset exothermic temperatures of 231.0 °C. When considering the first and second cooling down data, it was noted that endothermic onset temperature of PETG 30-GF does not demonstrate a substantial change, where PETG 30-GF reached temperatures of 239.0 °C.

7.2. RECOMMENDATIONS

Future work on thermal characterization on engineering thermoplastic composites should include TGA/DTG and DSC studies under air to identify the thermo-oxidative degradation and thermomechanical data for large-area AM, since this research only accounted for inert conditions. Further, it is recommended to consider the impact of pre-drying and storage conditions, that is currently done before printing in BAAM, on the thermomechanical properties. In addition, master batching is recommended to optimize the data dispersion of the collected results. These examinations may reveal realistic results for BAAM printing that were not taken in consideration in this research. Similarly, the integration of moisture absorption in PETG should also be pursued to study the effect on thermomechanical properties, since PETG is hygroscopic. Lastly, future research efforts on TGA and DSC should encompass the construction of induction time plots in the context of thermal and thermo-oxidative degradation.

References

1. Aduba, D. C., Margaretta, E. D., Marnot, A. E., Heifferon, K. V., Surbey, W. R., Chartrain, N. A., … Williams, C. B. (2019). Vat photopolymerization 3D printing of acid-cleavable PEG-methacrylate networks for biomaterial applications. *Materials Today Communications*, *19*, 204–211. doi: 10.1016/j.mtcomm.2019.01.003
2. Ahmad, N., Gopinath, P., & Dutta, R. (2019). *3D printing technology in nanomedicine*. St. Louis, MO: Elsevier. doi:10.1016/C2017-0-03828-4
3. Askeland, D. R., & Wright, W. J. (2015). *The Science and Engineering of Materials* (7th ed.). Boston: Cengage Learning.
4. ASTM International. (2002). *ASTM D4673-02 Standard Classification System for Acrylonitrile-Butadiene-Styrene (ABS) Plastics and Alloys Molding and Extrusion Materials*. Retrieved from https://doi.org/10.1520/D4673-02
5. ASTM International. (2014). *ASTM E1356-08(2014) Standard Test Method for Assignment of the Glass Transition Temperatures by Differential Scanning Calorimetry*. Retrieved from https://doi.org/10.1520/E1356-08R14
6. ASTM International. (2015). *ASTM E1142-15 Standard Terminology Relating to Thermophysical Properties*. Retrieved from https://doi.org/10.1520/E1142-15
7. ASTM International. (2017). *ASTM E2550-17 Standard Test Method for Thermal Stability by Thermogravimetry*. Retrieved from https://doi.org/10.1520/E2550-17
8. ASTM International. (2018). *ASTM E473-18 Standard Terminology Relating to Thermal Analysis and Rheology*. Retrieved from https://doi.org/10.1520/E0473-18
9. ASTM International. (2019). *ASTM D883-19c Standard Terminology Relating to Plastics*. Retrieved from https://doi.org/10.1520/D0883-19C
10. Balderrama-Armendariz, C. O., Macdonald, E., Roberson, D. A., Ruiz-Huerta, L., Maldonado-Macias, A., Valadez-Gutierrez, E., … Espalin, D. (2019). Folding behavior of thermoplastic hinges fabricated with polymer extrusion additive manufacturing. *The International Journal of Advanced Manufacturing Technology*, 1–13. doi: 10.1007/s00170-019-04196-x
11. Biron, M. (2018). *Thermoplastics and thermoplastic composites* (3rd ed.). Oxford: William Andrew Applied Science /Elsevier. doi:10.1016/C2017-0-01099-6
12. Brandt, M. (2017). *Laser additive manufacturing: Materials, Design, Technologies, and Applications*. Amsterdam: Elsevier, Woodhead. doi: 10.1016/C2014-0-03891-9
13. BPF. (n.d.). British Plastics Federation: A History of Plastics. Retrieved December 1, 2019, from https://www.bpf.co.uk/plastipedia/plastics_history/default.aspx.
14. California Department of Public Health. (1990). *Styrene*. Richmond, CA.: Hazard Evaluation System & Information Service, California Dept. of Health Services, Occupational Health Branch.

15. Chergui, A., Hadj-Hamou, K., & Vignat, F. (2018). Production scheduling and nesting in additive manufacturing. *Computers and Industrial Engineering*, *126* (May), 292– 301. https://doi.org/10.1016/j.cie.2018.09.048

16. Cordella, C., Moussa, I., Martel, A.-C., Sbirrazzuoli, N., & Lizzani-Cuvelier, L. (2002). Recent Developments in Food Characterization and Adulteration Detection: Technique-Oriented Perspectives. *Journal of Agricultural and Food Chemistry*, *50*(7), 1751–1764. doi: 10.1021/jf011096z

17. Corkery, M. (2019, August 12). A Giant Factory Rises to Make a Product Filling Up the World: Plastic. Retrieved December 1, 2019, from https://www.nytimes.com/2019/08/12/business/energy-environment/plastics-shell-pennsylvania-plant.html.

18. Compton, B. G., Post, B. K., Duty, C. E., Love, L., & Kunc, V. (2017). Thermal analysis of additive manufacturing of large-scale thermoplastic polymer composites. *Additive Manufacturing*, *17*, 77–86. doi: 10.1016/j.addma.2017.07.006

19. Dupaix, R. B. (2003). *Temperature and rate dependent finite strain behavior of poly (ethylene terephthalate) and poly (ethylene terephthalate)-glycol above the glass transition temperature* (Doctoral dissertation, Massachusetts Institute of Technology).

20. Espalin, David, "Development of a multi-material, multi-technology FDM system for process improvement experimentation" (2012). ETD Collection for University of Texas, El Paso. AAI1533221

21. Espalin, David, "High Feed Rate Wire Heating and Embedding for Large Area Additive Manufacturing of Parts Containing Embedded Electronic Functionality" (2017). *ETD Collection for University of Texas, El Paso*. AAI10825126 https://digitalcommons.utep.edu/dissertations/AAI10825126

22. Gibson, I., Rosen, D. W., & Stucker, B. (2016). *Additive manufacturing technologies: 3D printing, rapid prototyping, and direct digital manufacturing*. New York: Springer. doi: 10.1007/978-1-4939-2113-3

23. Gilbert, M. (2017). *Brydson's Plastics Materials* (8th ed.). Kidlington, Oxford, United Kingdom: Butterworth-Heinemann, an imprint of Elsevier.

24. González-Vidal, N., Martínez De Ilarduya, A., & Muñoz-Guerra, S. (2009). Poly (ethylene-co-1, 4-cyclohexylenedimethylene terephthalate) copolyesters obtained by ring opening polymerization. *Journal of Polymer Science Part A: Polymer Chemistry, 47* (22), 5954-5966.

25. Gibson, I., Rosen, D. W., & Stucker, B. (2016). *Additive manufacturing technologies: 3D printing, rapid prototyping, and direct digital manufacturing* (2nd. ed.). New York: Springer. doi:10.1007/978-1-4939-2113-3

26. Gooch, J. W. (2007). *Encyclopedic dictionary of polymers with 710 figures and 38 tables*. New York, NY: Springer.

27. Heyes, G. B. (2018). ASTM E691–87 Standard Practice for Conducting an Interlaboratory Study to Determine the Precision of a Test Method. *Journal of Quality Technology*, *25*(4), 313–314. https://doi.org/10.1080/00224065.1993.11979478

28. Hitachi High-Tech Science Corporation. (1995). *Thermal Decomposition Measurement of ABS resin I - Analysis by Quasi-Isothermal TG/FTIR Measurements* (TA NO. 66.). Tokio: Hitachi

29. Hughes, K., Meek, M. E., Walker, M., Beauchamp, R., & International Programme on Chemical Safety. (2001). *1,3-Butadiene: Human health aspects*. Geneva: World Health Organization.

30. International Programme on Chemical Safety INCHEM. (2001, March). Acrylonitrile. Retrieved December 1, 2019, from http://www.inchem.org/documents/icsc/icsc/eics0092.htm.

31. International Programme on Chemical Safety INCHEM. (2017, April). 1,3-Butadiene. Retrieved December 1, 2019, from http://www.inchem.org/documents/icsc/icsc/eics0017.htm.

32. International Programme on Chemical Safety INCHEM. (2006, April). Styrene. Retrieved December 1, 2019, from http://www.inchem.org/documents/icsc/icsc/eics0073.htm.

33. Kutz, M. (2017). *Applied plastics engineering handbook: Processing, materials, and applications* (2nd ed.). Kidlington, Oxford, United Kingdom: William Andrew, an imprint of Elsevier. doi:10.1016/C2014-0-04118-4

34. Larson, E. R. (2015). *Thermoplastic material selection: A practical guide*. Amsterdam: Elsevier. doi:10.1016/C2013-0-18851-4

35. Long, G., Meek, M. E., Cureton, P., & International Programme on Chemical Safety. (2002). *Acrylonitrile*. Geneva: World Health Organization.

36. Love, L. J., Kunc, V., Rios, O., Duty, C. E., Elliott, A. M., Post, B. K., … Blue, C. A. (2014). The importance of carbon fiber to polymer additive manufacturing. *Journal of Materials Research*, *29*(17), 1893–1898. doi: 10.1557/jmr.2014.212

37. McKeen, L. W. (2014). *The Effect of Long Term Thermal Exposure on Plastics and Elastomers*. Oxford: William Andrew. doi:10.1016/C2013-0-00091-6

38. Menczel, J. D., & Prime, R. B. (2009). *Thermal analysis of polymers: Fundamentals and applications*. Hoboken, NJ: John Wiley. doi:10.1002/9780470423837

39. Mireles, Jorge, "Process study and control of electron beam melting technology using infrared thermography" (2013). *ETD Collection for University of Texas, El Paso*. AAI1551238. https://digitalcommons.utep.edu/dissertations/AAI1551238

40. National Center for Biotechnology Information. PubChem Database. Styrene, CID=7501, https://pubchem.ncbi.nlm.nih.gov/compound/Styrene (accessed on July. 21, 2019)

41. National Center for Biotechnology Information. PubChem Database. 1,3-Butadiene, CID=7845, https://pubchem.ncbi.nlm.nih.gov/compound/1_3-Butadiene (accessed on July 31, 2019)

42. National Center for Biotechnology Information. PubChem Database. Acrylonitrile, CID=7855, https://pubchem.ncbi.nlm.nih.gov/compound/Acrylonitrile (accessed on July 21, 2019)

43. Neff, C., Trapuzzano, M., & Crane, N. B. (2018). Impact of vapor polishing on surface quality and mechanical properties of extruded ABS. *Rapid Prototyping Journal*, *24*(2), 501–508. doi: 10.1108/rpj-03-2017-0039

44. New Jersey Department of Health. (2011). *Right to Know Hazardous Substance Fact Sheets: Styrene monomer*. Trenton, NJ.: New Jersey Department of Health.

45. Paszkiewicz, S., Szymczyk, A., Pawlikowska, D., Irska, I., Taraghi, I., Pilawka, R., . . . Piesowicz, E. (2017). Synthesis and characterization of poly(ethylene terephthalate-co-1,4-cyclohexanedimethylene terephtlatate)-block- poly(tetramethylene oxide) copolymers. *RSC Advances,7*(66), 41311-41954. doi:10.1039/c7ra07172h

46. Paszkiewicz, S, Taraghi, I, Pawlikowska, D, et al. Influence of hybrid system of nanofillers on the functional properties of postconsumer PET-G–based nanocomposites. *Polym Adv Technol*. 2019; 1– 10. https://doi.org/10.1002/pat.4729

47. Polymer Chemistry. (n.d.). Retrieved November 30, 2019, from https://www.acs.org/content/acs/en/careers/college-to-career/areas-of-chemistry/polymer-chemistry.html.

48. Ranade, A. , D'Souza, N. , Thellen, C. and Ratto, J. A. (2005), Surfactant concentration effects on amorphous PETG–montmorillonite layered silicate (MLS) nanocomposite films. Polym. Int., 54: 875-881. doi:10.1002/pi.1777

49. Roschli, A., Gaul, K. T., Boulger, A. M., Post, B. K., Chesser, P. C., Love, L. J., … Borish, M. (2019). Designing for Big Area Additive Manufacturing. Additive Manufacturing, 25(September 2018), 275–285. https://doi.org/10.1016/j.addma.2018.11.006

50. Rosemond, Z., Chou, S., Wilson, J., Schwartz, M., Tomei-Torres, F., ATSDR, … Citra, M. (2010). *Toxicological profile for styrene*. Atlanta, GA: U.S. Dept. of Health and Human Services, Public Health Service, Agency for Toxic Substances and Disease Registry.

51. Rothon, R., & DeArmitt, C. (2017). Fillers (Including Fiber Reinforcements). *Brydson's Plastics Materials*, 169–204. https://doi.org/10.1016/B978-0-323-35824-8.00008- 6

52. Scheirs, J. (2000). *Compositional and failure analysis of polymers: A practical approach*. Chichester: Wiley.

53. Stevenson, A. C. (1948). Ammonolysis. *Industrial and Engineering Chemistry*, *40*(9), 1584–1589. https://doi.org/10.1021/ie50465a006

54. Suzuki, M., & Wilkie, C. A. (1995). T*he thermal degradation of acrylonitrile-butadiene-styrene terpolymei as studied by TGA/FTIR. Polymer Degradation and Stability*, 47(2), 217–221. doi:10.1016/0141-3910(94)00122-o

55. The Basics: Polymer Definition and Properties. (n.d.). Retrieved November 30, 2019, from https://plastics.americanchemistry.com/plastics/The-Basics/.

56. Thomas, D. S. (2013). Economics of the U.S. Additive Manufacturing Industry. doi: 10.6028/nist.sp.1163

57. White, W. C. (2007). Butadiene production process overview. *Chemico-Biological Interactions*, *166*(1–3), 10–14. https://doi.org/10.1016/j.cbi.2007.01.009

58. Yang, M.-H. (2000). *The thermal degradation of acrylonitrile-butadiene-styrene terpolymer under various gas conditions*. Polymer Testing, 19(1), 105–110. https://doi.org/10.1016/S0142-9418(98)00067-1

59. Yang, S., Rafael Castilleja, J., Barrera, E. V., & Lozano, K. (2004). Thermal analysis of an acrylonitrile–butadiene–styrene/SWNT composite. *Polymer Degradation and Stability*, *83*(3), 383–388. https://doi.org/10.1016/J.POLYMDEGRADSTAB.2003.08.002

60. Zhang, N., Bao, X. X., Tan, Z. Y., Sun, S. L., Zhou, C., Yang, H. D. and Zhang, H. X. (2007), *Morphology and mechanical properties of ABS blends prepared from emulsion-polymerized PB-g-SAN impact modifier with AIBN as initiator.* J. Appl. Polym. Sci., 105: 1237-1243. doi:10.1002/app.26035

61. Zhang, J., & Jung, Y.-G. (2018). Additive manufacturing: materials, processes, quantifications and applications. Cambridge, MA: Butterworth-Heinemann. doi: 10.1016/C2016-0-01595-4

Appendix A

A.1. TGA ABS 20-CF

ABS 20 wt. % CF (carbon fiber) reinforced by weight, compounded by Techmer PM Polymer Modifiers:

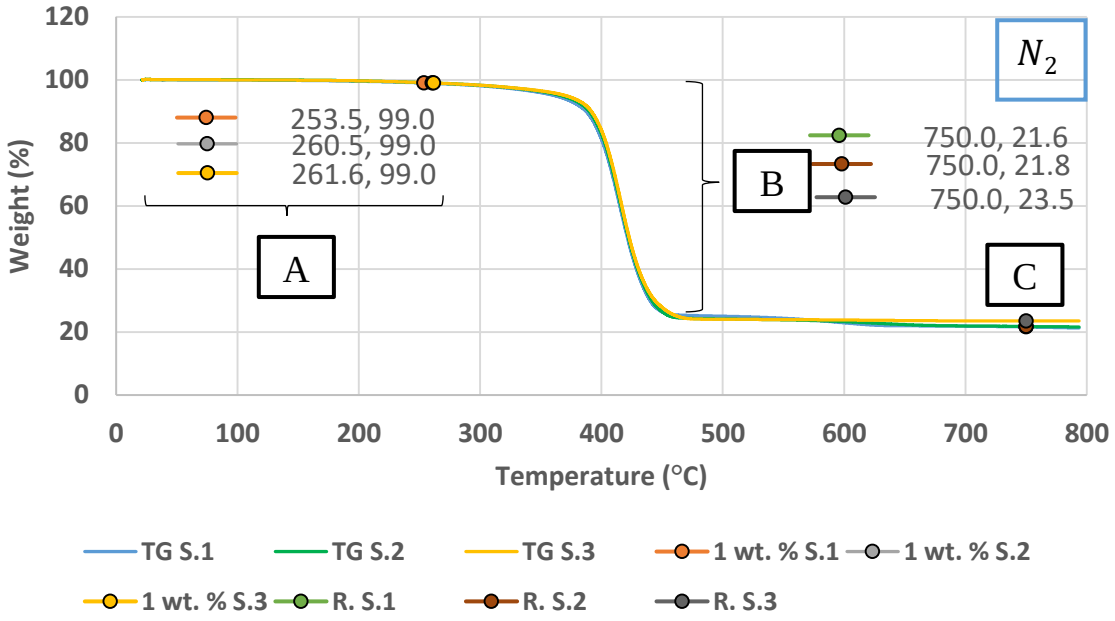

Figure A.1:The TGA readings obtained from three ABS 20-CF samples after heated to a temperature of 800 °C in nitrogen.

A.2. DTG ABS 20-CF

ABS 20 wt. % CF (carbon fiber) reinforced by weight, compounded by Techmer PM Polymer Modifiers:

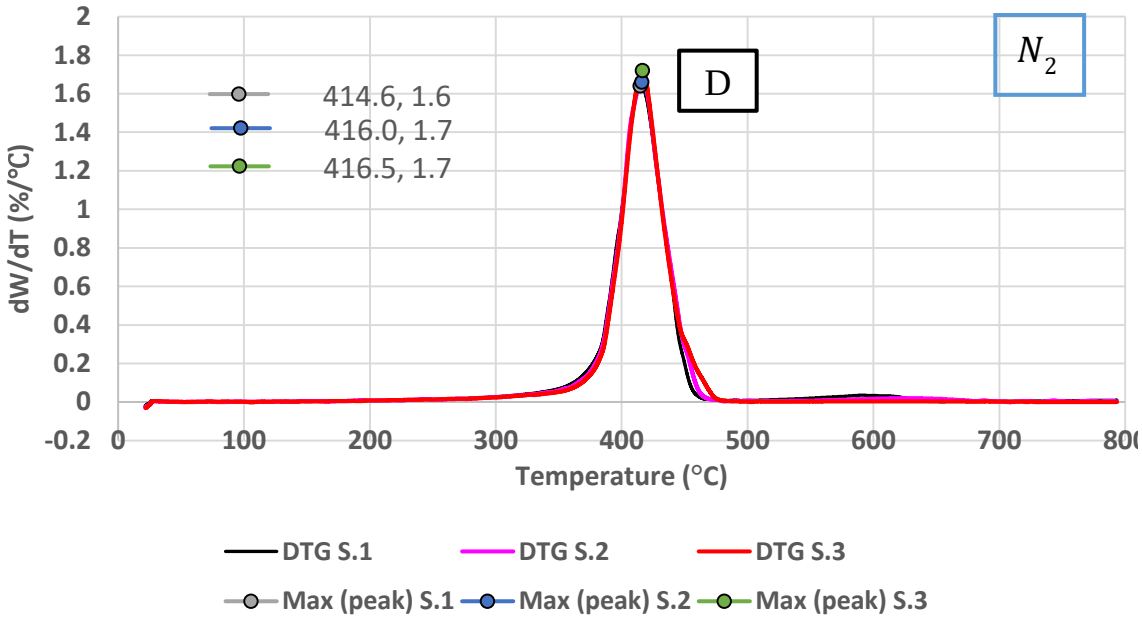

Figure A.2: The DTG readings obtained from three ABS 20-CF samples after heated to a temperature of 800 °C in nitrogen.

A.3. TGA ABS 20-CF (Average)

ABS 20 wt. % CF (carbon fiber) reinforced by weight, compounded by Techmer PM Polymer Modifiers:

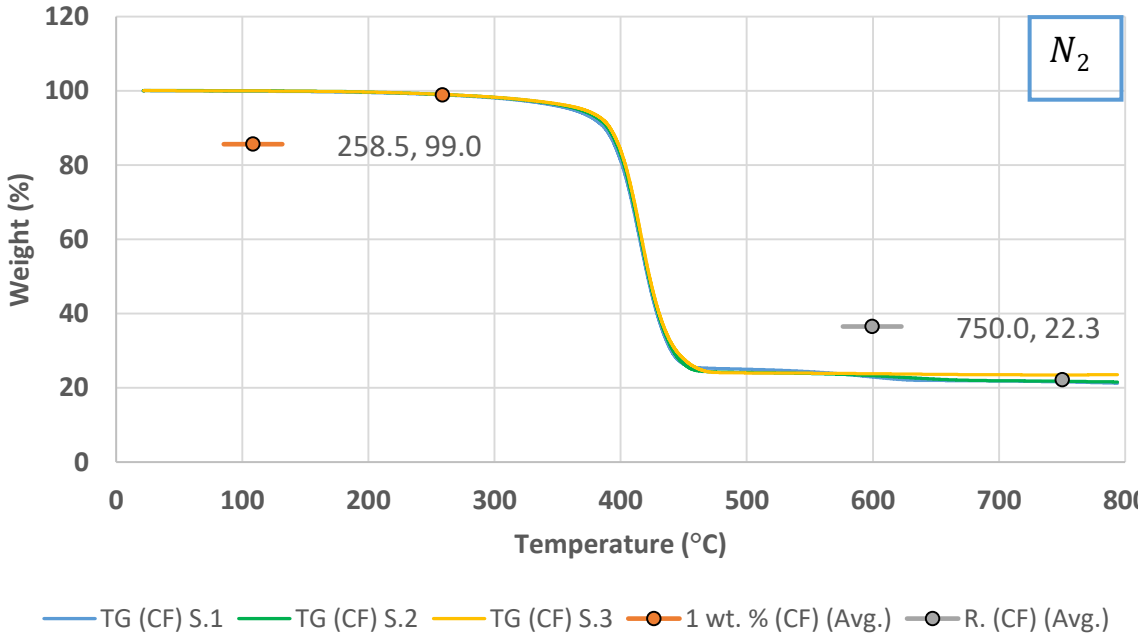

Figure A.3: The arithmetic averages for the 1 % percentage weight loss and residual analyses at 750 °C, obtained from three ABS 20-CF samples.

A.4. DTG ABS 20-CF (Average)

ABS 20 wt. % CF (carbon fiber) reinforced by weight, compounded by Techmer PM Polymer Modifiers:

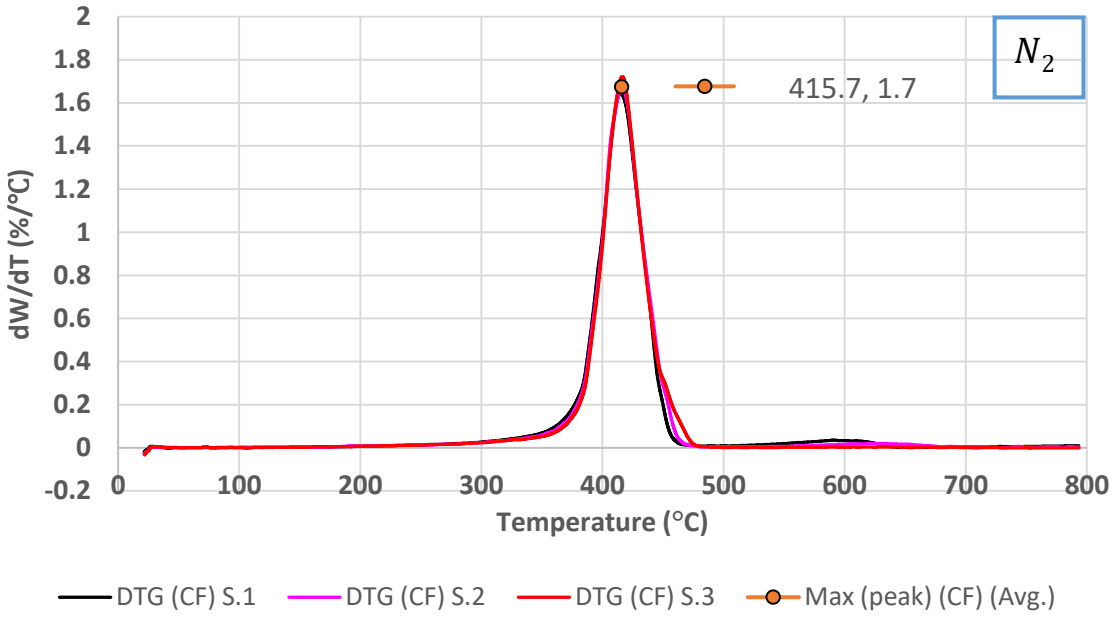

Figure A.4: The arithmetic averages for the maximum peak temperature analysis, obtained from the DTG curves of three ABS 20-CF samples.

A.5. TGA ABS 20-GF

ABS 20 wt. % GF (glass fiber) reinforced by weight, compounded by Techmer PM Polymer Modifiers:

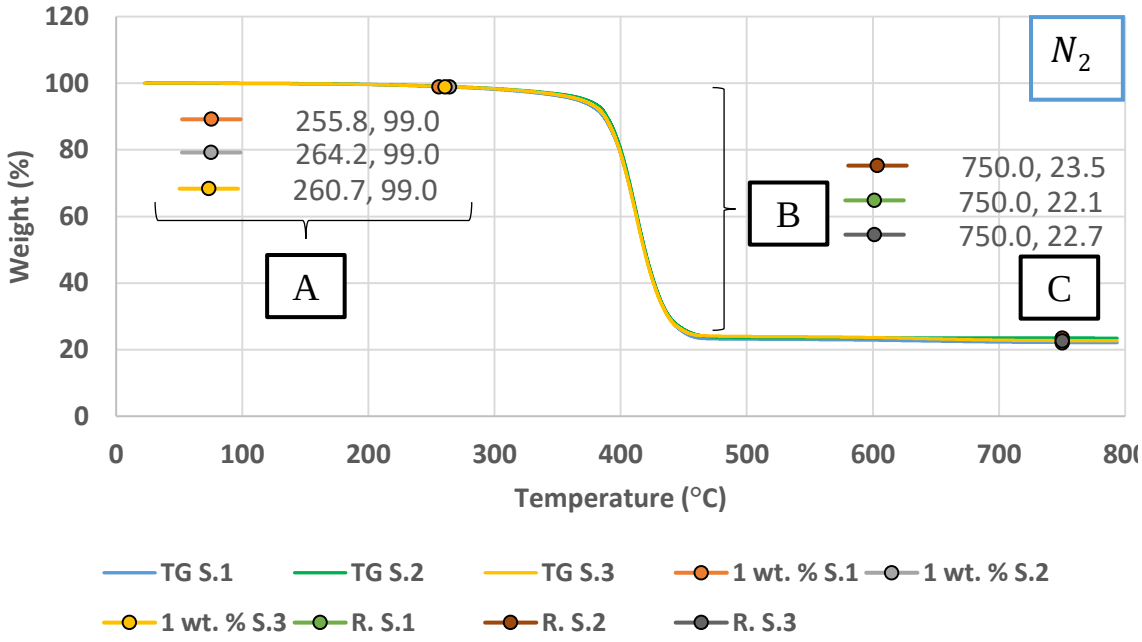

Figure A.5: The TGA readings obtained from three ABS 20-GF samples after heated to a temperature of 800 °C in nitrogen.

A.6. DTG ABS 20-GF

ABS 20 wt. % GF (glass fiber) reinforced by weight, compounded by Techmer PM Polymer Modifiers:

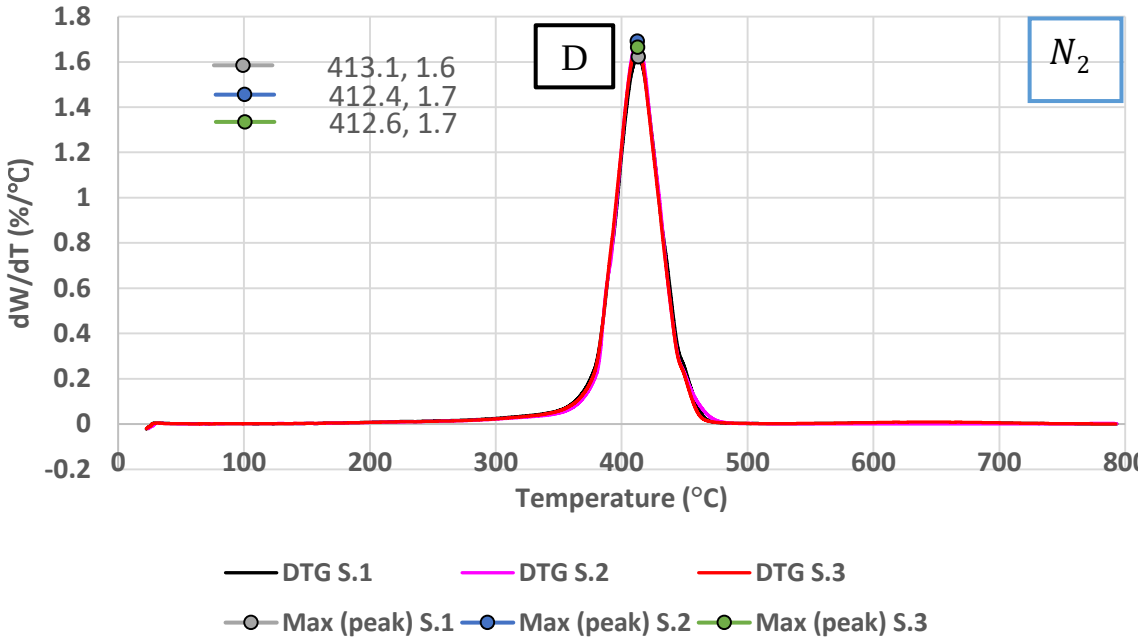

Figure A.6: The DTG readings obtained from three ABS 20-GF samples after heated to a temperature of 800 °C in nitrogen.

A.7. TGA ABS 20-GF (Average)

ABS 20 wt. % GF (glass fiber) reinforced by weight, compounded by Techmer PM Polymer Modifiers:

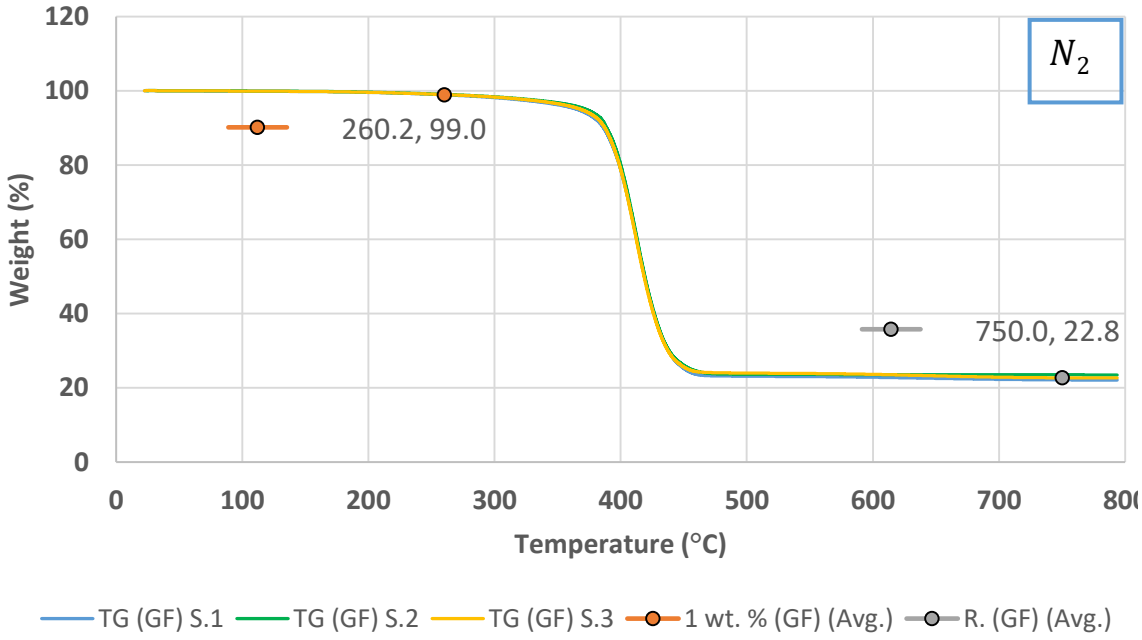

Figure A.7: The arithmetic averages for the 1 % percentage weight loss and residual analyses at 750 °C, obtained from three ABS 20-GF samples.

A.8. DTG ABS 20-GF (Average)

ABS 20 wt. % GF (glass fiber) reinforced by weight, compounded by Techmer PM Polymer Modifiers:

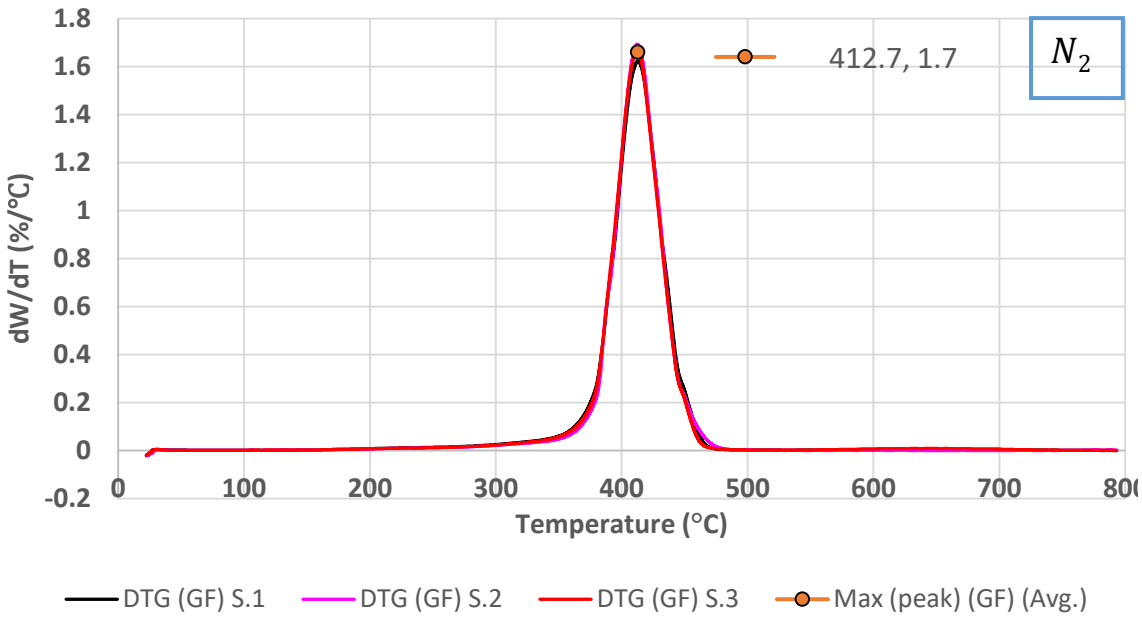

Figure A.8: The arithmetic averages for the maximum peak temperature analysis, obtained from the DTG curves of three ABS 20-GF samples.

A.9. TGA ABS 40-GF

ABS 40 wt. % GF (glass fiber) reinforced by weight, compounded by Techmer PM Polymer Modifiers:

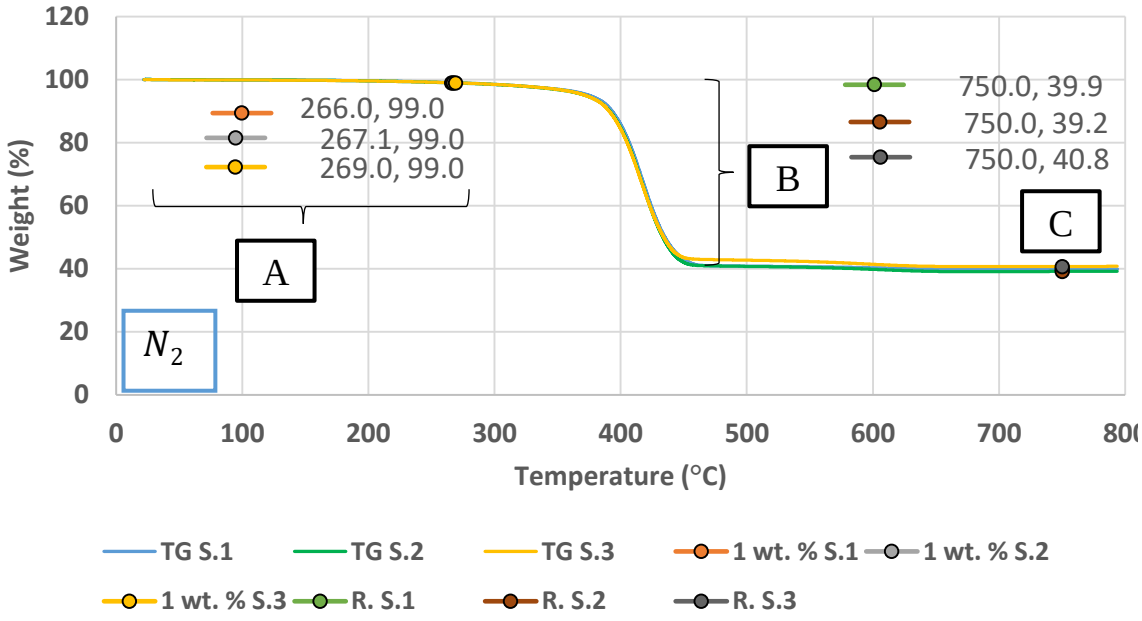

Figure A.9: The TGA readings obtained from three ABS 40-GF samples after heated to a temperature of 800 °C in nitrogen.

A.10. DTG ABS 40-GF

ABS 40 wt. % GF (glass fiber) reinforced by weight, compounded by Techmer PM Polymer Modifiers:

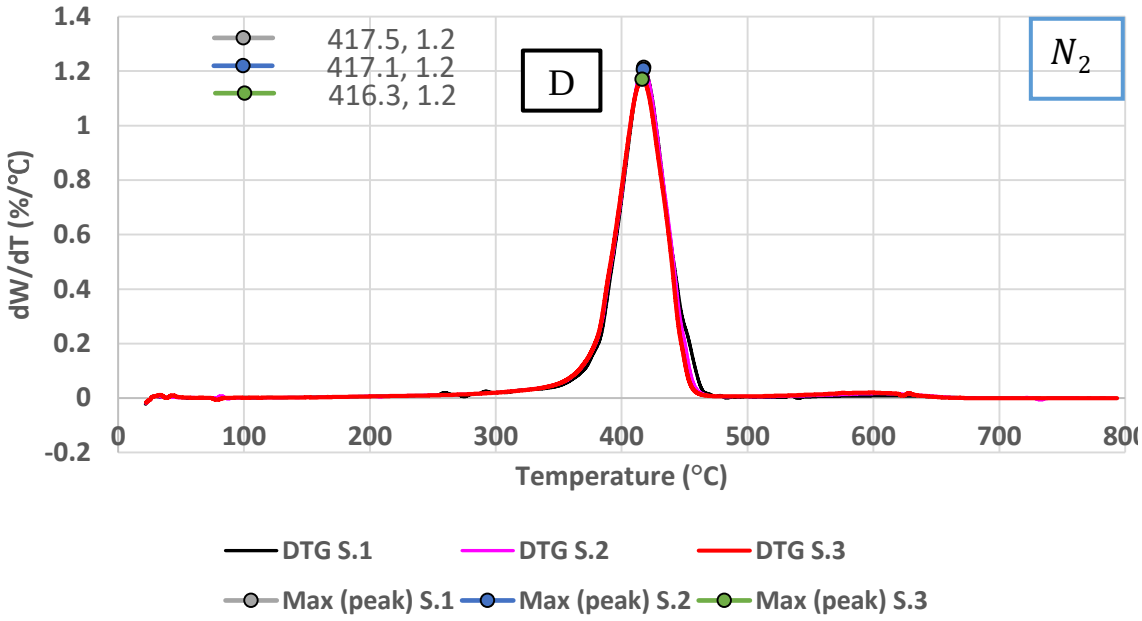

Figure A.10: The DTG readings obtained from three ABS 40-GF samples after heated to a temperature of 800 °C in nitrogen.

A.11. TGA ABS 40-GF (Average)

ABS 40 wt. % GF (glass fiber) reinforced by weight, compounded by Techmer PM Polymer Modifiers:

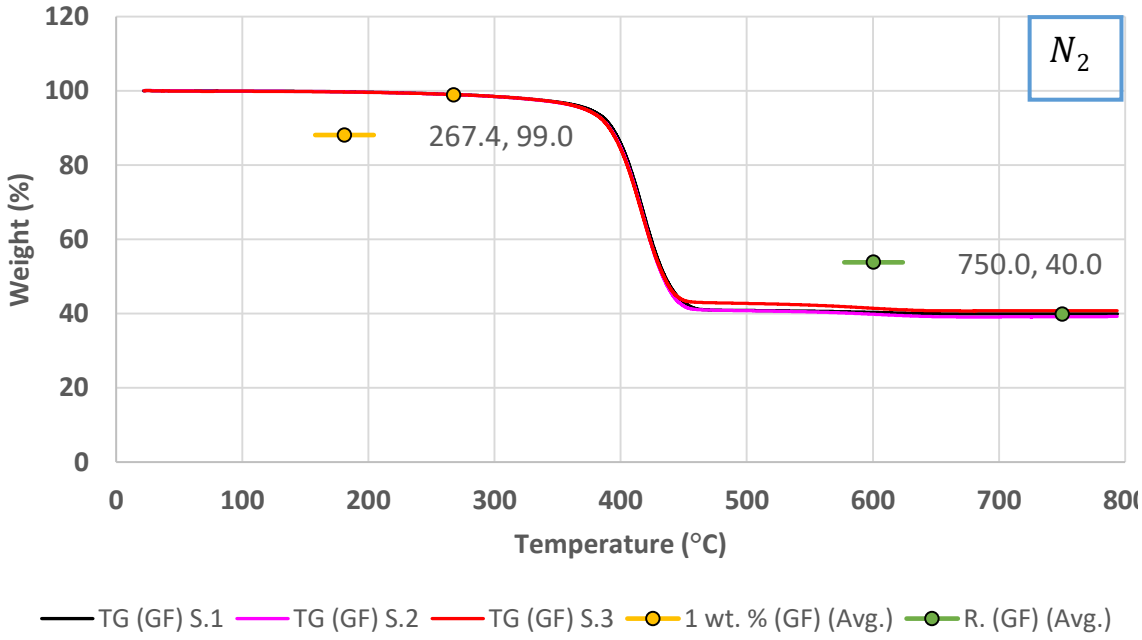

Figure A.11: The arithmetic averages for the 1 % percentage weight loss and residual analyses at 750 °C, obtained from three ABS 40-GF samples.

A.12. DTG ABS 40-GF (Average)

ABS 40 wt. % GF (glass fiber) reinforced by weight, compounded by Techmer PM Polymer Modifiers:

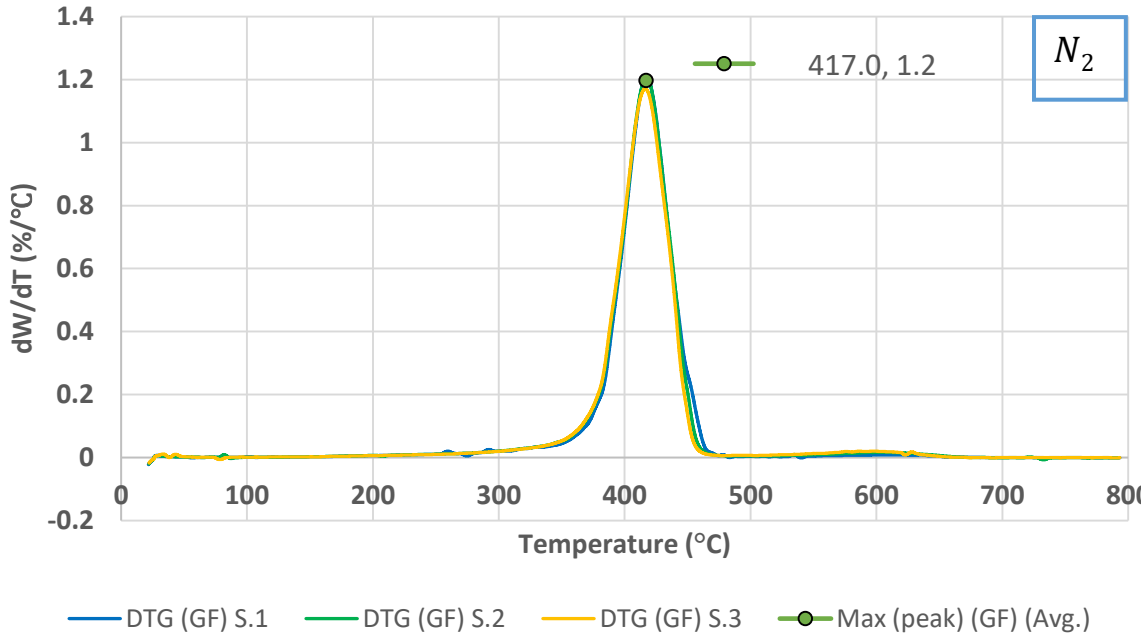

Figure A.12: DTG curves of ABS 40 wt. % GF arithmetic averages for the maximum peak temperature analysis.

A.13. TGA ABS 20-GF (SABIC)

ABS 20 wt. % GF reinforced by weight compounded by SABIC:

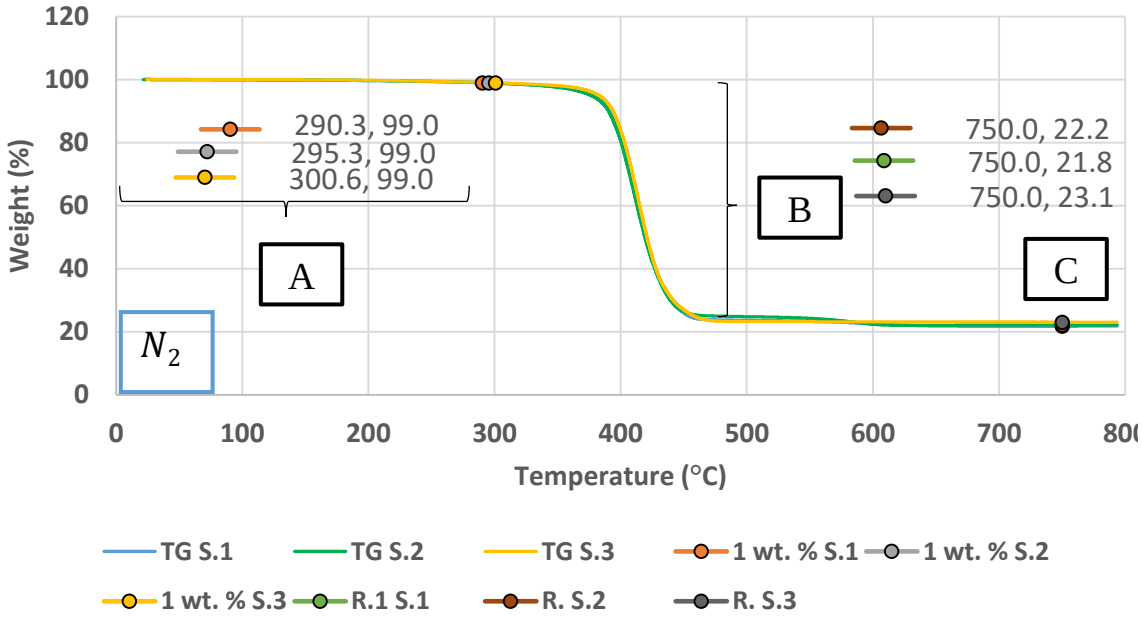

Figure A.13: The TGA readings obtained from three ABS 20-GF samples, by SABIC, after heated to a temperature of 800 °C in nitrogen.

A.14. DTG ABS 20-GF (SABIC)

ABS 20 wt. % GF reinforced by weight compounded by SABIC:

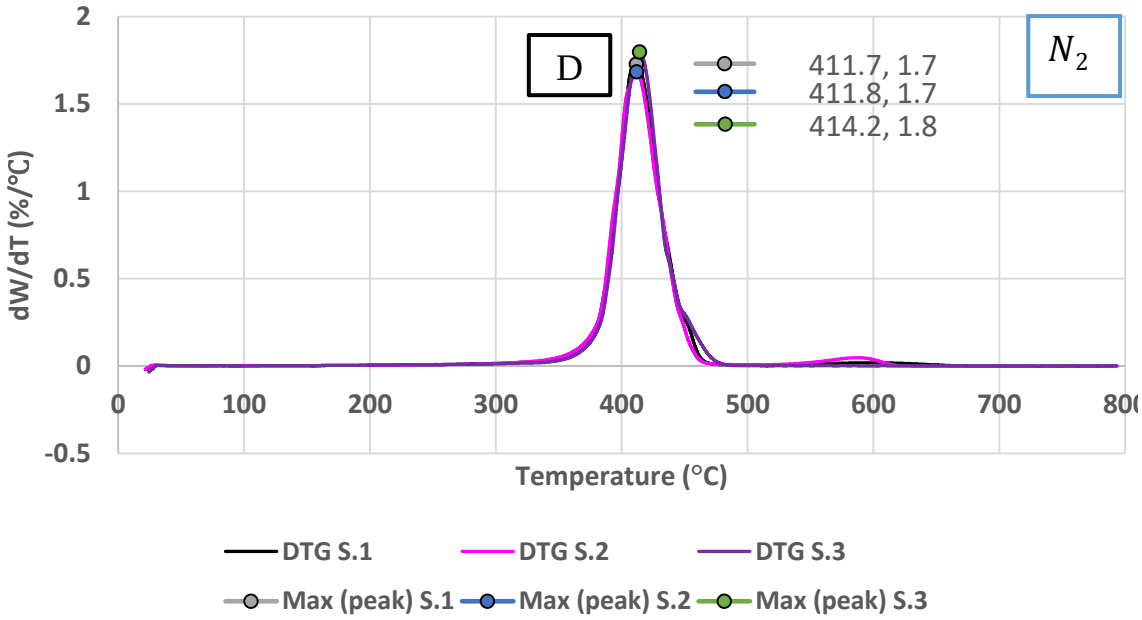

Figure A.14: The DTG readings obtained from three ABS 20-GF samples, by SABIC, after heated to a temperature of 800 °C in nitrogen.

A.15. TGA ABS 20-GF (SABIC) (Average)

ABS 20 wt. % GF reinforced by weight compounded by SABIC:

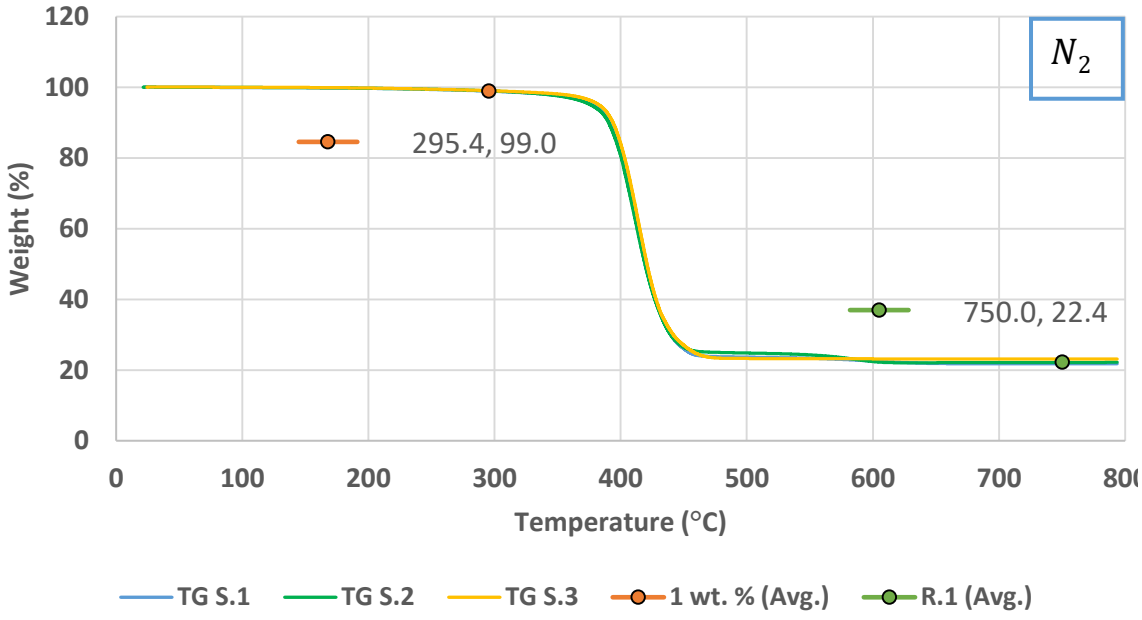

Figure A.15: The arithmetic averages for the 1 % percentage weight loss and residual analyses at 750 °C, obtained from three ABS 20-GF samples by SABIC.

A.16. DTG ABS 20-GF (SABIC) (Average)

ABS 20 wt. % GF reinforced by weight compounded by SABIC:

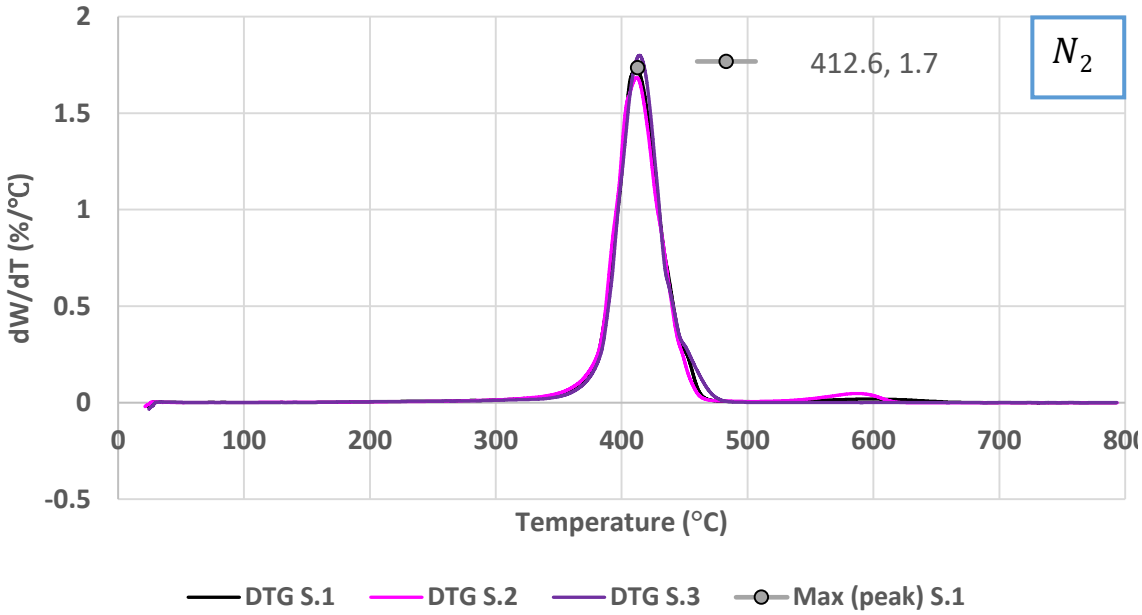

Figure A.16: The arithmetic averages for the maximum peak temperature analysis, obtained from the DTG curves of three ABS 20-GF samples by SABIC.

A.17. TGA PETG 30-GF

PETG 30 wt. % GF reinforced by weight, compounded by Techmer PM Polymer Modifiers:

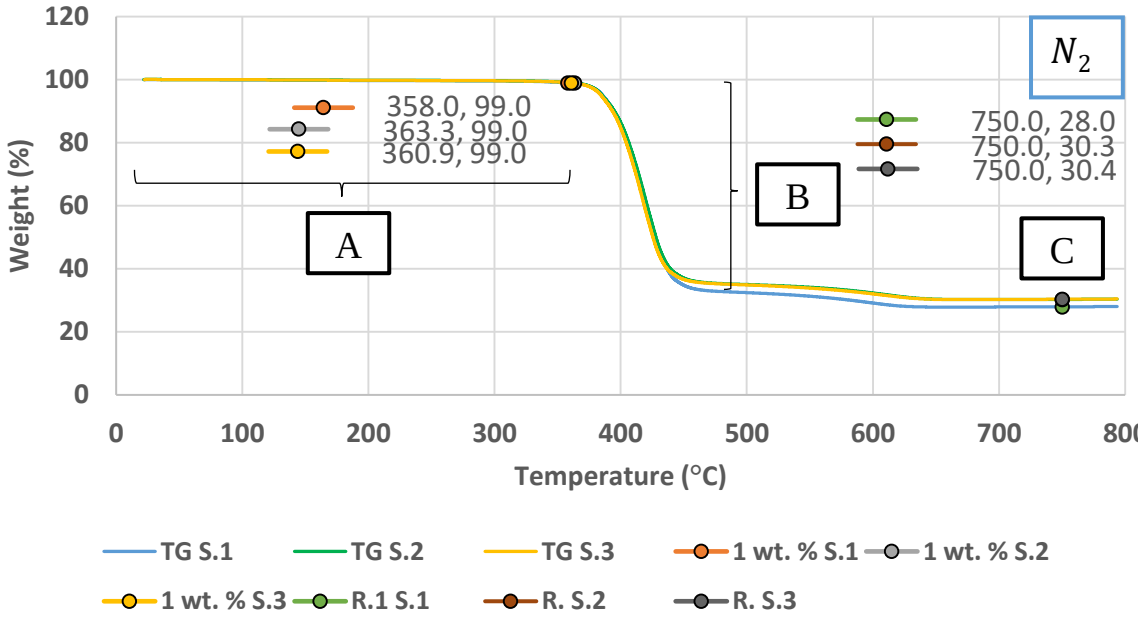

Figure A.17: The TGA readings obtained from three PETG 30-GF samples after heated to a temperature of 800 °C in nitrogen.

A.18. DTG PETG 30-GF

PETG 30 wt. % GF reinforced by weight, compounded by Techmer PM Polymer Modifiers:

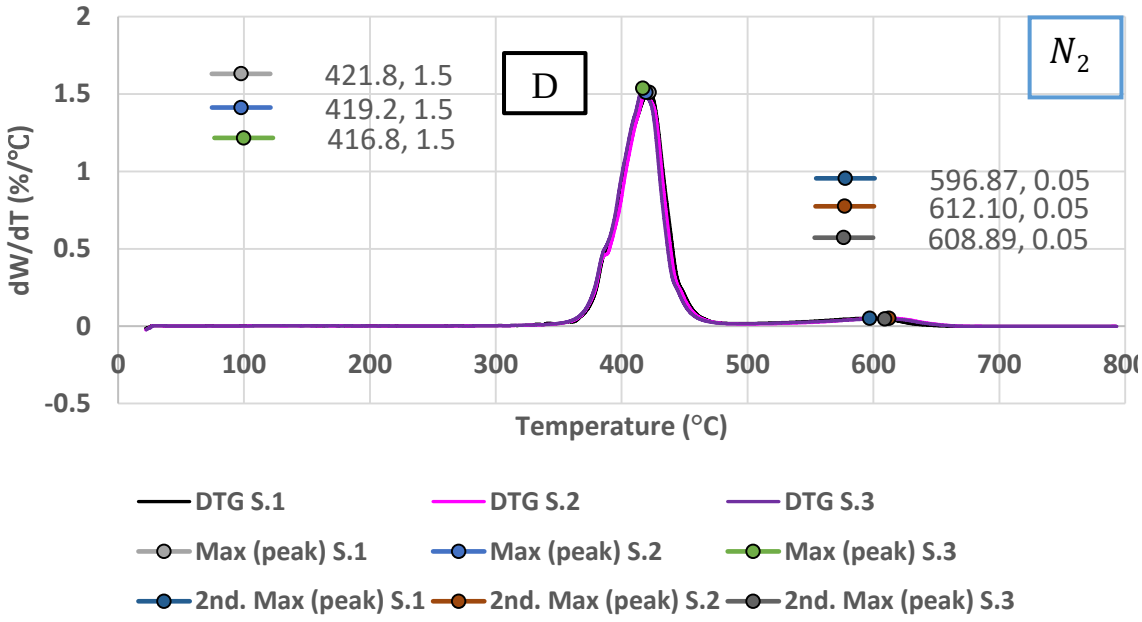

Figure A.18. The DTG readings obtained from three PETG 30-GF samples after heated to a temperature of 800 °C in nitrogen.

A.19. TGA PETG 30-GF (Averages)

PETG 30 wt. % GF reinforced by weight, compounded by Techmer PM Polymer Modifiers:

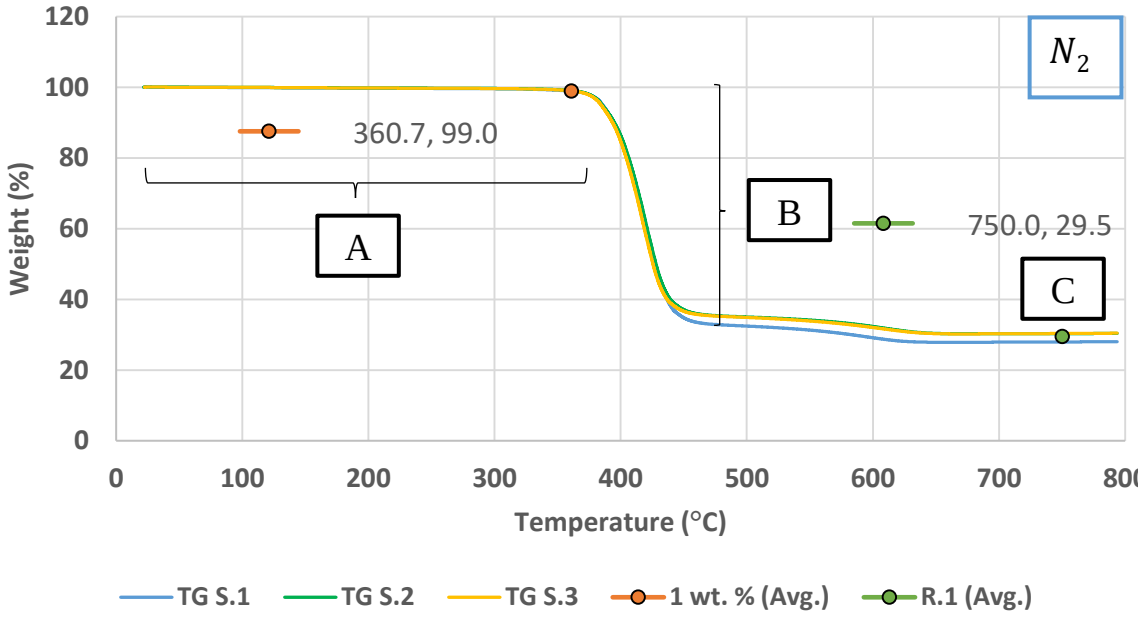

Figure A.19: The arithmetic averages for the 1 % percentage weight loss and residual analyses at 750 °C, obtained from three PETG 30-GF samples.

A.20. DTG PETG 30-GF (Averages)

PETG 30 wt. % GF reinforced by weight, compounded by Techmer PM Polymer Modifiers:

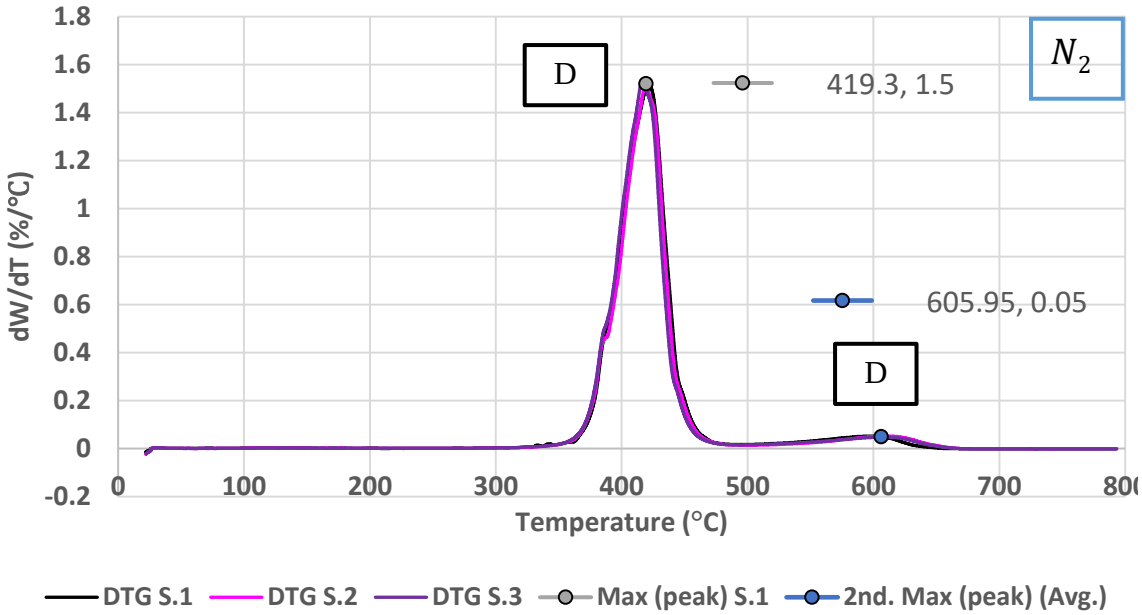

Figure A.20: The arithmetic averages for the maximum peak temperature analysis, obtained from the DTG curves of three PETG 30-GF samples.

A.21. The Trios Analysis for ABS 20-CF (S.1.)

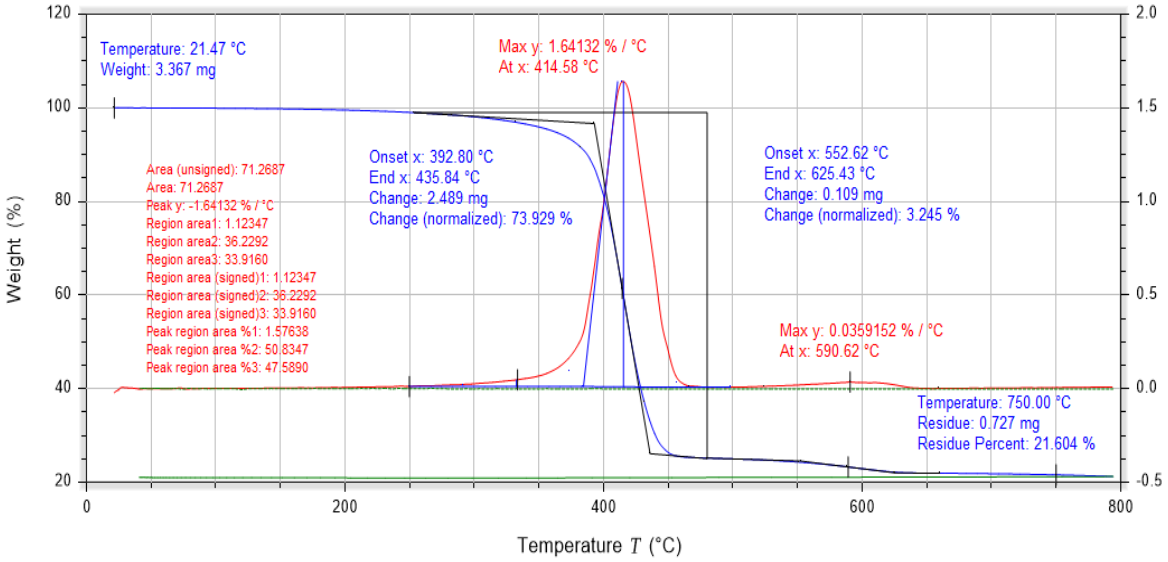

Figure A.21: The inert thermal stability history of the first ABS 20-CF, TG/DTG curves, sample. Notice that all the retrieved Trios graphs in Appendix A are courtesy of Trios v.4.5.0. software package.

A.22. The Trios Analysis for ABS 20-CF (S.2.)

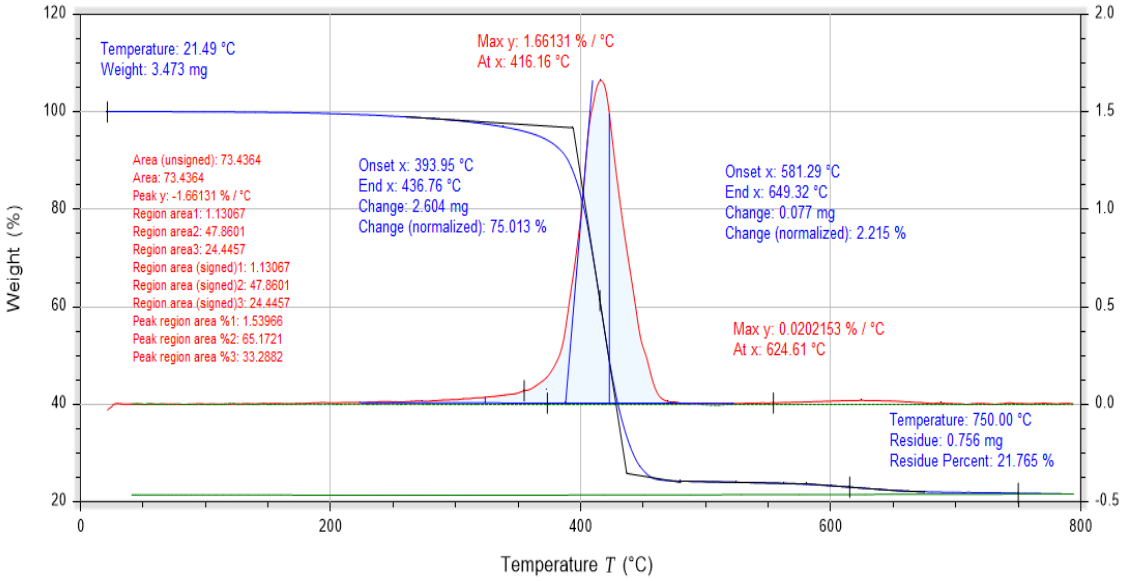

Figure A.22: The inert thermal stability history of the second ABS 20-CF sample.

A.23. The Trios Analysis for ABS 20-CF (S.3.)

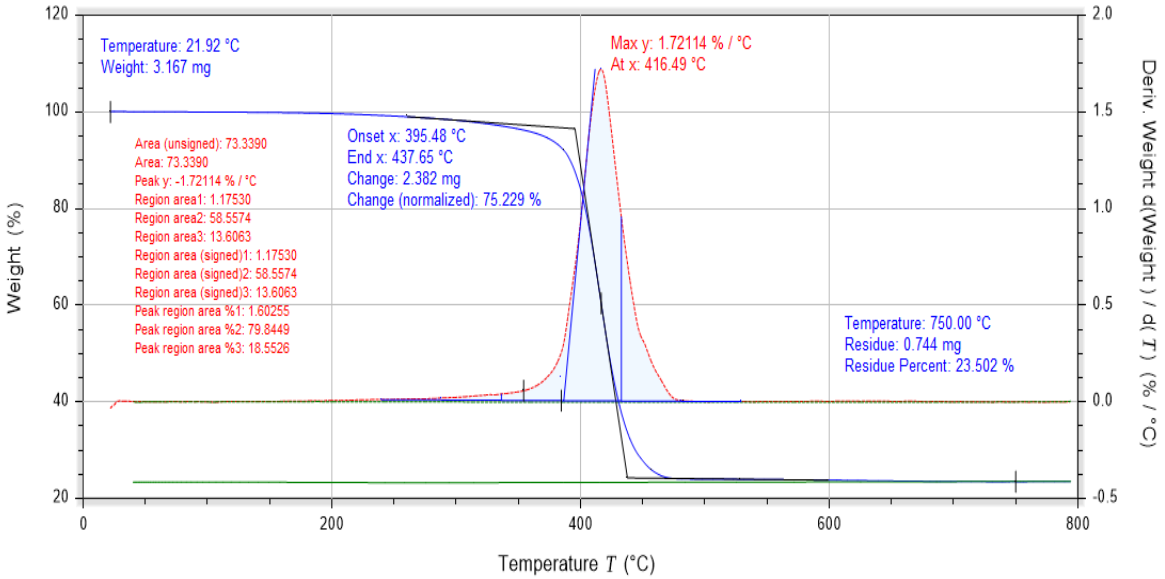

Figure A.23: The inert thermal stability history of the third ABS 20-CF sample.

A.24. The Trios Analysis for ABS 20-GF (S.1.)

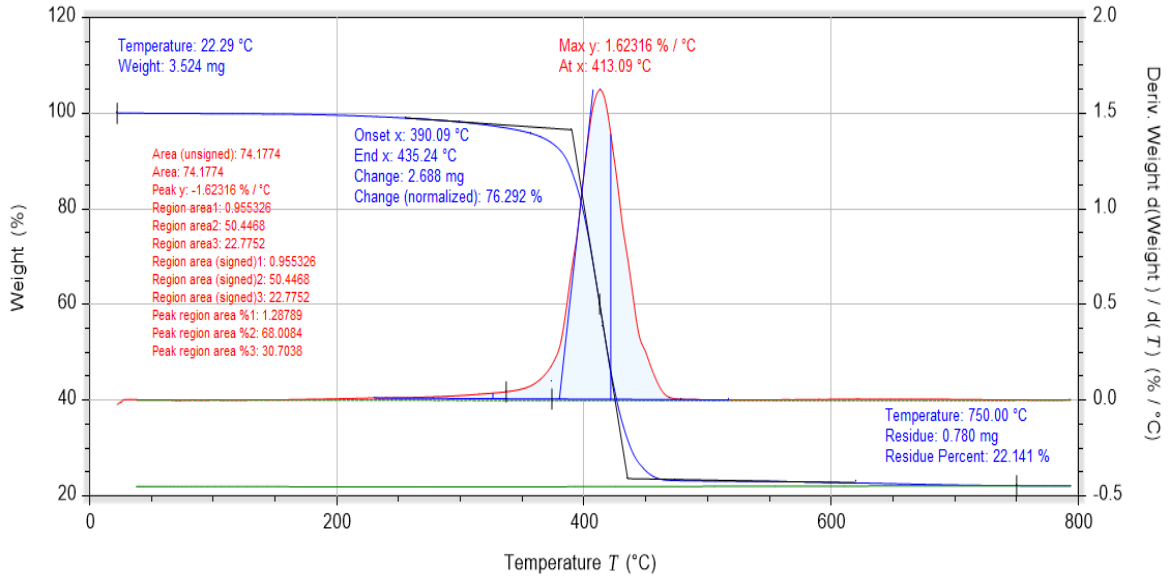

Figure A.24: The inert thermal stability history of the first ABS 20-GF sample.

A.25. The Trios Analysis for ABS 20-GF (S.2.)

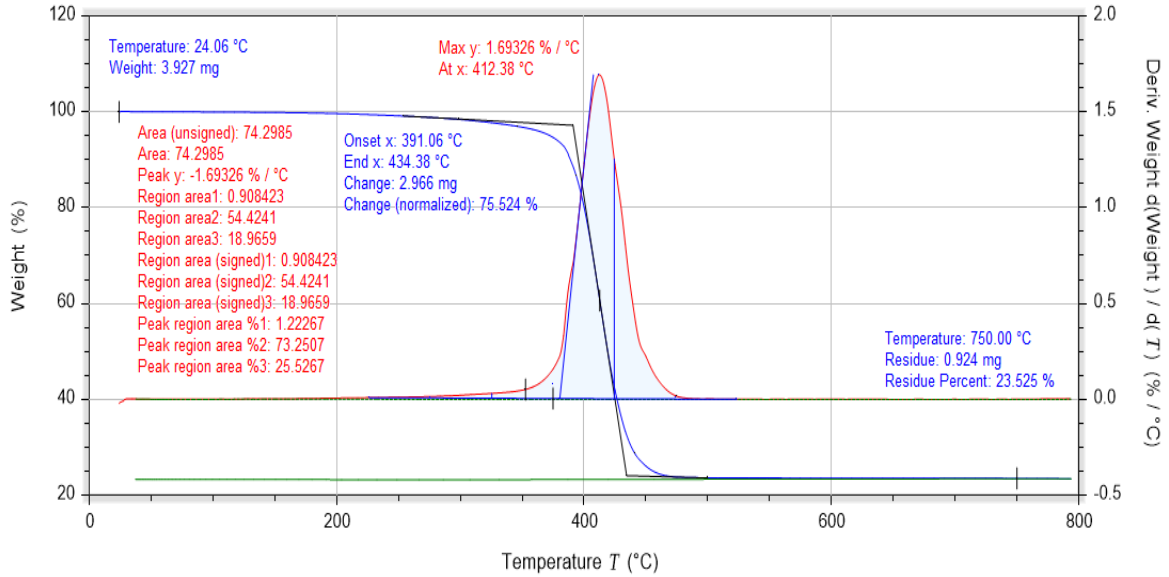

Figure A.25: The inert thermal stability history of the second ABS 20-GF sample.

A.26. The Trios Analysis for ABS 20-GF (S.3.)

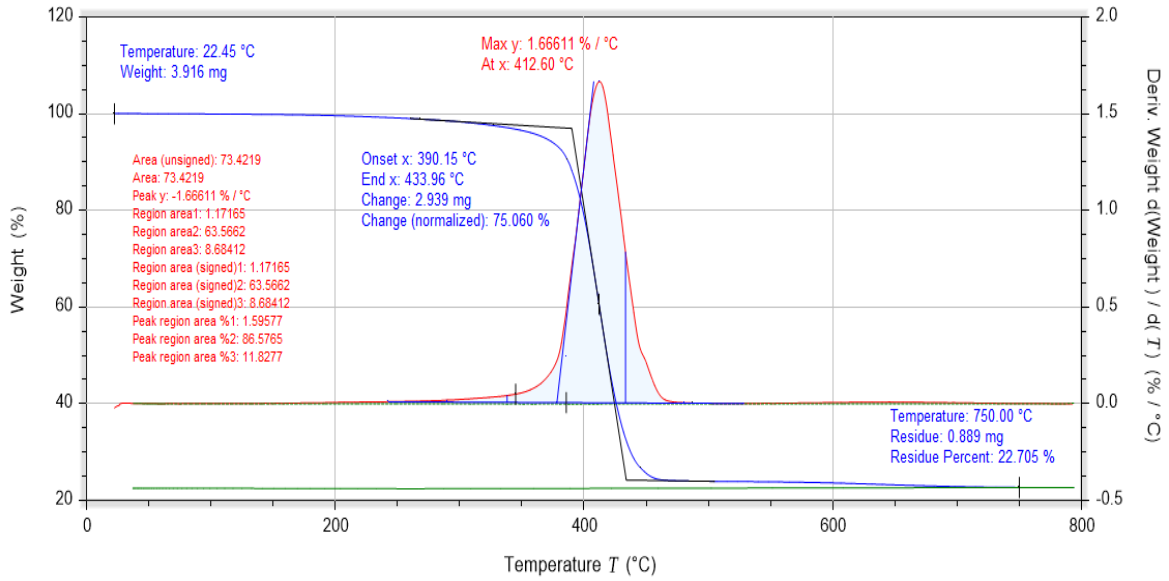

Figure A.26: The inert thermal stability history of the third ABS 20-GF sample.

A.27. The Trios Analysis for ABS 40-GF (S.1.)

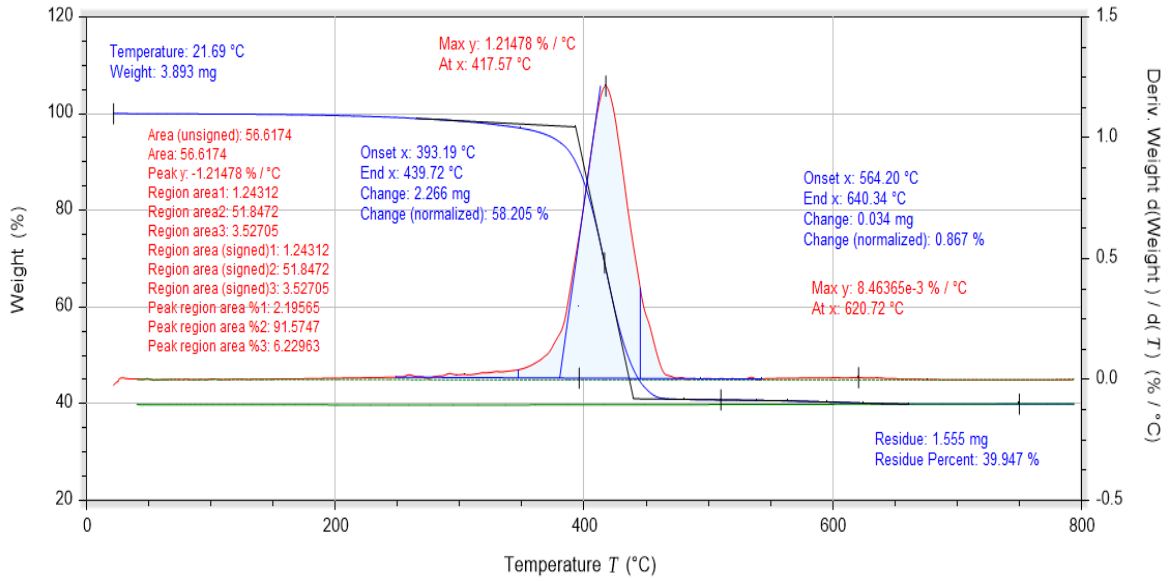

Figure A.27: The inert thermal stability history of the first ABS 40-GF sample

A.28. The Trios Analysis for ABS 40-GF (S.2.)

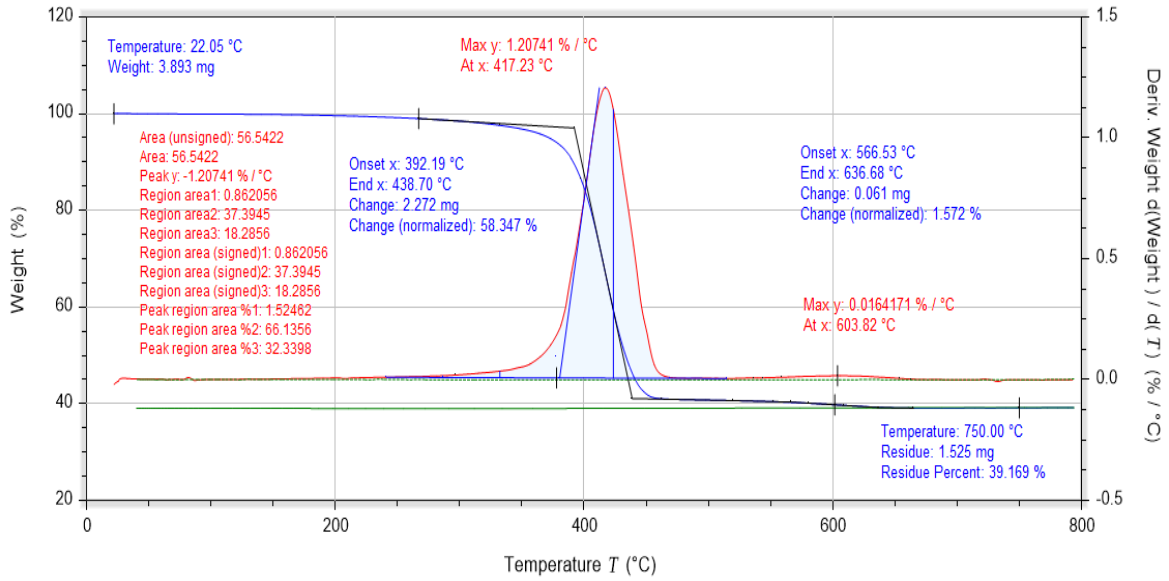

Figure A.28: The inert thermal stability history of the second ABS 20-GF sample.

A.29. The Trios Analysis for ABS 40-GF (S.3.)

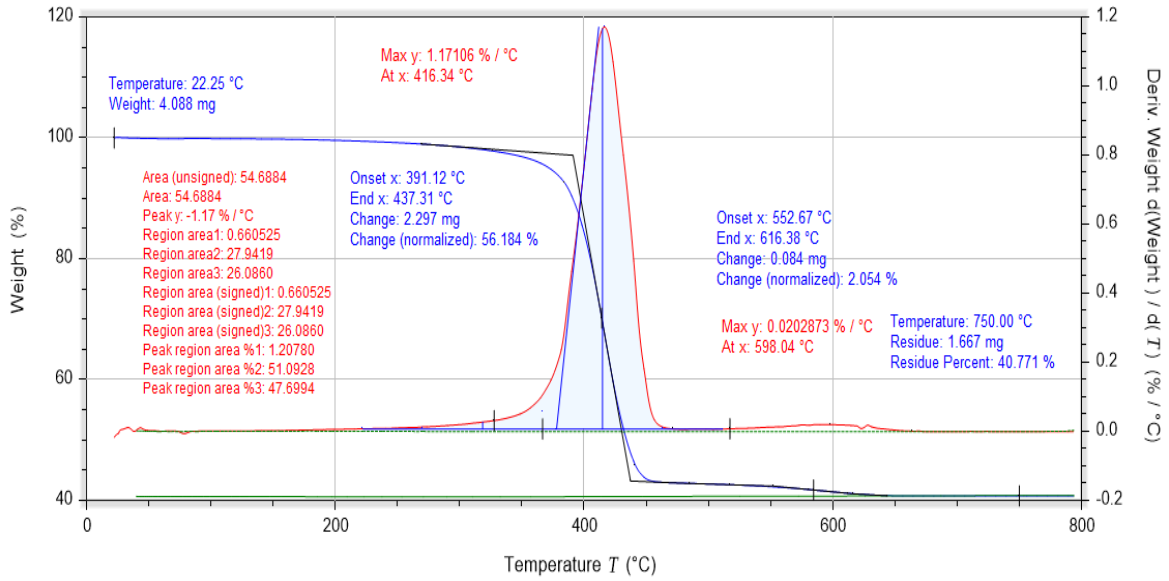

Figure A.29: The inert thermal stability history of the third ABS 40-GF sample.

A.30. The Trios Analysis for ABS 20-GF (SABIC) (S.1.)

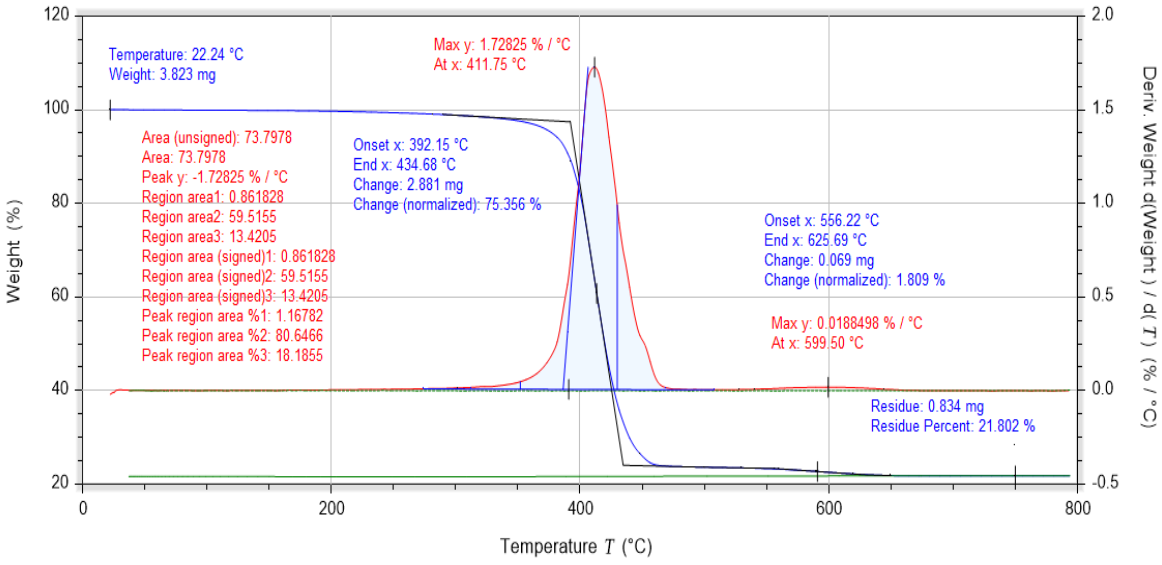

Figure A.30: The inert thermal stability history of the first ABS 20-GF (SABIC) sample.

A.31. The Trios Analysis for ABS 20-GF (SABIC) (S.2.)

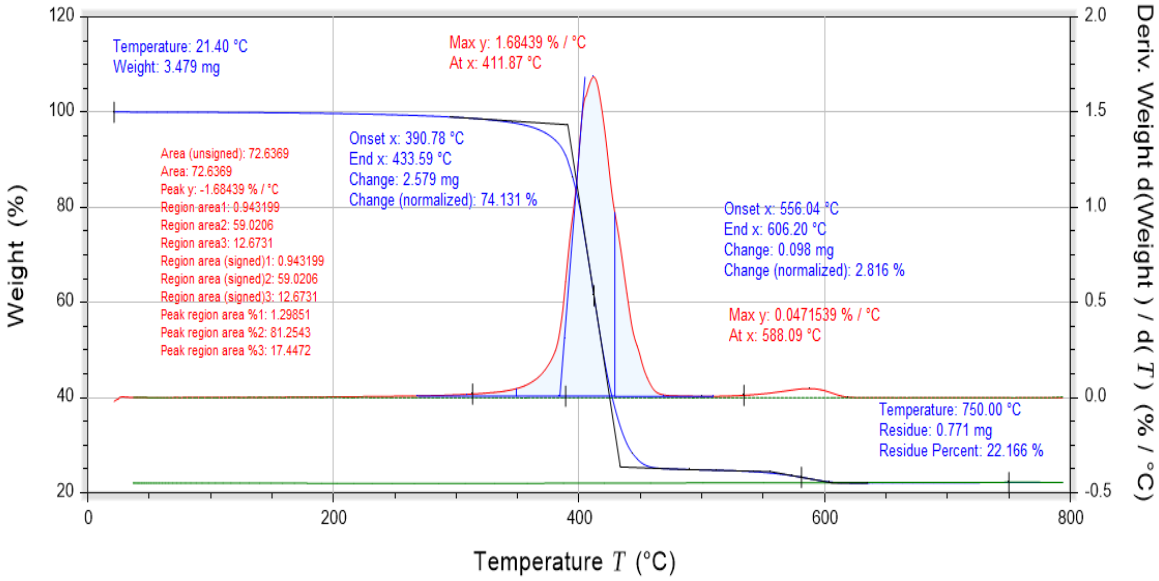

Figure A.31: The inert thermal stability history of the second ABS 20-GF (SABIC) sample.

A.32. The Trios Analysis for ABS 20-GF (SABIC) (S.3.)

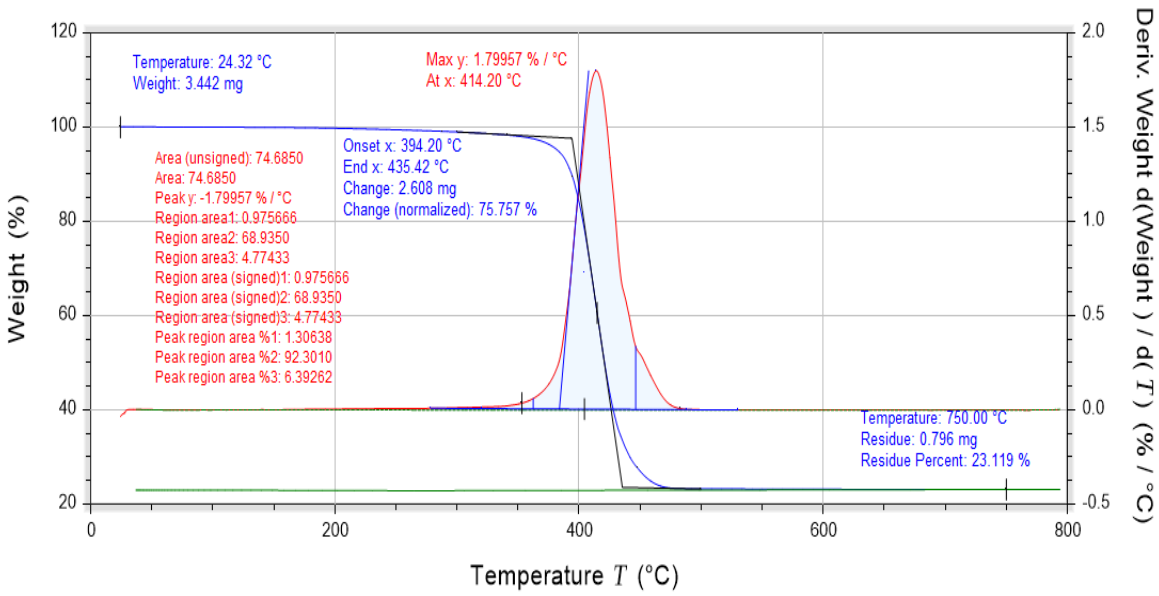

Figure A.32: The inert thermal stability history of the third ABS 20-GF (SABIC) sample.

A.33. The Trios Analysis for PETG 30-GF (S.1.)

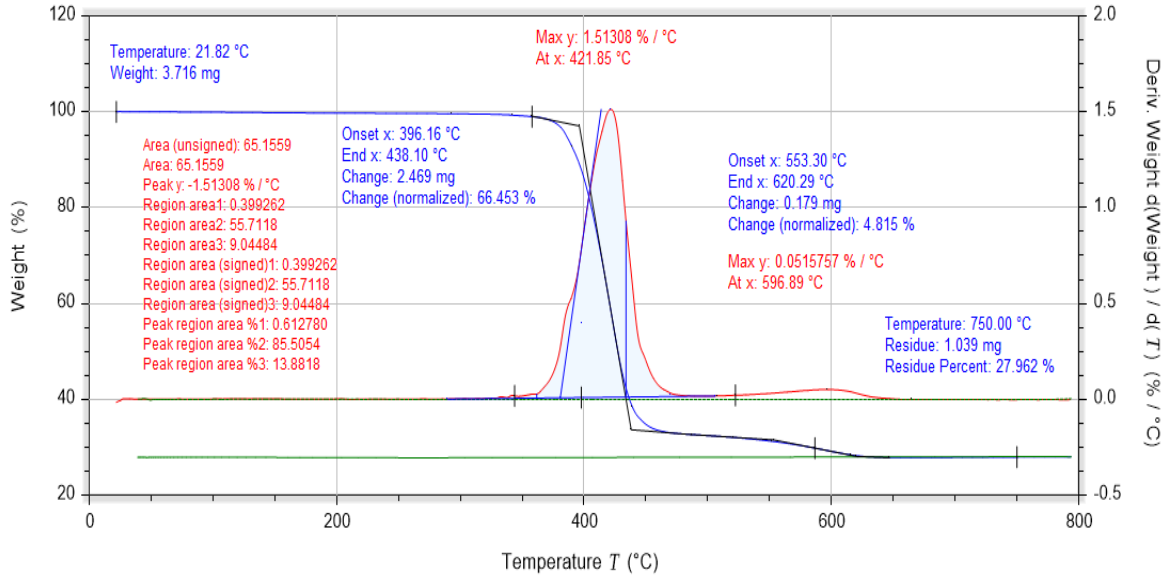

Figure A.33: The inert thermal stability history of the first PETG 30-GF (SABIC) sample.

A.34. The Trios Analysis for PETG 30-GF (S.2.)

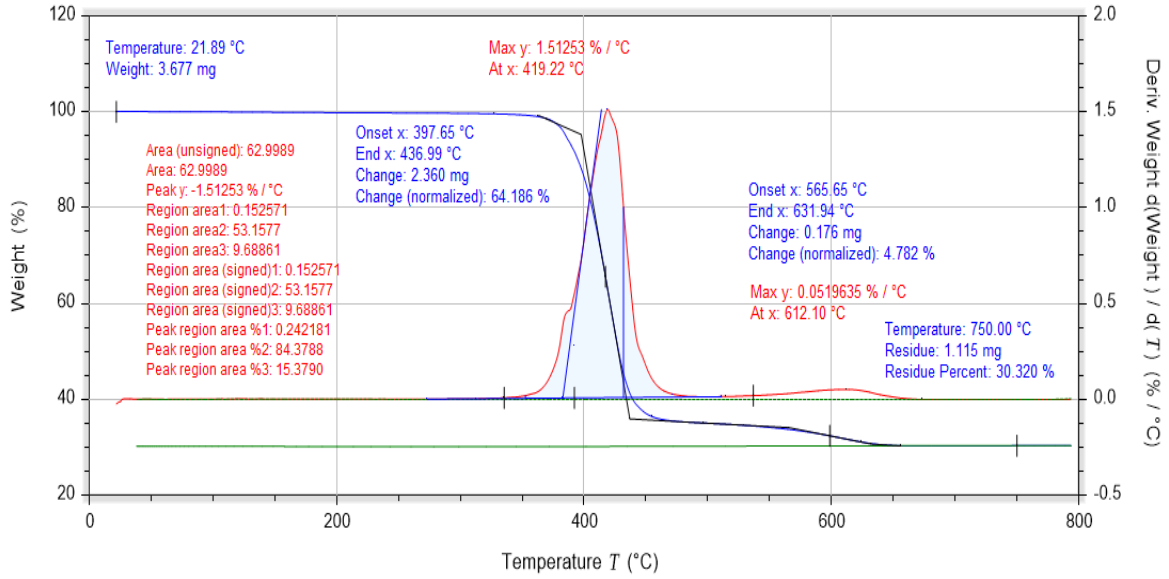

Figure A.34: The inert thermal stability history of the second PETG 30-GF (SABIC) sample.

A.35. The Trios Analysis for PETG 30-GF (S.3.)

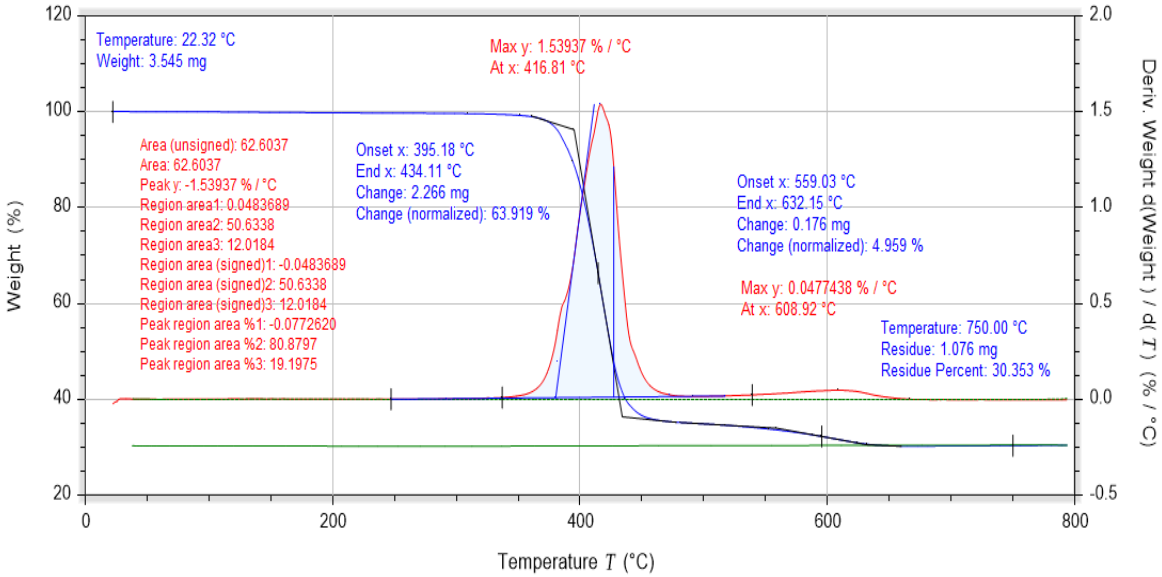

Figure A.35: The inert thermal stability history of the third PETG 30-GF (SABIC) sample.

A.42. The Decomposition Temperature (1 wt.%)

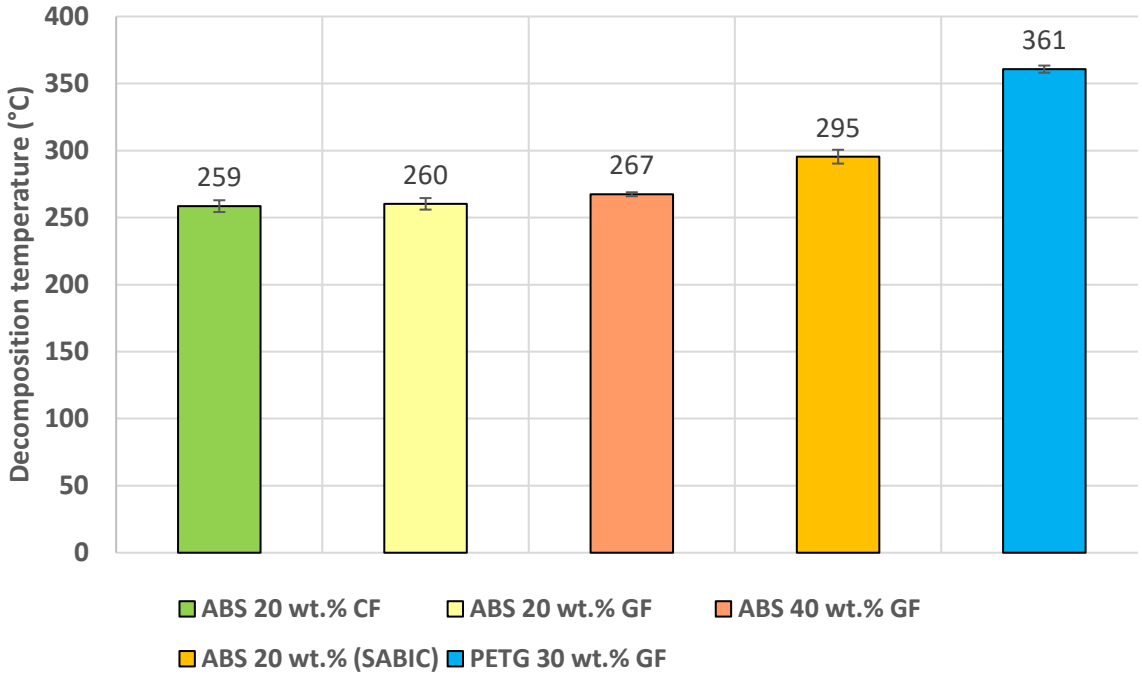

Figure A.36: The average decomposition temperature for a set of three replicate experiments per material investigated. This was stablished according to the 1 wt. % loss from the overall sample mass. There was not statistical difference among the results. Vertical error bars are illustrating the ± standard deviation.

A.43. The Weight Loss (1st. Decomposition Step Transition)

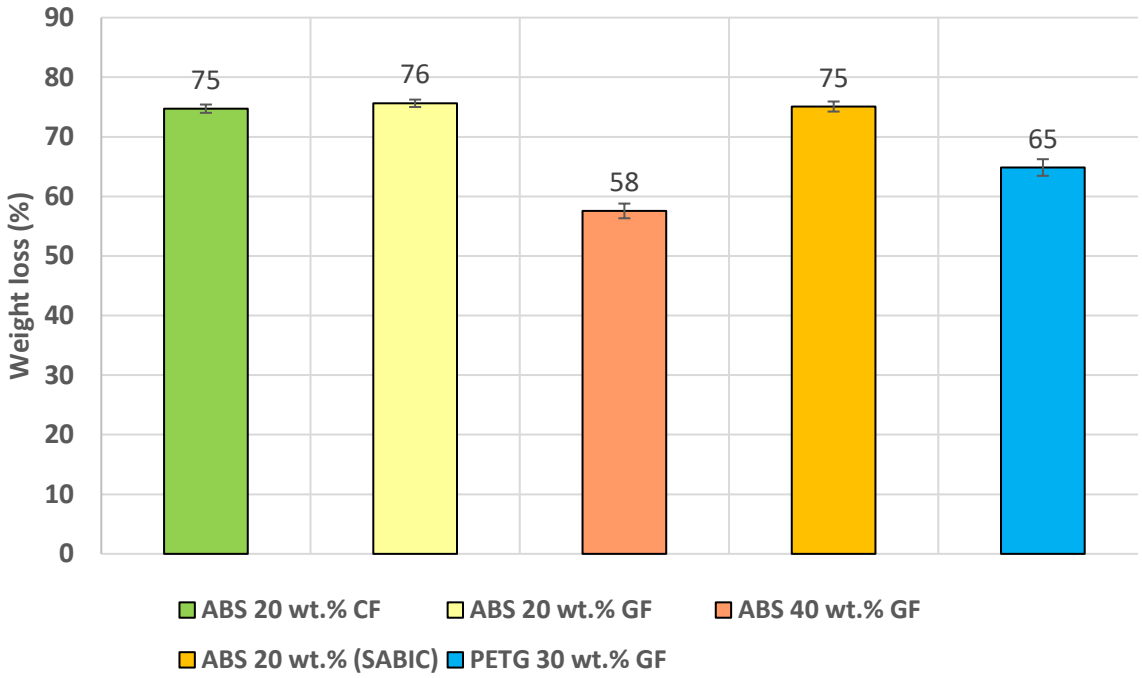

Figure A. 37: The average weight loss for a set of three replicate experiments per material investigated. This analysis was stablished between the decomposition temperature up to a visible plateau region after the decomposition event. There was a relatively low statically difference among the results. Vertical error bars are illustrating the ± standard deviation.

A.44. Maximum Peak Temperature

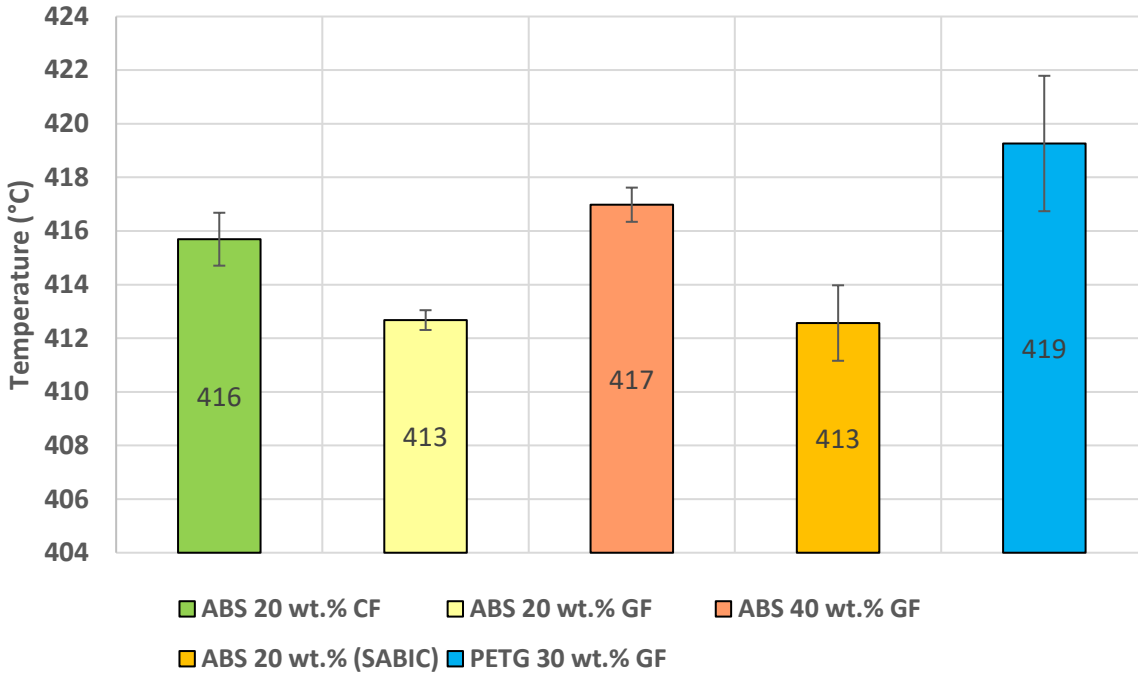

Figure A. 38: The average maximum peak temperature for a set of three replicate experiments per material investigated. Notice it is shown a significant statistical difference among the results, please note the temperature scale range shown, 404 °C to 424 °C, in the y-axis. Vertical error bars are illustrating the ± standard deviation.

A.45. Residue Percent

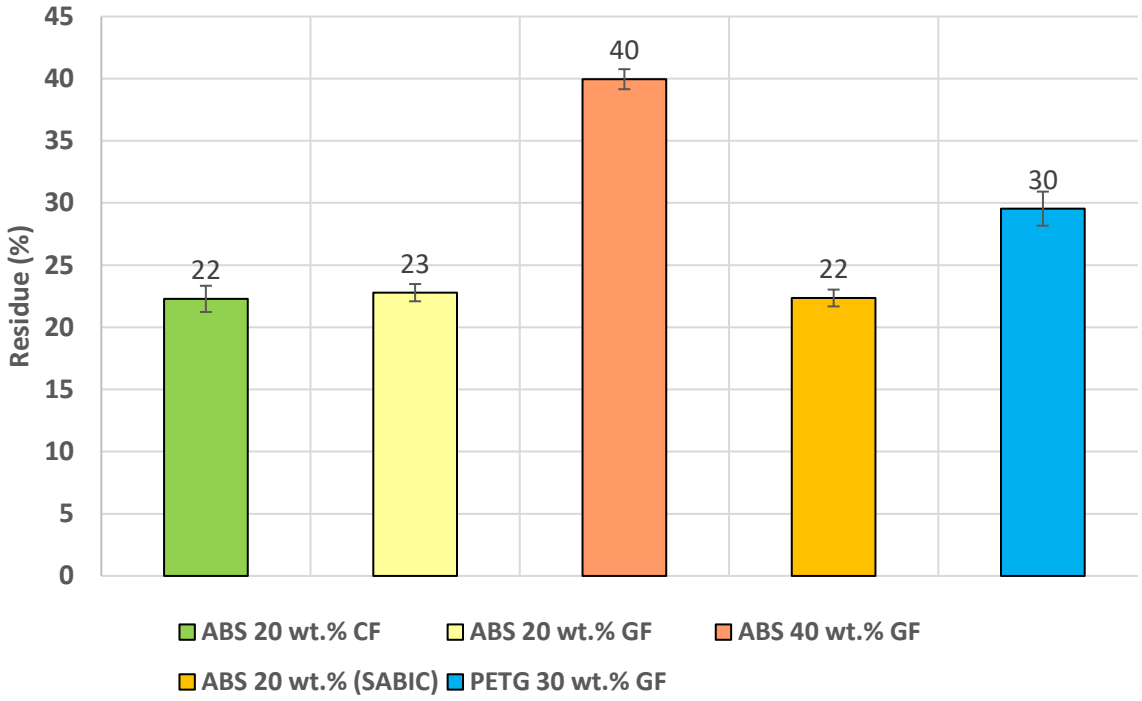

Figure A. 39: The average residue percent measured at 750 °C for a set of three replicate experiments per material investigated. There was not significant statistical difference among the results. Vertical error bars are illustrating the ± standard deviation.

A.46. Area Under the DTG Peak Integration

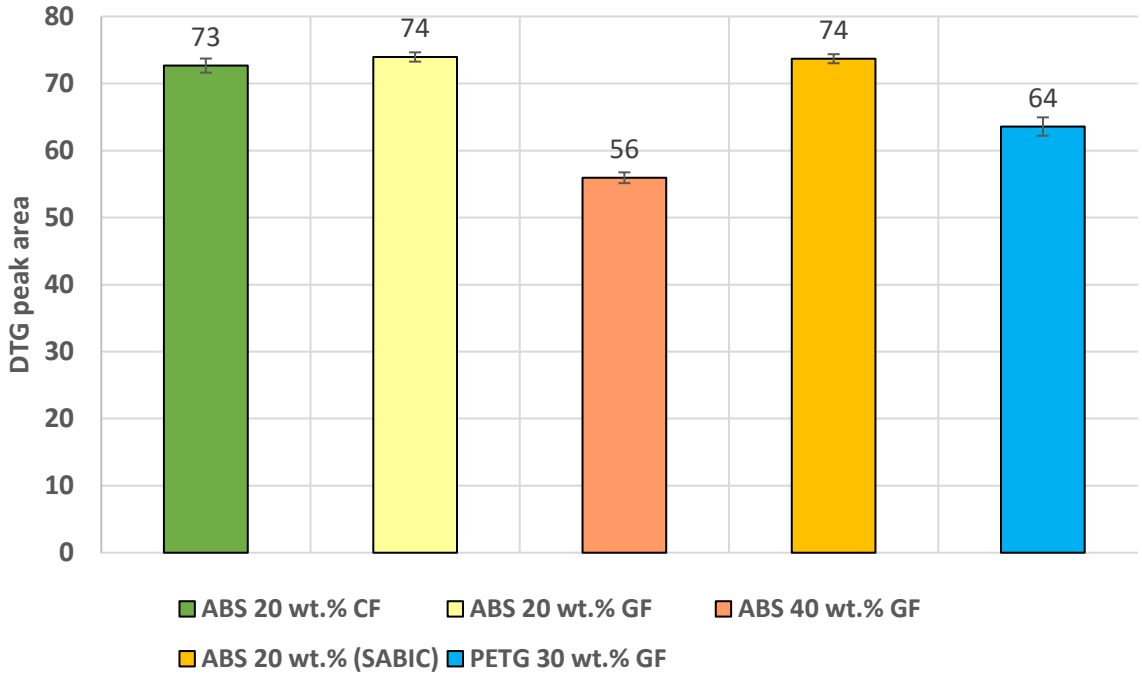

Figure A. 40: The area under the DTG curve identifying the amount of decomposed material matrix for a set of three replicate for five engineering thermoplastics, ABS and PETG, respectively. There was not significant statistical difference among the results. Vertical error bars are illustrating the ± standard deviation.

A.47. Materials

Table A.1: The material's model and description for the thermal characterization of ABS and PETG.

Manufacturer	Model	Description	Product	Lot number
ABS 20 wt. % CF				
Techmer	Electrafil J-1200/CF/20 3DP	ELECTRAFIL ® ABS 1501 3DP	TES11372	TN1701128549
ABS 20 wt. % GF				
Techmer	HiFill ABS 1511 3DP	HIFILL® ABS 1511 3DP	TES11412	TN1706142683
ABS 40 wt. % GF				
Techmer	HiFill J-1200/40 3DP Nat	HIFILL® ABS 1601 3DP	TES11492	TL1611021793
PETG 30 wt. % GF				
Techmer	HiFill PETG GF30 3DP	HIFILL® PETG 1701 3DP	PTM112532	TN1703134886
ABS 20 wt. % GF				
Sabic	LNP THERMOCOMP AM, COMPOUND AF004XXAR1	N/A	N/A	0008301951

A.48. Materials

Table A.2: The material's description for ABS and PETG.

Material	Material matrix	Reinforcing material	Fiber percentage by weight (wt. %)
ABS 20-CF	ABS	Carbon fiber	20
ABS 20-GF	ABS	Glass fiber	20
ABS 40-GF	ABS	Glass fiber	40
PETG 30-GF	PETG	Glass fiber	30
ABS 20-GF (SABIC)	ABS	Glass fiber	20

A.49. TG summary (Initial mass, 1st step transition and Residue Percent)

Table A.3 : The initial sample mass, major step transitions, minor step transitions and residual percentage for five engineering thermoplastics.

TG (in Nitrogen)	Initial mass (mg.)	1st step transition (wt.%)	2nd step transition (wt.%)	Residue percentage (wt.%)
ABS 20-CF (Techmer)				
Sample I	3.367	73.92	3.24	21.60
Sample II	3.473	75.01	2.21	21.76
Sample III	3.167	75.22	N/A	23.50
ABS 20-GF (Techmer)				
Sample I	3.524	76.29	N/A	22.14
Sample II	3.927	75.52	N/A	23.52
Sample III	3.916	75.06	N/A	22.70
ABS 40-GF (Techmer)				
Sample I	3.893	58.20	0.86	39.94
Sample II	3.893	58.34	1.57	39.16
Sample III	4.088	56.14	2.05	40.77
PETG 30-GF (Techmer)				
Sample I	3.823	66.45	4.81	27.96
Sample II	3.479	64.18	4.78	30.32
Sample III	3.442	63.91	4.95	30.35
ABS 20-GF (SABIC)				
Sample I	3.716	75.35	1.80	21.80
Sample II	3.667	74.13	2.81	22.16
Sample III	3.554	75.75	N/A	23.11

A.50. TG summary (Initial Mass)

Table A.4: The initial sample mass initial mass prior thermal decomposition.

TG (in Nitrogen)	Initial mass (mg.)	Initial mass ($\bar{X}$)	Initial mass (σ)	CV
ABS 20-CF (Techmer)				
S.1	3.367	3.33	0.15	4.49
S.2	3.473			
S.3	3.167			
ABS 20-GF (Techmer)				
S.1	3.524	3.78	0.22	5.82
S.2	3.927			
S.3	3.916			
ABS 40-GF (Techmer)				
S.1	3.893	3.95	0.11	2.78
S.2	3.893			
S.3	4.088			
PETG 30-GF (Techmer)				
S.1	3.823	3.58	0.21	5.86
S.2	3.479			
S.3	3.442			
ABS 20-GF (SABIC)				
S.1	3.716	3.64	0.08	2.19
S.2	3.667			
S.3	3.554			

A.51. TGA summary (Decomposition Temperature)

Table A.5: The 1.0 % weight loss, decomposition temperature, for five engineering thermoplastics.

TG (in Nitrogen)	$T_{decomposition}$ (° C)	$T_{decomposition}$ ($\bar{X}$)	$T_{decomposition}$ (σ)	CV
ABS 20-CF (Techmer)				
S.1	253.50	258.52	4.37	1.69
S.2	260.49			
S.3	261.56			
ABS 20-GF (Techmer)				
S.1	255.75	260.21	4.26	1.63
S.2	264.23			
S.3	260.66			
ABS 40-GF (Techmer)				
S.1	266.00	267.36	1.50	0.56
S.2	267.10			
S.3	268.98			
PETG 30-GF (Techmer)				
S.1	357.96	360.73	2.68	0.74
S.2	363.32			
S.3	360.92			
ABS 20-GF (SABIC)				
S.1	290.32	295.41	5.15	1.74
S.2	295.29			
S.3	300.63			

A.52. TGA summary (Residue Percent)

Table A.6: The residual percentage at 750 °C, fixed mass loss, for five engineering thermoplastics.

TG (in Nitrogen)	Residue percentage (wt.%)	Residue percentage ($\bar{x}$)	Residue percentage (σ)	CV
ABS 20-CF (Techmer)				
S.1	21.60	22.28	1.05	4.71
S.2	21.76			
S.3	23.50			
ABS 20-GF (Techmer)				
S.1	22.14	22.78	.69	3.02
S.2	23.52			
S.3	22.70			
ABS 40-GF (Techmer)				
S.1	39.94	39.95	.80	2.0
S.2	39.16			
S.3	40.77			
PETG 30-GF (Techmer)				
S.1	27.96	29.54	1.37	4.63
S.2	30.32			
S.3	30.35			
ABS 20-GF (SABIC)				
S.1	21.80	22.35	.67	2.99
S.2	22.16			
S.3	23.11			

A.53. TGA summary (First Step Transition)

Table A.7: A single major step transitions for five engineering thermoplastics.

TG (in Nitrogen)	1st step transition (wt.%)	1st step transition ($\bar{x}$)	1st step transition (σ)	CV
ABS 20-CF (Techmer)				
S.1	73.92	74.71	.69	0.92
S.2	75.01			
S.3	75.22			
ABS 20-GF (Techmer)				
S.1	76.29	75.62	.62	0.81
S.2	75.52			
S.3	75.06			
ABS 40-GF (Techmer)				
S.1	58.20	57.56	1.23	2.13
S.2	58.34			
S.3	56.14			
PETG 30-GF (Techmer)				
S.1	66.45	64.84	1.39	2.01
S.2	64.18			
S.3	63.91			
ABS 20-GF (SABIC)				
S.1	75.35	75.07	.84	1.11
S.2	74.13			
S.3	75.75			

A.54. DTG summary (Max Peak Temperature)

Table A.8: The maximum peak temperature for five engineering thermoplastics.

TG (in Nitrogen)	Max peak temperature (° C)	Max peak temperature ($\bar{x}$)	Max peak temperature (σ)	CV
ABS 20-CF (Techmer)				
S.1	414.58	415.69	.98	0.23
S.2	416.04			
S.3	416.46			
ABS 20-GF (Techmer)				
S.1	413.07	412.66	.36	0.08
S.2	412.36			
S.3	412.56			
ABS 40-GF (Techmer)				
S.1	417.53	416.98	.63	0.15
S.2	417.13			
S.3	416.28			
PETG 30-GF (Techmer)				
S.1	421.82	419.26	2.52	0.60
S.2	419.20			
S.3	416.77			
ABS 20-GF (SABIC)				
S.1	411.68	412.57	1.40	0.33
S.2	411.83			
S.3	414.19			

A.55. DTG summary (Peak Integration)

Table A.9: The area under the DTG maximum peak for five engineering thermoplastics.

TG (in Nitrogen)	Area under the DTG curve	Area under the DTG curve ($\bar{X}$)	Area under the DTG curve (σ)	CV
ABS 20-CF (Techmer)				
S.1	71.26	72.67	1.22	1.67
S.2	73.43			
S.3	73.33			
ABS 20-GF (Techmer)				
S.1	74.17	73.96	0.47	0.63
S.2	74.29			
S.3	73.42			
ABS 40-GF (Techmer)				
S.1	56.61	55.94	1.09	1.94
S.2	56.54			
S.3	54.68			
PETG 30-GF (Techmer)				
S.1	65.15	63.58	1.37	2.15
S.2	62.99			
S.3	62.60			
ABS 20-GF (SABIC)				
S.1	73.79	73.7	1.02	1.38
S.2	72.63			
S.3	74.68			

A.56. TG and DTG (Summary)

Table A.10 The arithmetic mean values, TGA/DTG, for five engineering thermoplastics.

TGA	$\bar{x}$
ABS 20 wt. % CF (Techmer)	
Initial mass	3.33
Decomposition temperature (° C)	258.52
First step transition (wt.%)	74.71
Residue percentage (wt. %)	22.28
Max peak temperature	415.69
Area from the DTG peak integration	72.67

TGA	$\bar{x}$
ABS 20 wt. % GF (Techmer)	
Initial mass	3.78
Decomposition temperature (° C)	260.21
First step transition (wt.%)	75.62
Residue percentage (wt. %)	22.78
Max peak temperature	412.66
Area from the DTG peak integration	73.96

TGA	$\bar{x}$
ABS 40 wt. % GF (Techmer)	
Initial mass	3.95
Decomposition temperature (° C)	267.36
First step transition (wt.%)	57.56
Residue percentage (wt. %)	39.95
Max peak temperature	416.26
Area from the DTG peak integration	55.94

A.57. TGA and DTG (Summary)

Table A.11 The arithmetic mean values, TGA/DTG, for five engineering thermoplastics.

TGA	$\bar{x}$
PETG 30 wt. % GF (Techmer)	
Initial mass	3.58
Decomposition temperature (° C)	360.73
First step transition (wt.%)	64.84
Residue percentage (wt. %)	29.54
Max peak temperature	419.26
Area from the DTG peak integration	63.58

TGA	$\bar{x}$
ABS 20 wt. % GF (SABIC)	
Initial mass	3.64
Decomposition temperature (° C)	295.41
First step transition (wt.%)	75.07
Residue percentage (wt. %)	22.35
Max peak temperature	412.57
Area from the DTG peak integration	73.70

A.58. Standard Deviation

Table A.12: The standard deviations, TGA/DTG, for five engineering thermoplastics.

TGA/DTG	σ
ABS 20 wt. % CF (Techmer)	
Initial mass	0.15
Decomposition temperature	4.37
First step transition	0.69
Residue percentage	1.05
Max peak temperature	0.98
Area from the DTG peak integration	1.22

TGA/DTG	σ
ABS 20 wt. % GF (Techmer)	
Initial mass	0.22
Decomposition temperature	4.26
First step transition	0.62
Residue percentage	0.69
Max peak temperature	0.36
Area from the DTG peak integration	0.47

TG/DTG	σ
ABS 40 wt. % GF (Techmer)	
Initial mass	0.11
Decomposition temperature	1.50
First step transition	1.23
Residue percentage	0.80
Max peak temperature	0.63
Area from the DTG peak integration	1.09

A.59. Standard Deviation

Table A.13:The standard deviations, TGA/DTG, for five engineering thermoplastics.

TGA/DTG	σ
PETG 30 wt. % GF (Techmer)	
Initial mass	0.21
Decomposition temperature	2.68
First step transition	1.39
Residue percentage	1.37
Max peak temperature	2.52
Area from the DTG peak integration	1.37

TGA/DTG	σ
ABS 20 wt. % GF (SABIC)	
Initial mass	0.08
Decomposition temperature	5.15
First step transition	0.84
Residue percentage	0.67
Max peak temperature	1.40
Area from the DTG peak integration	1.02

A.60. Coefficient of variation

Table A.14: The coefficient of variance, TGA/DTG, for five engineering thermoplastics.

TGA/DTG	CV
ABS 20 wt. % CF (Techmer)	
Initial mass	4.49
Decomposition temperature	1.69
First step transition	0.92
Residue percentage	4.71
Max peak temperature	0.23
Area from the DTG peak integration	1.67

TGA/DTG	CV
ABS 20 wt. % GF (Techmer)	
Initial mass	5.82
Decomposition temperature	1.63
First step transition	0.81
Residue percentage	3.02
Max peak temperature	0.08
Area from the DTG peak integration	0.63

TGA/DTG	CV
ABS 40 wt. % GF (Techmer)	
Initial mass	2.78
Decomposition temperature	0.56
First step transition	2.13
Residue percentage	2.00
Max peak temperature	0.15
Area from the DTG peak integration	1.94

A.59. Coefficient of variation

Table A.15: The coefficient of variance, TGA/DTG, for five engineering thermoplastics.

TGA/DTG	CV
PETG 30 wt. % GF (Techmer)	
Initial mass	5.86
Decomposition temperature	0.74
First step transition	2.01
Residue percentage	4.63
Max peak temperature	0.60
Area from the DTG peak integration	2.15

TGA/DTG	CV
ABS 20 wt. % GF (SABIC)	
Initial mass	2.19
Decomposition temperature	1.74
First step transition	1.11
Residue percentage	2.99
Max peak temperature	0.33
Area from the DTG peak integration	1.38

A.61. DSC candidate temperatures

Table A.16: The candidate temperatures for the DSC studies of five engineering thermoplastics.

TGA	$T_{decomposition}$ (° C)	T_{DSC} (° C)
ABS 20 wt. % CF	258.52	220
ABS 20 wt. % GF	260.21	220
ABS 40 wt. % GF	267.36	227
PETG 30 wt. % GF	360.73	340
ABS 20 wt. % GF (SABIC)	295.41	255

A.62. TGA/DTG thermal analysis comparison (Summary)

Table A.17: The percentage changes from the comparison of ABS 20-GF and ABS 20-CF compounded by Techmer.

ABS 20-GF compared to ABS 20-CF		
TGA/DTG	Change	Percentage change (%)
Decomposition temperature (° C)	1.69	0.65
First step transition (wt.%)	.91	1.21
Residue percentage **(**wt. %)	.50	2.24
Max peak temperature (° C)	-3.03	-0.73
Area from the DTG peak integration	1.29	1.77

A.63. TGA/DTG thermal analysis comparison (Summary)

Table A.18: The percentage improvements from the comparison of ABS 40-GF and ABS 20-GF compounded by Techmer.

ABS 40-GF compared to ABS 20-GF		
TGA/DTG	Improvement	Percentage improvement (%)
Decomposition temperature (° C)	7.15	2.74
First step transition (wt.%)	18.06	31.37
Residue percentage **(**wt. %)	17.17	75.37
Max peak temperature (° C)	3.60	0.87
Area from the DTG peak integration	18.02	32.21

A.64. TGA/DTG thermal analysis comparison (Summary)

Table A.19: The percentage improvements from the comparison of ABS 20-GF (SABIC) and ABS 20-GF compounded by Techmer.

ABS 20-GF (SABIC) compared to ABS 20-GF (Techmer)		
TGA/DTG	Improvement	Percentage improvement (%)
Decomposition temperature (° C)	35.20	13.52
First step transition (wt.%)	0.55	0.73
Residue percentage **(**wt. %)	-0.43	-1.92
Max peak temperature (° C)	-0.09	-.0.02
Area from the DTG peak integration	0.26	0.35

Appendix B

B.1. DSC ABS 20-CF (S.1)

ABS 20 wt. % CF compounded by Techmer PM Polymer Modifiers:

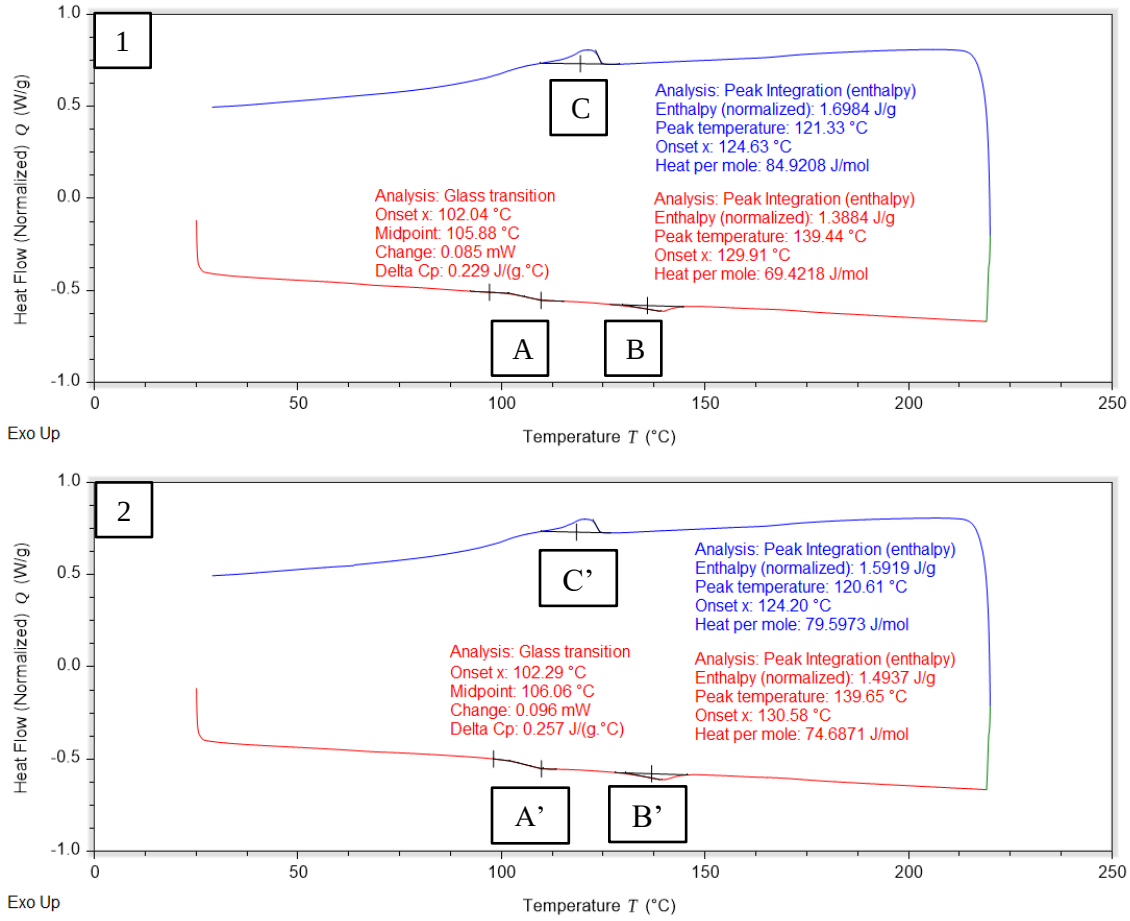

Figure B.1. The DSC curves, illustrating a heating up scan, red curve; in addition, a cooling down scan, blue curve, for the first sample. Please notice, Figure B.1 represents the initial experiment and Figure B.2 demonstrates the replicate experiment, both under the same processing parameters.

B.2. DSC ABS 20-CF (S.2)

ABS 20 wt. % CF compounded by Techmer PM Polymer Modifiers:

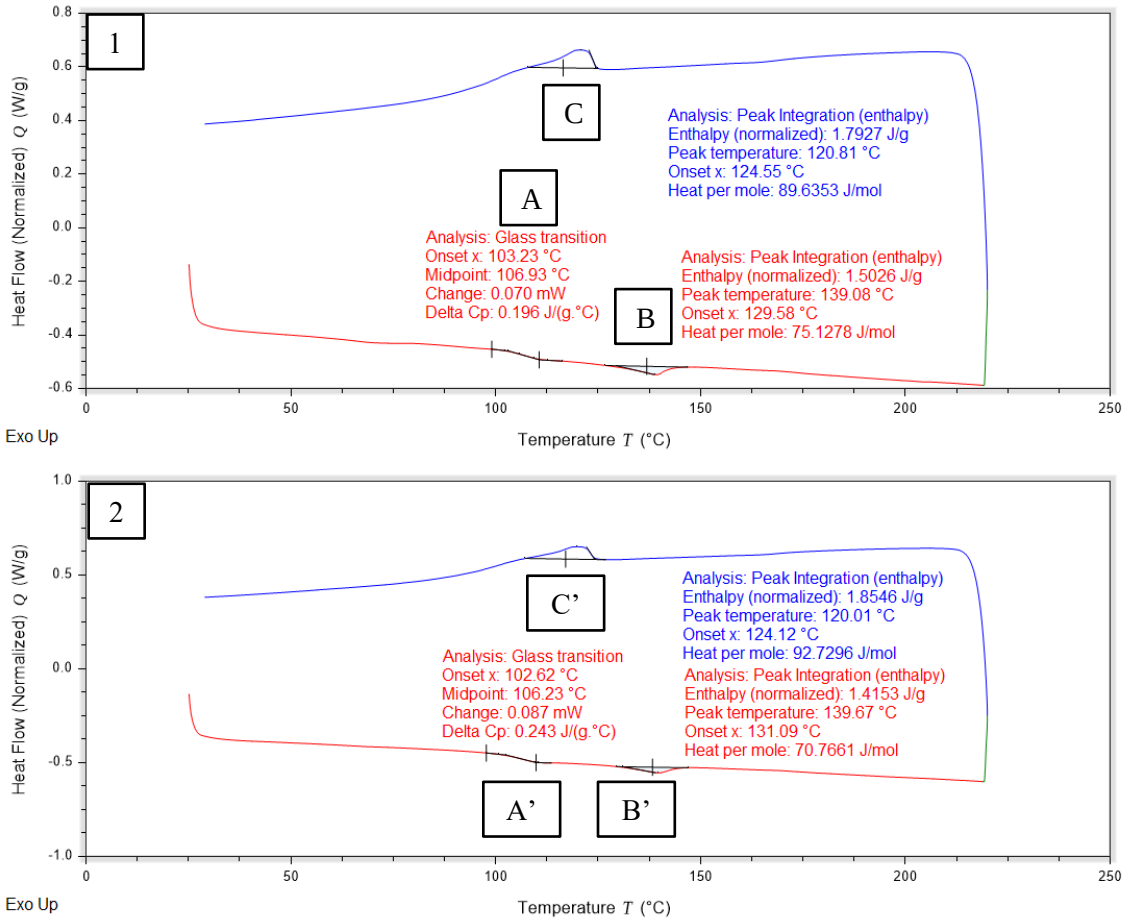

Figure B.2. The DSC curves, illustrating a heating up scan, red curve, and a cooling down scan, blue curve for the second sample.

B.3. DSC ABS 20-CF (S.3)

ABS 20 wt. % CF compounded by Techmer PM Polymer Modifiers:

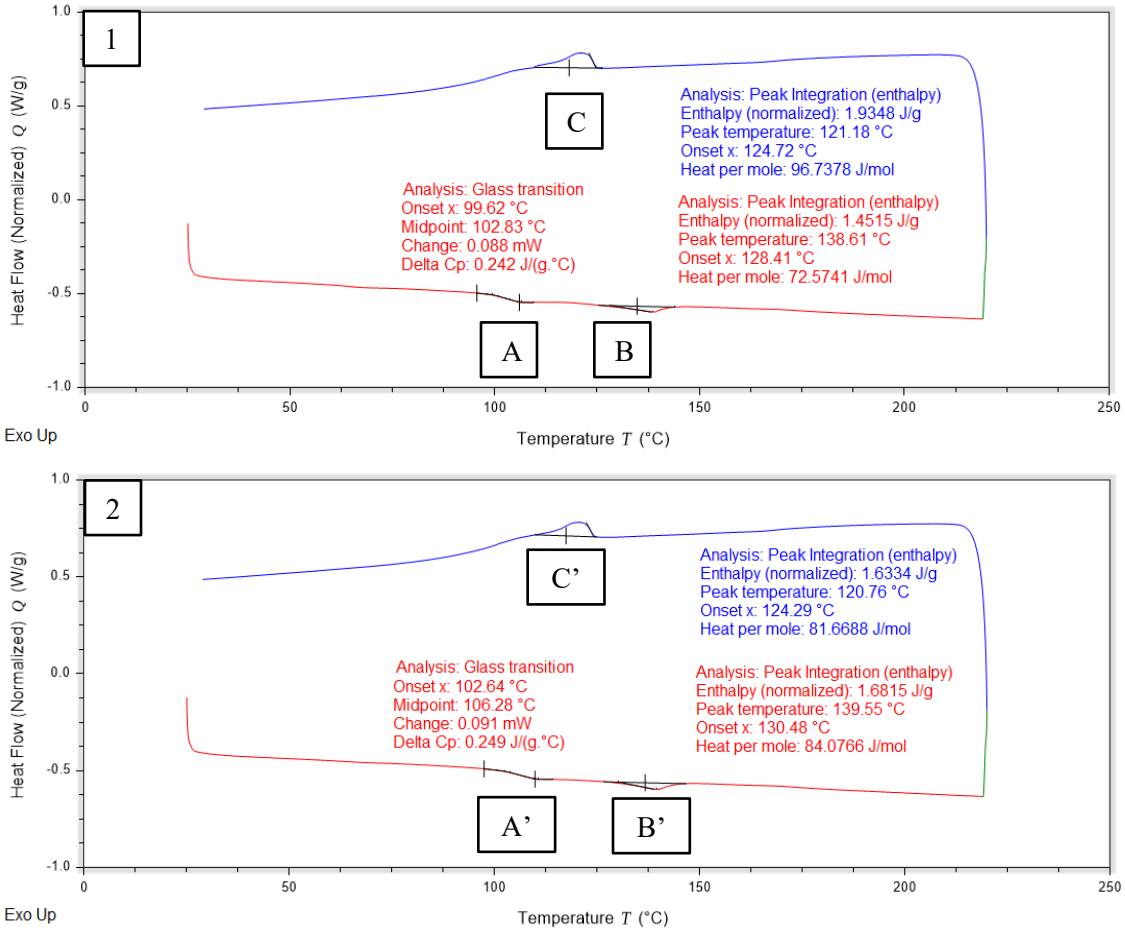

Figure B.3. The DSC curves, illustrating a heating up scan, red curve, and a cooling down scan, blue curve for the third sample.

B.4. DSC ABS 20-CF (overlay)

ABS 20 wt. % CF compounded by Techmer PM Polymer Modifiers:

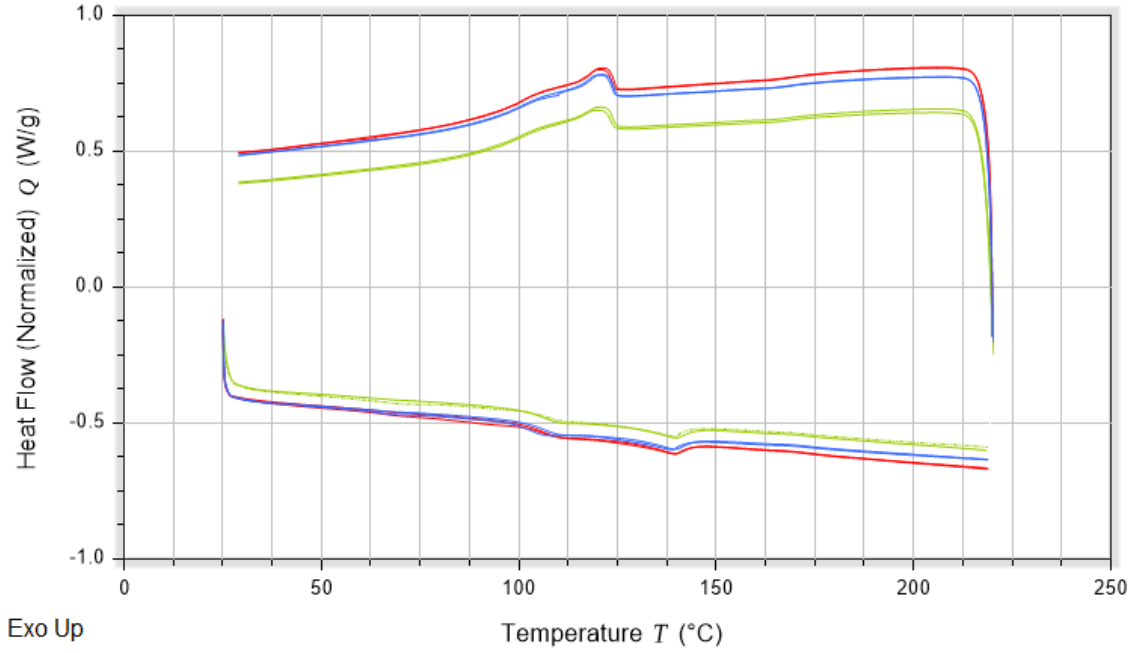

Figure B.4. The overlay for a set of three sample, notice the red curves represent the first sample, the blue curves illustrates the second sample and the green curve is attributed to the third sample.

B.5. DSC ABS 20-GF (S.1)

ABS 20 wt. % GF compounded by Techmer PM Polymer Modifiers:

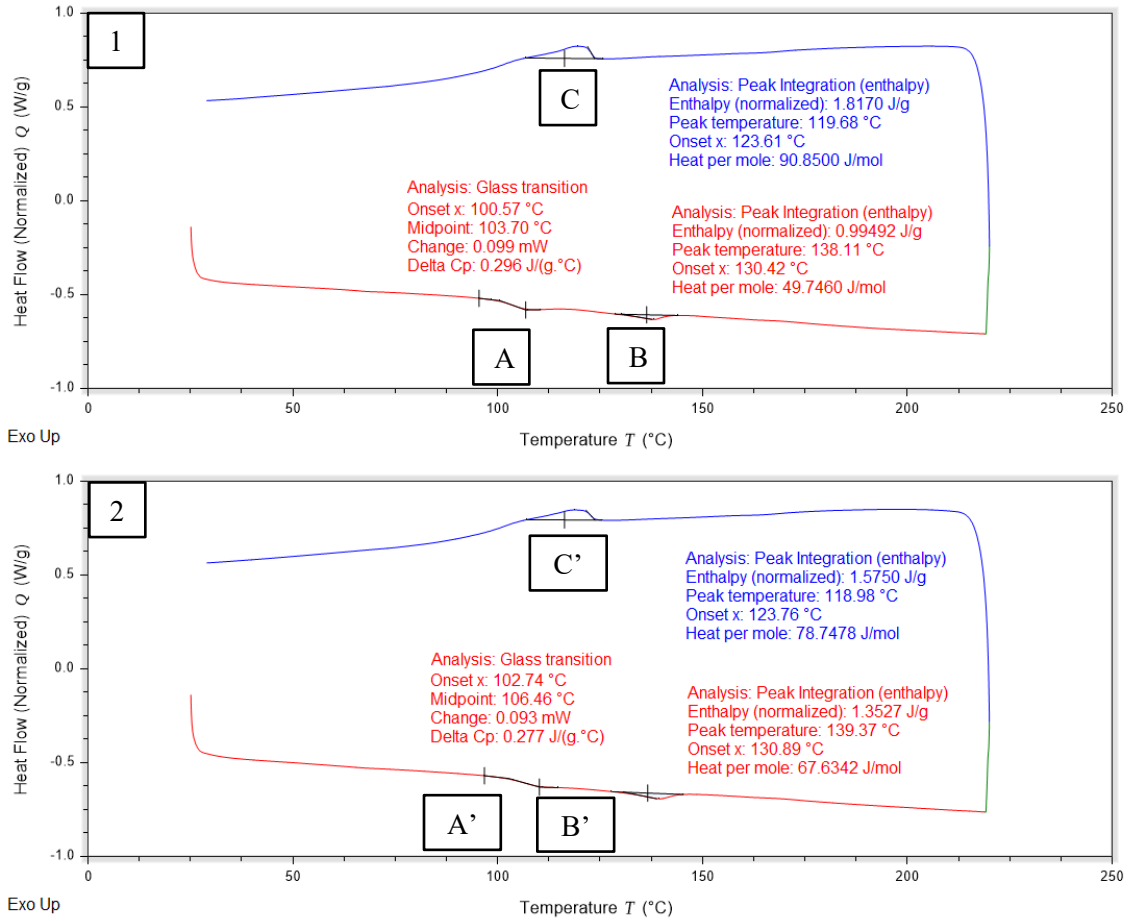

Figure B.5. The DSC curves, illustrating a heating up scan, red curve; in addition, a cooling down scan, blue curve, for the first sample. Please notice, Figure B.1 represents the initial experiment and Figure B.2 demonstrates the replicate experiment, both under the same processing parameters.

B.6. DSC ABS 20-GF (S.2)

ABS 20 wt. % GF compounded by Techmer PM Polymer Modifiers:

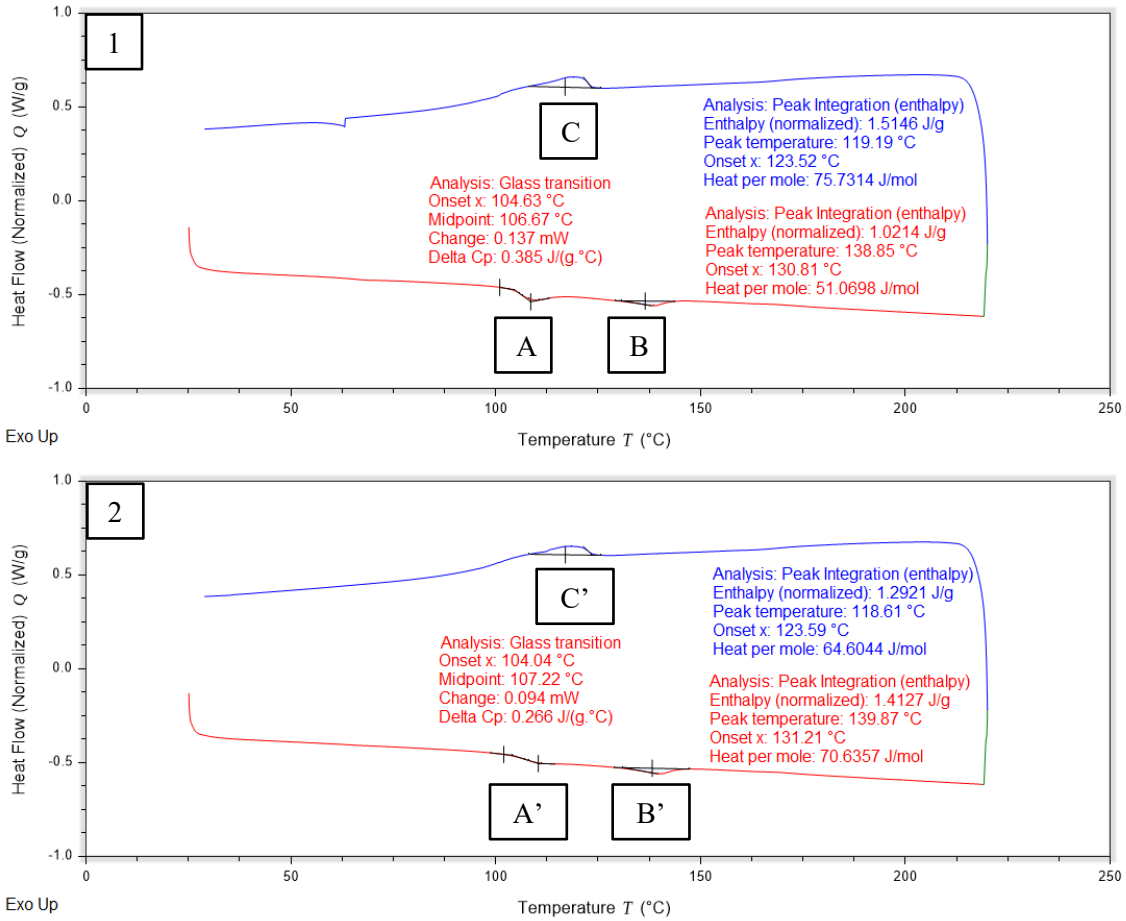

Figure B.6. The DSC curves, illustrating a heating up scan, red curve, and a cooling down scan, blue curve for the second sample.

B.7. DSC ABS 20-GF (S.3)

ABS 20 wt. % GF compounded by Techmer PM Polymer Modifiers:

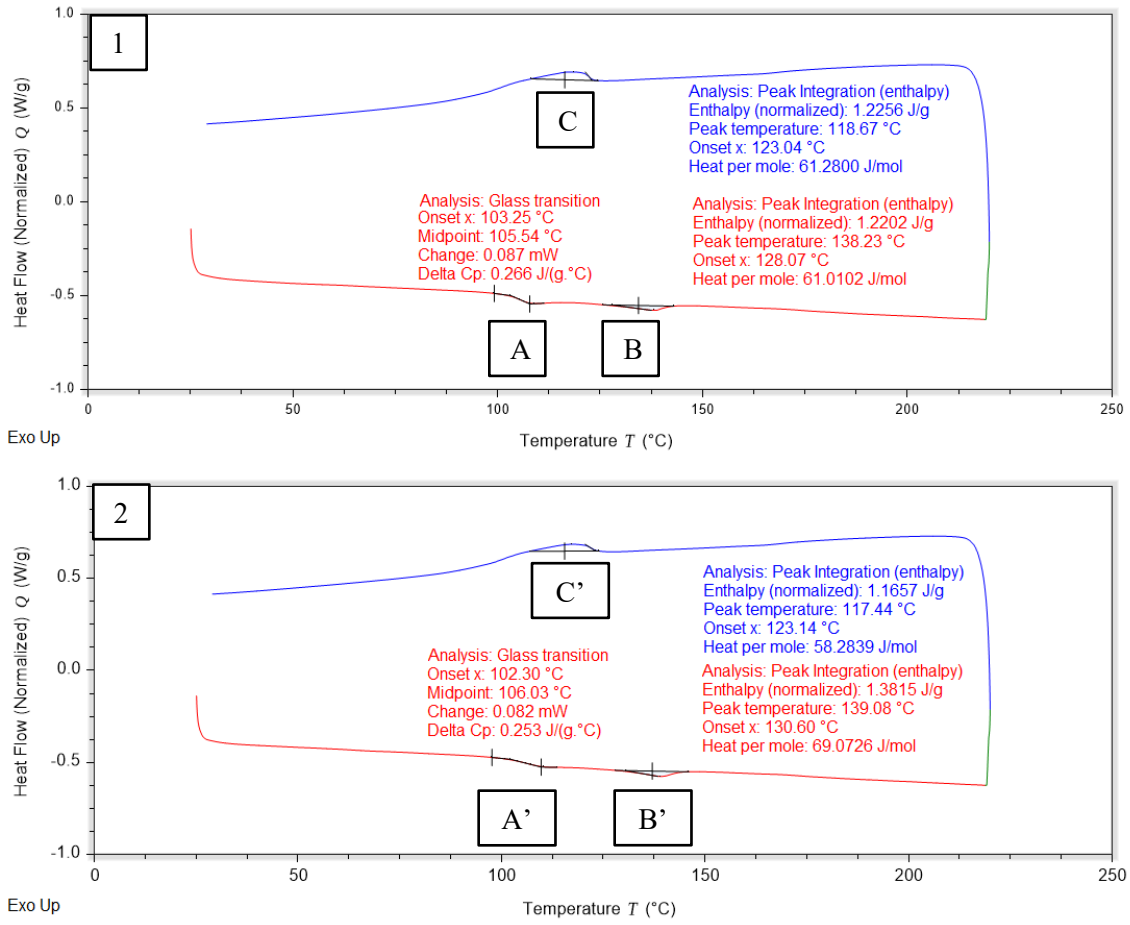

Figure B.7 The DSC curves, illustrating a heating up scan, red curve, and a cooling down scan, blue curve for the third sample.

B.8. DSC ABS 20-GF (overlay)

ABS 20 wt. % GF compounded by Techmer PM Polymer Modifiers:

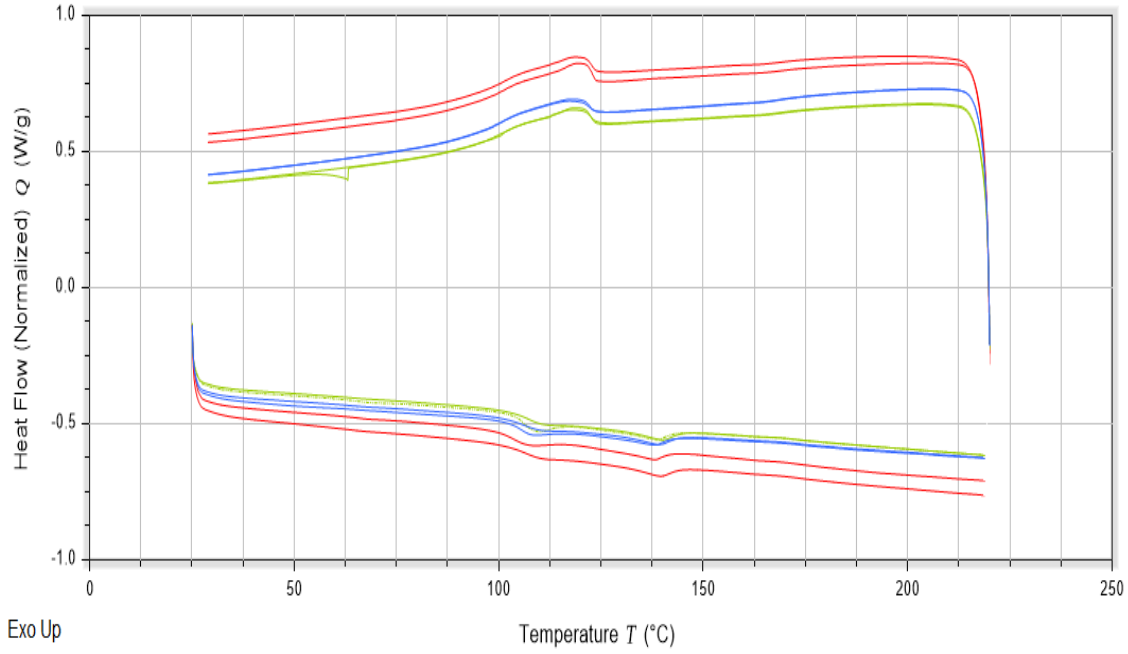

Figure B.8. The overlay for a set of three sample, notice the red curves represent the first sample, the blue curves illustrates the second sample and the green curve is attributed to the third sample.

B.9. DSC ABS-GF (S.1)

ABS 40 wt. % GF compounded by Techmer PM Polymer Modifiers:

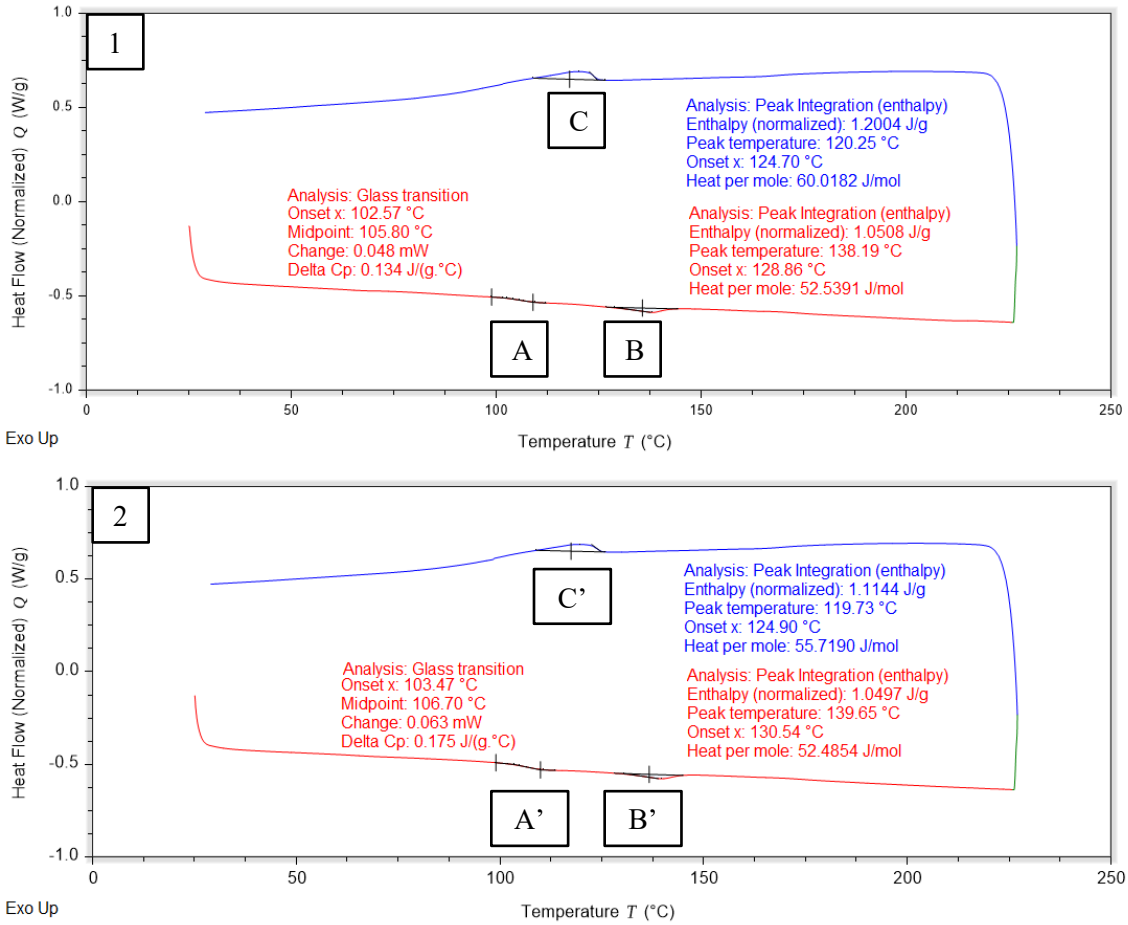

Figure B.9. The DSC curves, illustrating a heating up scan, red curve; in addition, a cooling down scan, blue curve, for the first sample. Please notice, Figure B.1 represents the initial experiment and Figure B.2 demonstrates the replicate experiment, both under the same processing parameters.

B.10. DSC ABS 40-GF (S.2)

ABS 40 wt. % GF compounded by Techmer PM Polymer Modifiers:

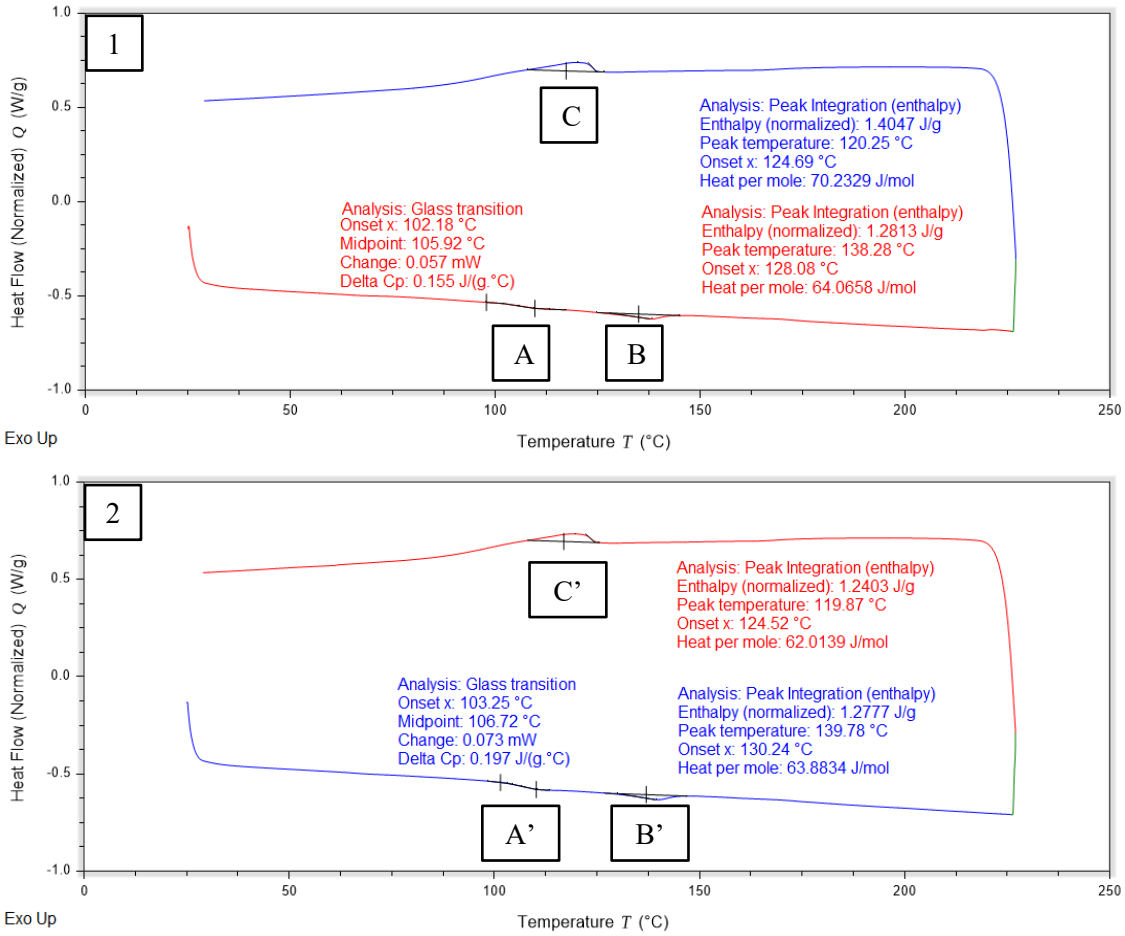

Figure B.10. The DSC curves, illustrating a heating up scan, red curve, and a cooling down scan, blue curve for the second sample.

B.11. DSC ABS 40-GF (S.3)

ABS 40 wt. % GF compounded by Techmer PM Polymer Modifiers:

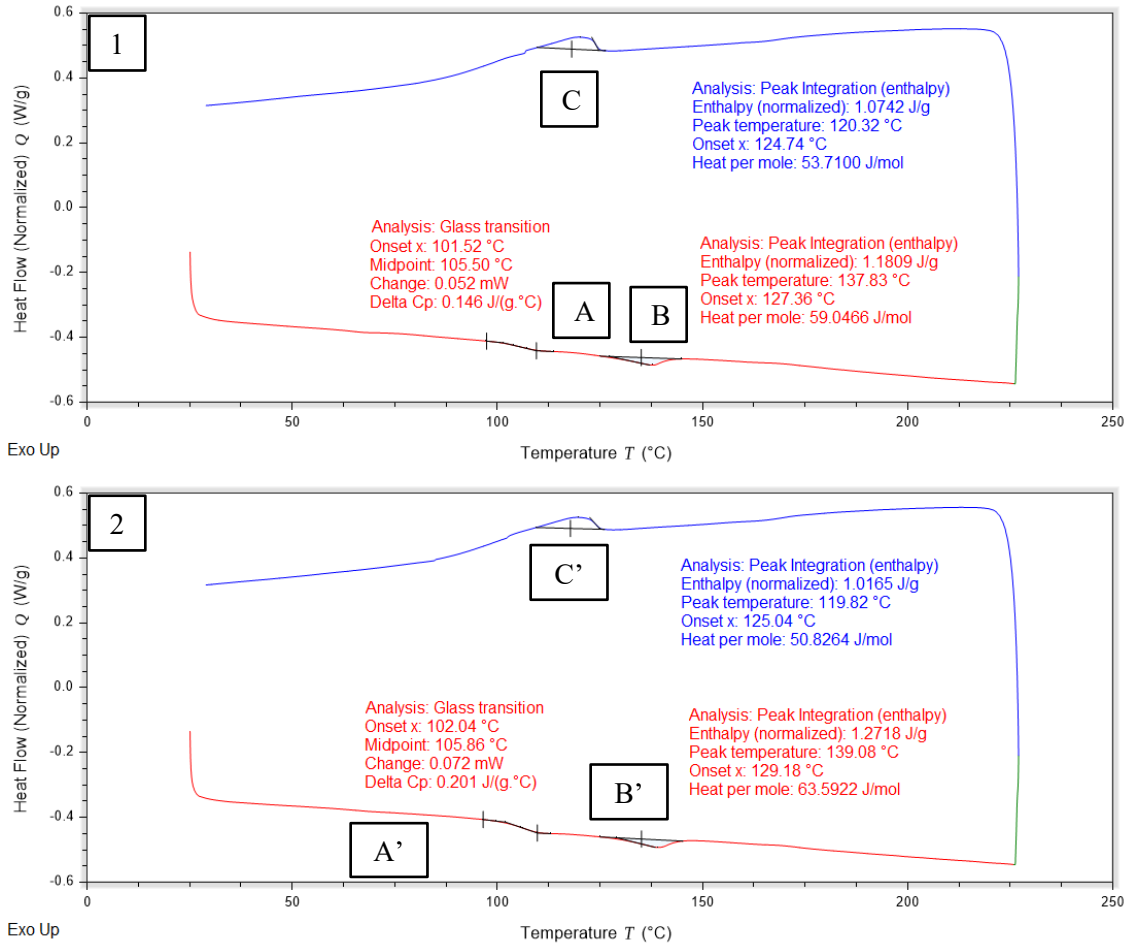

Figure B.11. The DSC curves, illustrating a heating up scan, red curve, and a cooling down scan, blue curve for the third sample.

B.12. DSC ABS 40-GF (overlay)

ABS 40 wt. % GF compounded by Techmer PM Polymer Modifiers:

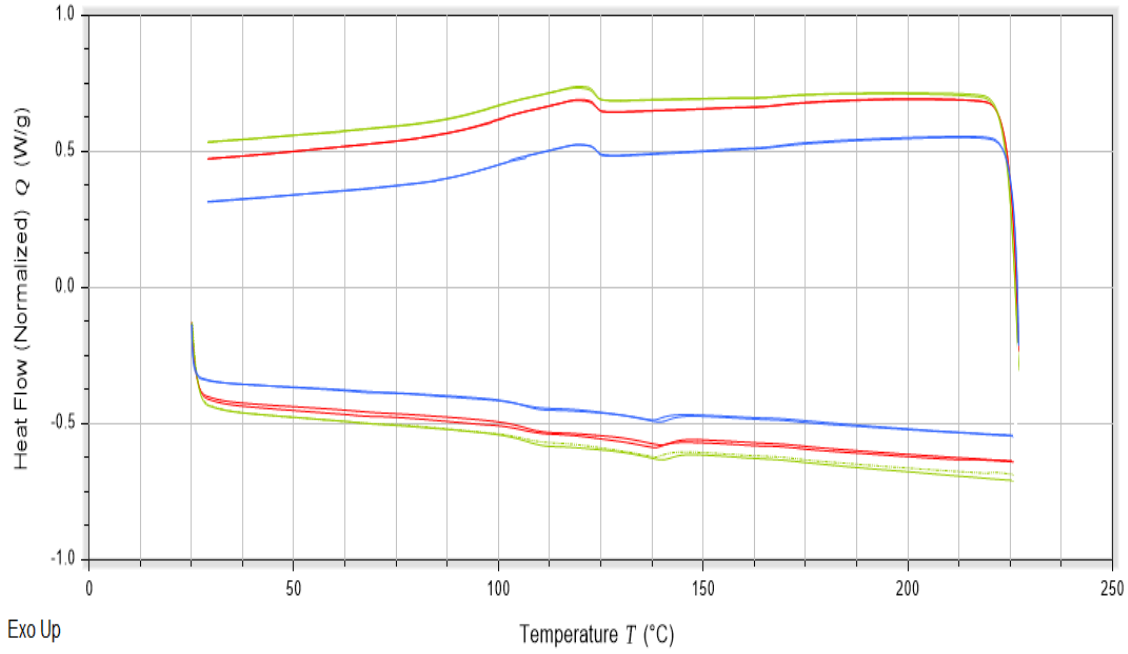

Figure B.12. The overlay for a set of three sample, notice the red curves represent the first sample, the blue curves illustrates the second sample and the green curve is attributed to the third sample.

B.13. DSC ABS 20-GF (SABIC) (S.1)

ABS 20 wt. % GF compounded by SABIC:

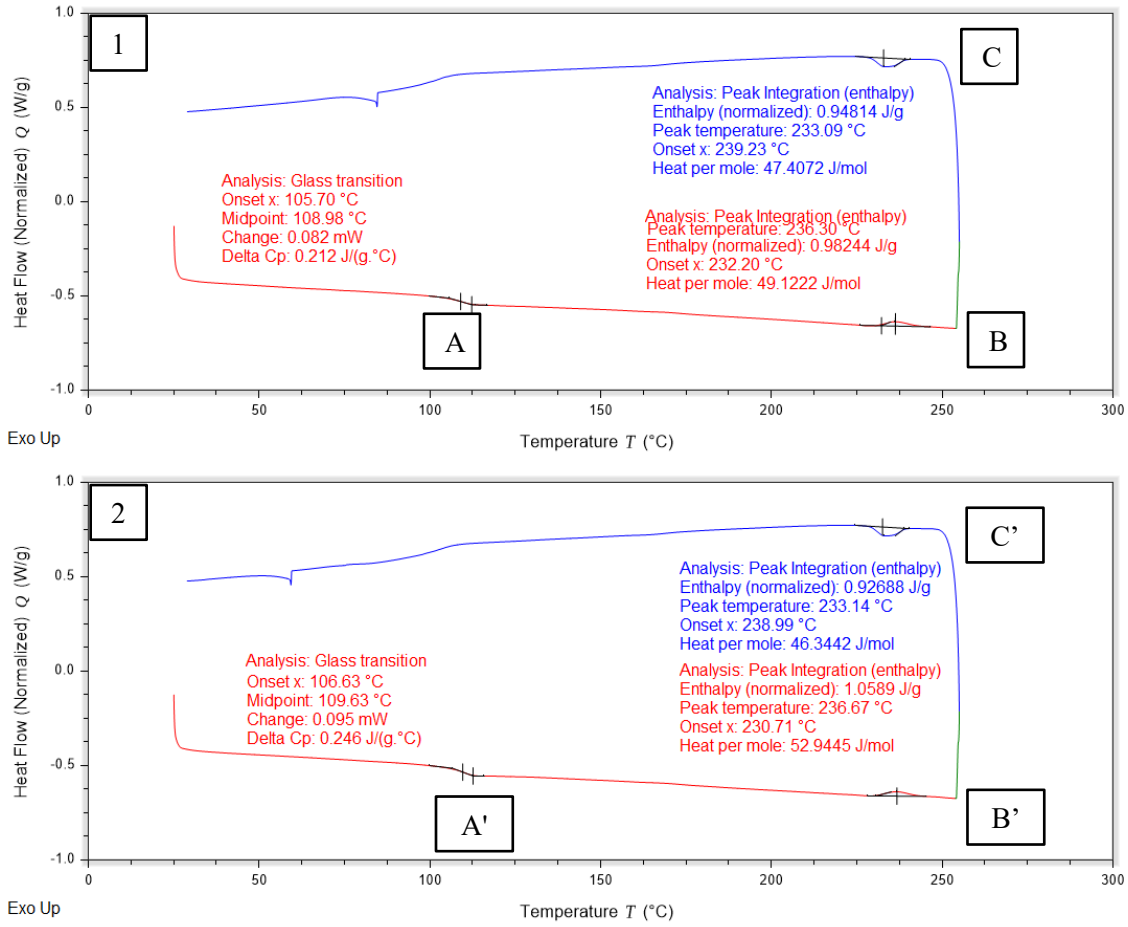

Figure B.13. The DSC curves, illustrating a heating up scan, red curve; in addition, a cooling down scan, blue curve, for the first sample. Please notice, Figure B.1 represents the initial experiment and Figure B.2 demonstrates the replicate experiment, both under the same processing parameters.

B.14. DSC ABS 20-GF (SABIC) (S.2)

ABS 20 wt. % GF compounded by SABIC:

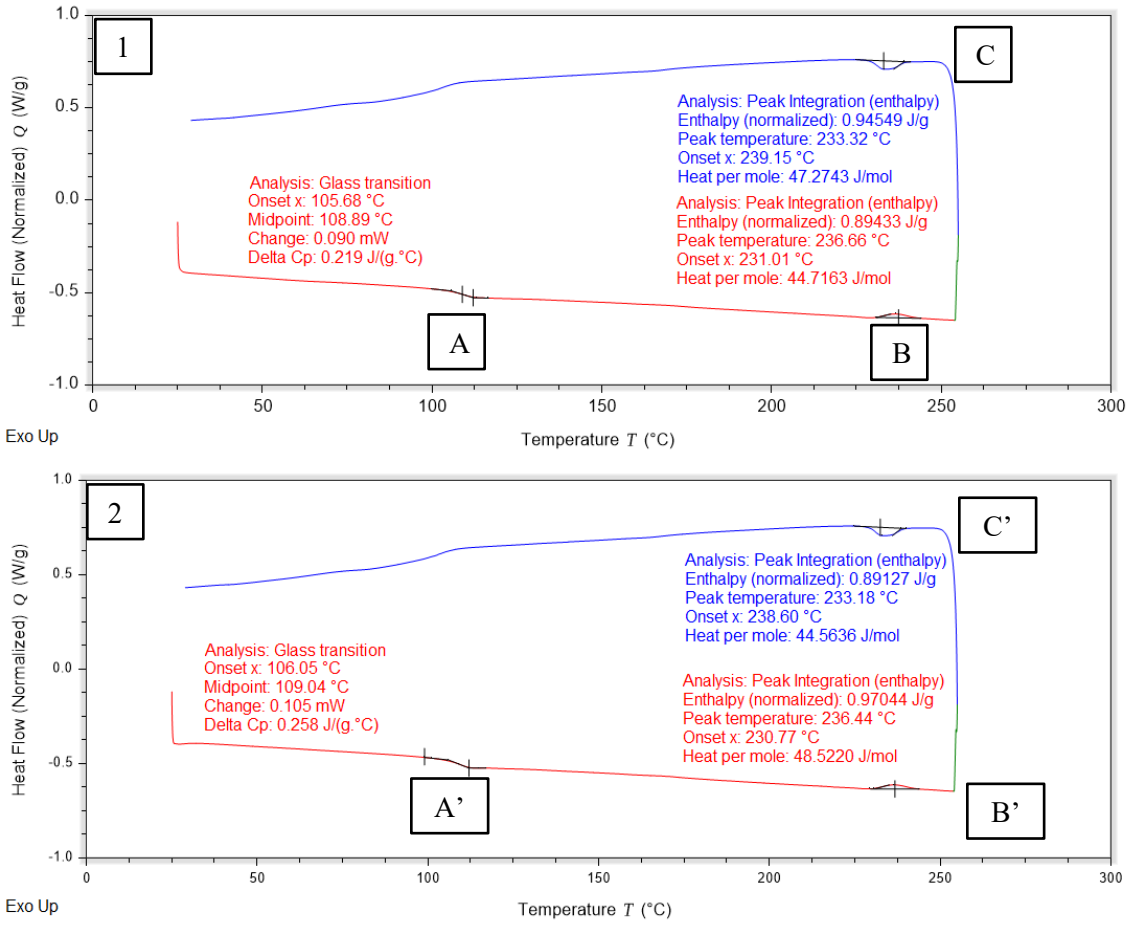

Figure B.14. The DSC curves, illustrating a heating up scan, red curve, and a cooling down scan, blue curve for the second sample.

B.15. DSC ABS 20-GF (SABIC) (S.3)

ABS 20 wt. % GF compounded by SABIC:

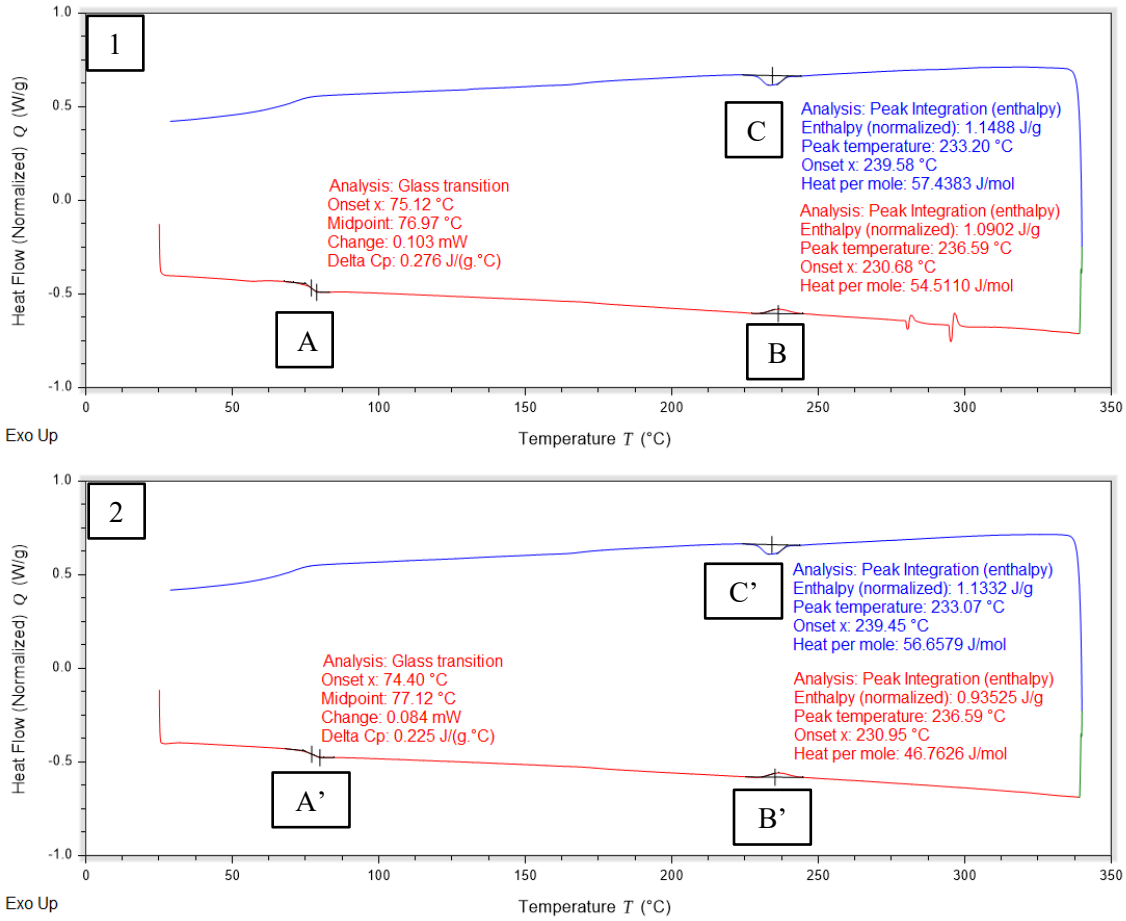

Figure B.15. The DSC curves, illustrating a heating up scan, red curve, and a cooling down scan, blue curve for the third sample.

B.16. DSC ABS 20-GF (SABIC) (overlay)

ABS 20 wt. % GF compounded by SABIC:

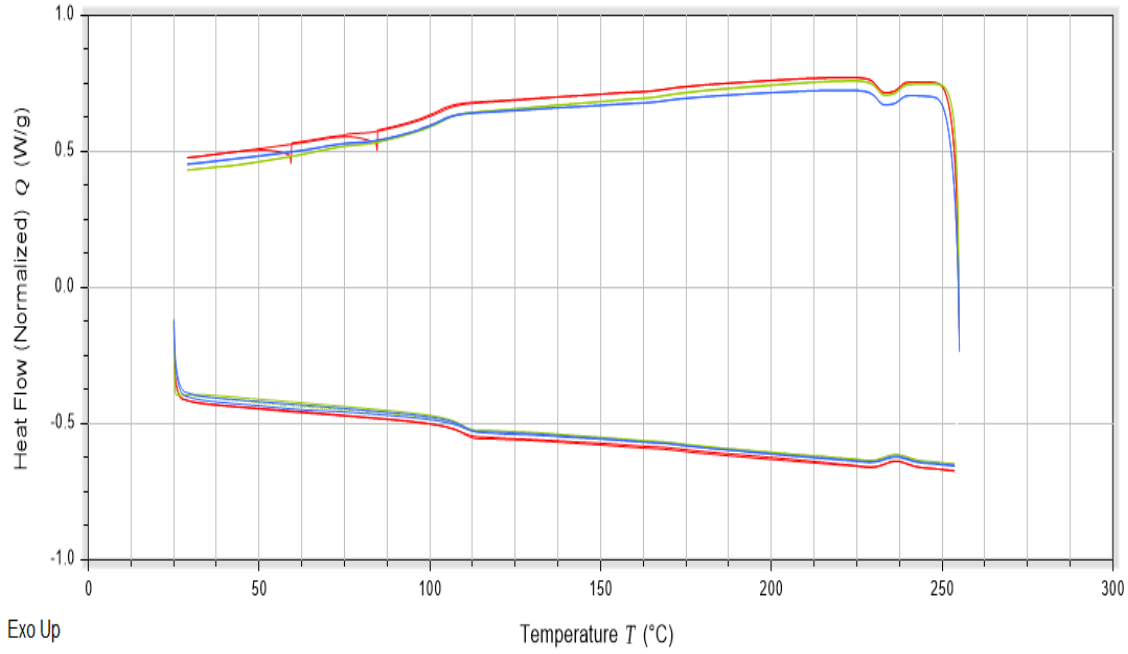

Figure B.16. The overlay for a set of three sample, notice the red curves represent the first sample, the blue curves illustrates the second sample and the green curve is attributed to the third sample.

B.17. DSC PETG 30-GF (S.1)

PETG 30 wt. % GF compounded by Techmer PM Polymer Modifiers:

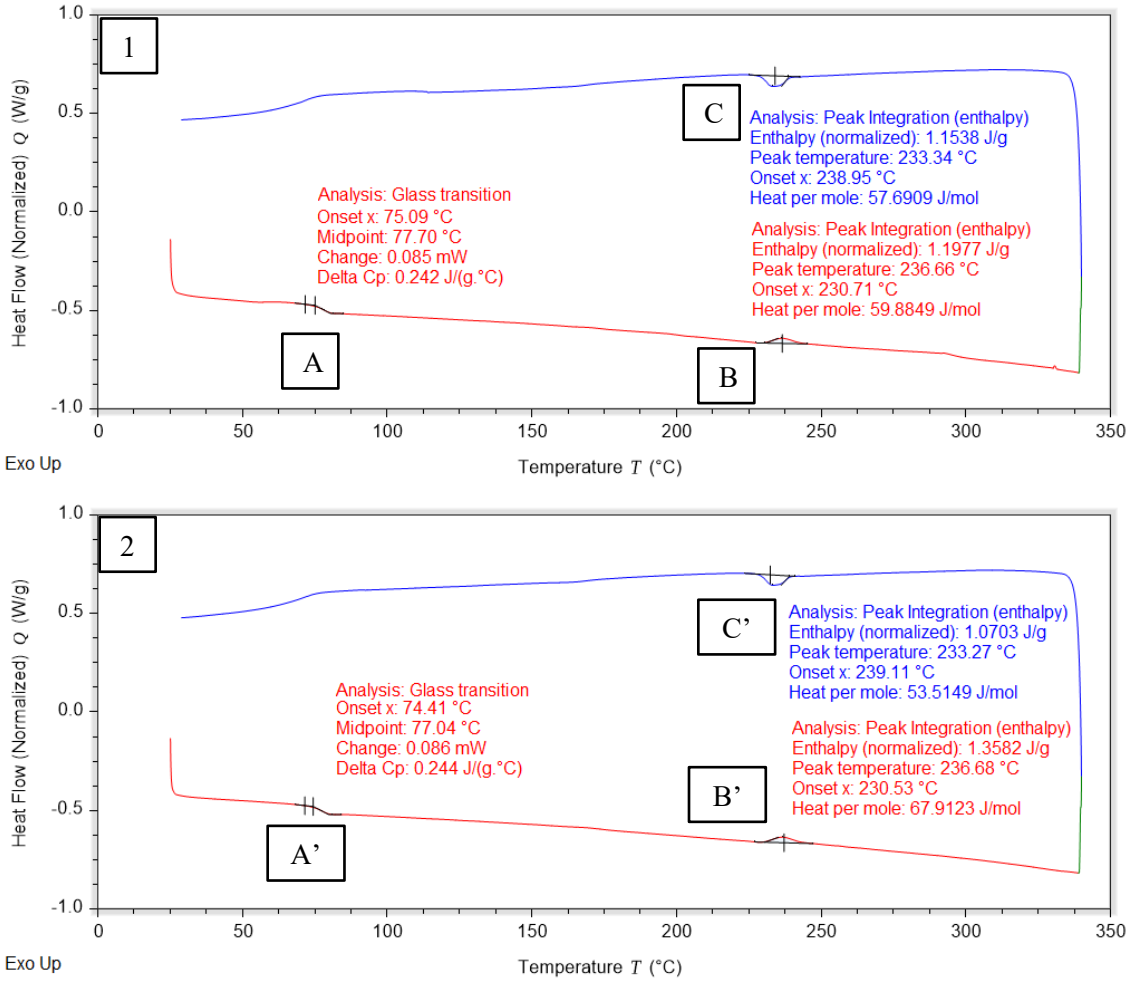

Figure B.17. The DSC curves, illustrating a heating up scan, red curve; in addition, a cooling down scan, blue curve, for the first sample. Please notice, Figure B.1 represents the initial experiment and Figure B.2 demonstrates the replicate experiment, both under the same processing parameters.

B.18. DSC PETG 30-GF (S.2)

PETG 30 wt. % GF compounded by Techmer PM Polymer Modifiers:

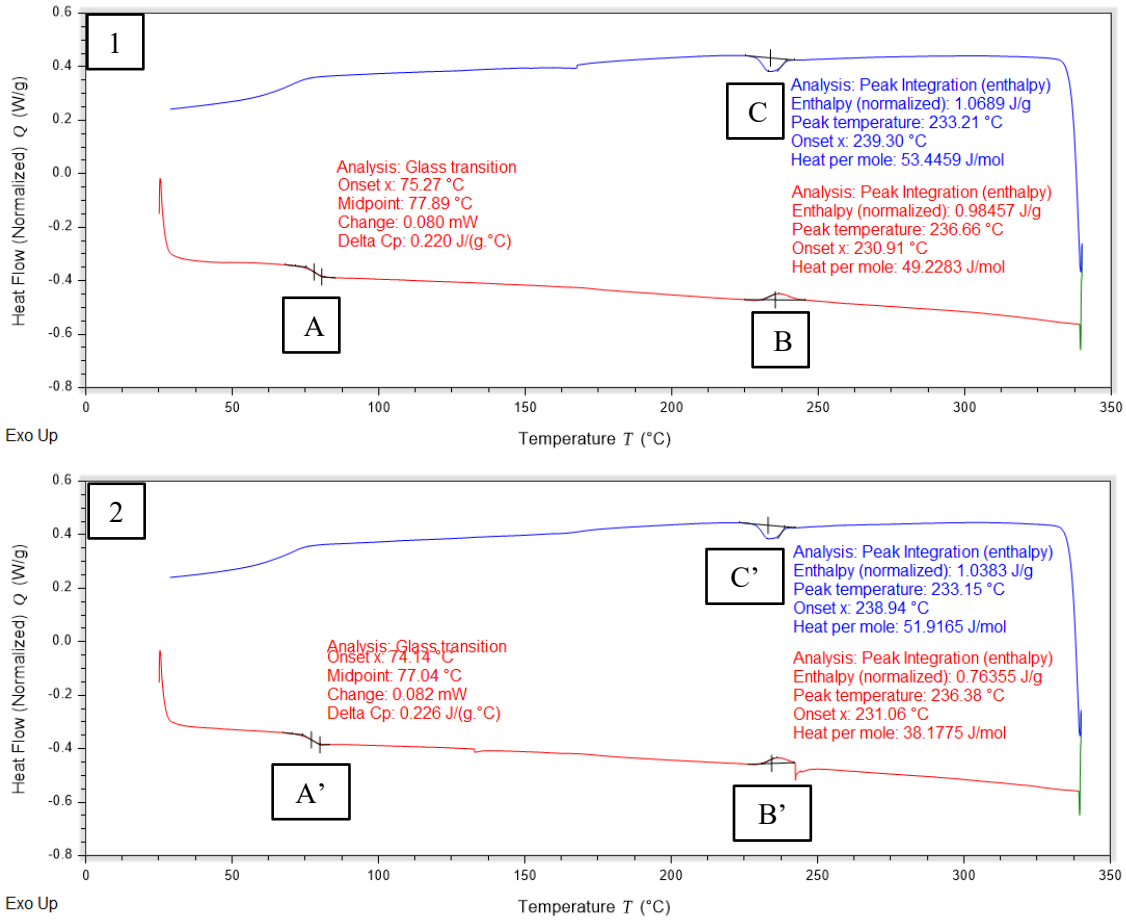

Figure B.18. DSC analyses displaying a heating up scan (red curve) and a cooling down scan (blue curve) Where figure B.1 represents the first experiment and figure B.2 represents is its replicate experiment under the same processing parameters.

B.19. DSC PETG 30-GF (S.3)

PETG 30 wt. % GF compounded by Techmer PM Polymer Modifiers:

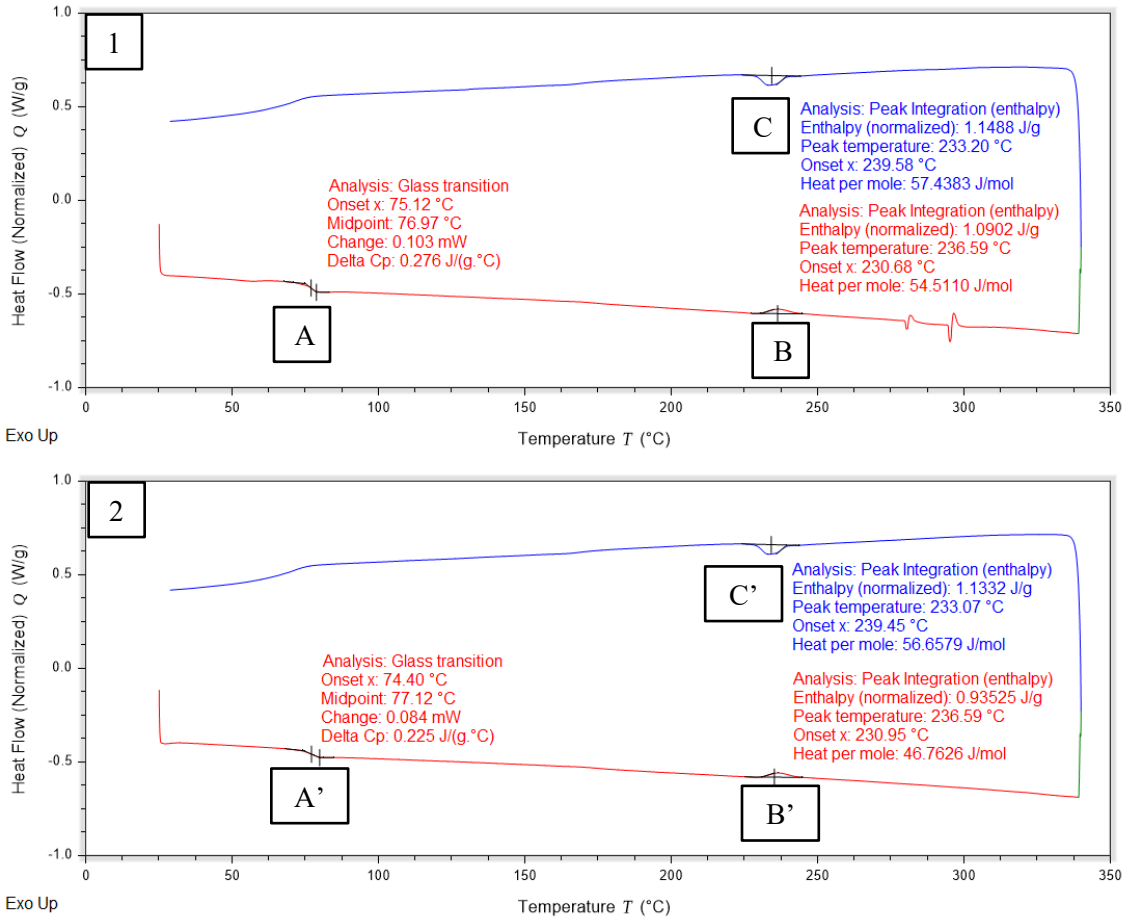

Figure B.19. DSC analyses displaying a heating up scan (red curve) and a cooling down scan (blue curve) Where figure B.1 represents the first experiment and figure B.2 represents is its replicate experiment under the same processing parameters.

B.20. DSC PETG 30-GF (overlay)

PETG 30 wt. % GF compounded by Techmer PM Polymer Modifiers:

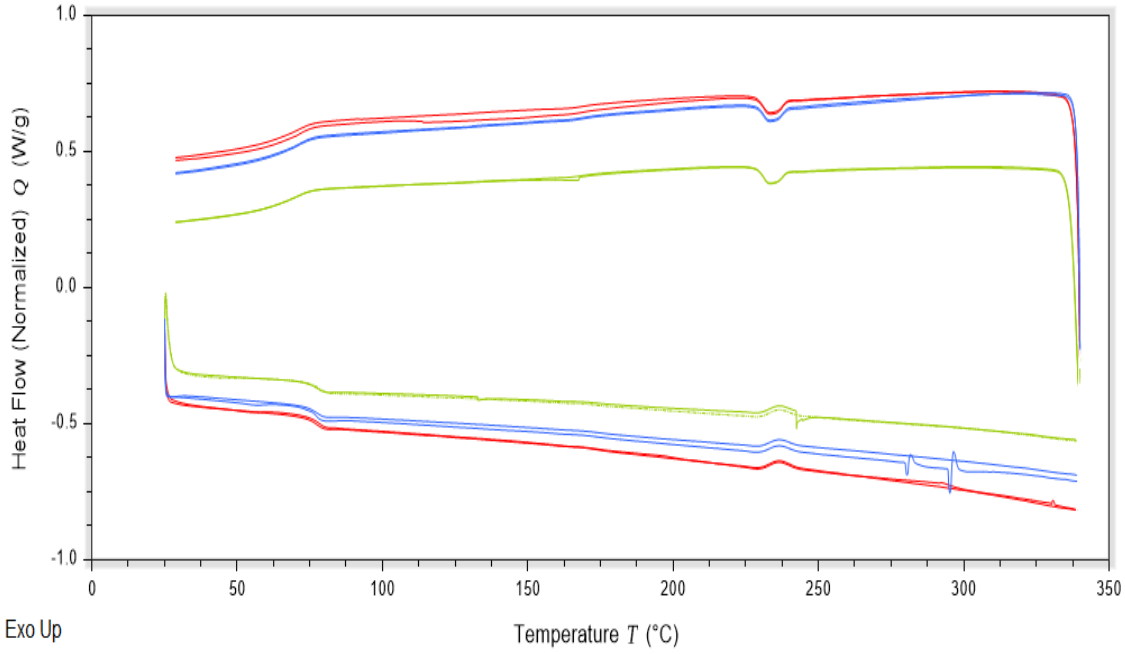

Figure B.20. The overlay for a set of three sample, notice the red curves represent the first sample, the blue curves illustrates the second sample and the green curve is attributed to the third sample.

B.21. DSC Summary (Initial Mass)

Table B.1. The initial sample mass prior the DSC examination.

DSC (in Nitrogen)	Initial mass (mg.)	Initial mass ($\bar{X}$)	Initial mass (σ)	CV
ABS 20-CF (Techmer)				
S.1	2.233	2.19	.04	1.82
S.2	2.147			
S.3	2.193			
ABS 20-GF (Techmer)				
S.1	2.010	2.03	.09	4.43
S.2	2.131			
S.3	1.954			
ABS 40-GF (Techmer)				
S.1	2.163	2.17	.03	1.38
S.2	2.212			
S.3	2.136			
PETG 30-GF (Techmer)				
S.1	2.119	2.18	.06	2.75
S.2	2.183			
S.3	2.240			
ABS 20-GF (SABIC)				
S.1	2.314	2.41	.09	3.73
S.2	2.453			
S.3	2.490			

B.22. DSC ABS 20-CF (Tg)

Table B.2. The average glass transition analysis of a set of three ABS 20-CF samples. Notice all the DSC analyses includes a replicate experiment.

DSC Nitrogen	Midpoint Tg (° C)	Midpoint Tg ($\bar{x}$)	Midpoint Tg (σ)	CV	Onset x (° C)	Onset x ($\bar{x}$)	Onset x (σ)	CV
First heating up cycle								
S.1	105.88	105.21	2.12	2.01	102.04	101.63	1.83	1.80
S.2	106.93				103.23			
S.3	102.83				99.62			
Second heating up cycle								
S.1	106.06	106.19	.11	0.10	102.29	102.51	.19	.18
S.2	106.23				102.62			
S.3	106.28				102.64			

DSC Nitrogen	Δ Cp (J/g·°C)	Δ Cp ($\bar{x}$)	Δ Cp (σ)	CV	Change (mW)	Change ($\bar{x}$)	Change (σ)	CV
First heating up cycle								
S.1	.22	.20	.02	10	.085	.08	.009	11.25
S.2	.19				.070			
S.3	.24				.088			
Second heating up cycle								
S.1	.25	.24	.005	2.08	.096	.09	.004	4.44
S.2	.24				.087			
S.3	.24				.091			

B.23. DSC ABS 20-CF (Endothermic Peak)

Table B.3. The average endothermic peak thermal event analysis of a set of three ABS 20-CF sample.

DSC Nitrogen	Peak (° C)	Peak ($\bar{x}$)	Peak (σ)	CV	Onset x (° C)	Onset x ($\bar{x}$)	Onset x (σ)	CV
First heating up cycle								
S.1	139.44	139.04	.41	.29	129.91	129.30	.78	.60
S.2	139.08				129.58			
S.3	138.61				128.41			
Second heating up cycle								
S.1	139.65	139.62	.06	.04	130.58	130.71	.32	.24
S.2	139.67				131.09			
S.3	139.55				130.48			

DSC Nitrogen	Heat per mole (J/mol)	Heat per mole ($\bar{x}$)	Heat per mole (σ)	CV	Enthalpy (J/g)	Enthalpy ($\bar{x}$)	Enthalpy (σ)	CV
First heating up cycle								
S.1	69.42	72.37	2.85	3.93	1.38	1.44	.06	4.16
S.2	75.12				1.50			
S.3	72.57				1.45			
Second heating up cycle								
S.1	74.68	76.50	6.83	8.92	1.49	1.52	.13	8.55
S.2	70.76				1.41			
S.3	84.07				1.68			

B.24. DSC ABS 20-CF (Exothermic Peak)

Table B.4. The average exothermic peak thermal event analysis of a set of three ABS 20-CF samples.

DSC Nitrogen	Peak (° C)	Peak ($\bar{x}$)	Peak (σ)	CV	Onset x (° C)	Onset x ($\bar{x}$)	Onset x (σ)	CV
First cooling down cycle								
S.1	121.33	121.10	.26	.21	124.63	124.63	.08	.06
S.2	120.81				124.55			
S.3	121.18				124.72			
Second cooling down cycle								
S.1	120.61	120.46	.39	.32	124.20	124.20	.08	.06
S.2	120.01				124.12			
S.3	120.76				124.29			

DSC Nitrogen	Heat per mole (J/mol)	Heat per mole ($\bar{x}$)	Heat per mole (σ)	CV	Enthalpy (J/g)	Enthalpy ($\bar{x}$)	Enthalpy (σ)	CV
First cooling down cycle								
S.1	96.73	90.42	5.94	6.56	1.69	1.80	.12	6.66
S.2	84.92				1.79			
S.3	89.63				1.93			
Second cooling down cycle								
S.1	79.59	84.65	7.05	8.32	1.59	1.69	.14	8.28
S.2	92.72				1.85			
S.3	81.66				1.63			

B.25. DSC ABS 20-GF (Tg)

Table B.5. The average glass transition analysis of a set of three ABS 20-GF samples.

DSC Nitrogen	Midpoint Tg (° C)	Midpoint Tg ($\bar{x}$)	Midpoint Tg (σ)	CV	Onset x (° C)	Onset x ($\bar{x}$)	Onset x (σ)	CV
First heating up cycle								
S.1	103.70	105.30	1.49	1.41	100.57	102.81	2.06	2.00
S.2	106.67				104.63			
S.3	105.54				103.25			
Second heating up cycle								
S.1	106.46	106.57	.60	.56	102.74	103.02	.90	.87
S.2	107.22				104.04			
S.3	106.03				102.30			

DSC Nitrogen	Δ Cp (J/g·°C)	Δ Cp ($\bar{x}$)	Δ Cp (σ)	CV	Change (mW)	Change ($\bar{x}$)	Change (σ)	CV
First heating up cycle								
S.1	.296	.31	.06	19.35	.099	.10	.02	20
S.2	.385				.137			
S.3	.266				.087			
Second heating up cycle								
S.1	.277	.26	.012	4.61	.093	.80	.006	.75
S.2	.266				.094			
S.3	.253				.082			

B.26. DSC ABS 20-GF (Endothermic Peak)

Table B.6. The average endothermic peak thermal event analysis of a set of three ABS 20-GF samples.

DSC Nitrogen	Peak (° C)	Peak ($\bar{x}$)	Peak (σ)	CV	Onset x (° C)	Onset x ($\bar{x}$)	Onset x (σ)	CV
First heating up cycle								
S.1	138.11	138.39	.39	.28	130.42	129.76	1.48	1.14
S.2	138.85				130.81			
S.3	138.23				128.07			
Second heating up cycle								
S.1	139.37	139.44	.39	.27	130.89	130.90	.30	.21
S.2	139.87				131.21			
S.3	139.08				130.60			

DSC Nitrogen	Heat per mole (J/mol)	Heat per mole ($\bar{x}$)	Heat per mole (σ)	CV	Enthalpy (J/g)	Enthalpy ($\bar{x}$)	Enthalpy (σ)	CV
First heating up cycle								
S.1	49.74	53.93	6.16	11.42	0.99	1.00	.02	2.0
S.2	51.06				1.02			
S.3	61.01				1.22			
Second heating up cycle								
S.1	67.63	69.11	1.50	2.17	1.35	1.38	.03	2.17
S.2	70.63				1.41			
S.3	69.07				1.38			

B.27. DSC ABS 20-GF (Exothermic Peak)

Table B.7. The average exothermic peak thermal event analysis of a set of three ABS 20-GF samples.

DSC Nitrogen	Peak (° C)	Peak ($\bar{x}$)	Peak (σ)	CV	Onset x (° C)	Onset x ($\bar{x}$)	Onset x (σ)	CV
First cooling down cycle								
S.1	119.68	119.18	.50	.41	123.61	123.39	.30	.24
S.2	119.19				123.52			
S.3	118.67				123.04			
Second cooling down cycle								
S.1	118.98	118.34	.80	.67	123.76	123.49	.18	.14
S.2	118.61				123.59			
S.3	117.44				123.14			

DSC Nitrogen	Heat per mole (J/mol)	Heat per mole ($\bar{x}$)	Heat per mole (σ)	CV	Enthalpy (J/g)	Enthalpy ($\bar{x}$)	Enthalpy (σ)	CV
First cooling down cycle								
S.1	90.85	75.95	14.78	19.46	1.81	1.51	.29	19.20
S.2	75.73				1.51			
S.3	61.28				1.22			
Second cooling down cycle								
S.1	78.74	67.20	10.47	15.58	1.57	1.34	.20	14.92
S.2	64.60				1.29			
S.3	58.28				1.16			

B.28. DSC ABS 40-GF (Tg)

Table B.8. The average glass transition analysis of a set of three ABS 40-GF samples.

DSC Nitrogen	Midpoint Tg (° C)	Midpoint Tg ($\bar{x}$)	Midpoint Tg (σ)	CV	Onset x (° C)	Onset x ($\bar{x}$)	Onset x (σ)	CV
First heating up cycle								
S.1	105.80	105.74	.21	.19	102.57	102.09	.53	.51
S.2	105.92				102.18			
S.3	105.50				101.52			
Second heating up cycle								
S.1	106.70	106.42	.49	.46	103.47	102.92	.77	.74
S.2	106.72				103.25			
S.3	105.86				102.04			

DSC Nitrogen	Δ Cp (J/g·°C)	Δ Cp ($\bar{x}$)	Δ Cp (σ)	CV	Change (mW)	Change ($\bar{x}$)	Change (σ)	CV
First heating up cycle								
S.1	.134	.145	.01	6.89	.048	.05	.004	8.0
S.2	.155				.057			
S.3	.146				.052			
Second heating up cycle								
S.1	.175	.191	.014	7.32	.063	.06	.005	8.33
S.2	.197				.073			
S.3	.201				.072			

B.29. DSC ABS 40 wt. % GF (Endothermic Peak)

Table B.9. The average endothermic peak thermal event analysis of a set of three ABS 40-GF samples.

DSC Nitrogen	Peak (° C)	Peak ($\bar{x}$)	Peak (σ)	CV	Onset x (° C)	Onset x ($\bar{x}$)	Onset x (σ)	CV
First heating up cycle								
S.1	138.19	138.10	.23	.16	128.86	128.10	.75	.58
S.2	138.28				128.08			
S.3	137.83				127.36			
Second heating up cycle								
S.1	139.65	139.50	.37	.26	130.54	129.98	.71	.54
S.2	139.78				130.24			
S.3	139.08				129.18			

DSC Nitrogen	Heat per mole (J/mol)	Heat per mole ($\bar{x}$)	Heat per mole (σ)	CV	Enthalpy (J/g)	Enthalpy ($\bar{x}$)	Enthalpy (σ)	CV
First heating up cycle								
S.1	52.53	58.54	5.78	9.87	1.05	1.17	.11	9.40
S.2	64.06				1.28			
S.3	59.04				1.18			
Second heating up cycle								
S.1	52.48	59.98	6.49	10.82	1.04	1.19	.13	10.92
S.2	63.88				1.27			
S.3	63.59				1.27			

B.30. DSC ABS 40 wt. % CF (Exothermic Peak)

Table B.10. The average exothermic peak thermal event analysis of a set of three ABS 40-GF samples.

DSC Nitrogen	Peak (° C)	Peak ($\bar{x}$)	Peak (σ)	CV	Onset x (° C)	Onset x ($\bar{x}$)	Onset x (σ)	CV
First cooling down cycle								
S.1	120.25	120.27	.04	.03	124.70	124.71	.02	.01
S.2	120.25				124.69			
S.3	120.32				124.74			
Second cooling down cycle								
S.1	119.73	119.80	.07	.05	124.90	124.82	.26	.20
S.2	119.87				124.52			
S.3	119.82				125.04			

DSC Nitrogen	Heat per mole (J/mol)	Heat per mole ($\bar{x}$)	Heat per mole (σ)	CV	Enthalpy (J/g)	Enthalpy ($\bar{x}$)	Enthalpy (σ)	CV
First cooling down cycle								
S.1	60.01	61.31	8.33	13.58	1.20	1.22	.16	13.11
S.2	70.23				1.40			
S.3	53.71				1.07			
Second cooling down cycle								
S.1	55.71	56.18	5.60	9.96	1.11	1.12	.11	9.82
S.2	62.01				1.24			
S.3	50.82				1.01			

B.31. DSC PETG 30-GF (Tg)

Table B.11. The average glass transition analysis of a set of three PETG 30-GF samples.

DSC Nitrogen	Midpoint Tg (° C)	Midpoint Tg ($\bar{x}$)	Midpoint Tg (σ)	CV	Onset x (° C)	Onset x ($\bar{x}$)	Onset x (σ)	CV
First heating up cycle								
S.1	77.70	77.52	.48	.61	75.09	75.16	.09	.11
S.2	77.89				75.27			
S.3	76.97				75.12			
Second heating up cycle								
S.1	77.04	77.06	.04	.05	74.41	74.31	.15	.20
S.2	77.04				74.14			
S.3	77.12				74.40			

DSC Nitrogen	Δ Cp (J/g·°C)	Δ Cp ($\bar{x}$)	Δ Cp (σ)	CV	Change (mW)	Change ($\bar{x}$)	Change (σ)	CV
First heating up cycle								
S.1	.242	.246	.02	8.13	.085	.08	.01	12.5
S.2	.220				.080			
S.3	.276				.103			
Second heating up cycle								
S.1	.244	.23	.01	4.34	.086	.08	.002	2.50
S.2	.226				.082			
S.3	.225				.084			

B.32. DSC PETG 30-GF (Exothermic Peak)

Table B.12. The average exothermic peak thermal event analysis of a set of three PETG 30-GF samples.

DSC Nitrogen	Peak (° C)	Peak ($\bar{x}$)	Peak (σ)	CV	Onset x (° C)	Onset x ($\bar{x}$)	Onset x (σ)	CV
First heating up cycle								
S.1	236.66	236.63	.04	.01	230.71	230.76	.12	.05
S.2	236.66				230.91			
S.3	236.59				230.68			
Second heating up cycle								
S.1	236.68	236.55	.15	.06	230.53	230.84	.27	.11
S.2	236.38				231.06			
S.3	236.59				230.95			

DSC Nitrogen	Heat per mole (J/mol)	Heat per mole ($\bar{x}$)	Heat per mole (σ)	CV	Enthalpy (J/g)	Enthalpy ($\bar{x}$)	Enthalpy (σ)	CV
First heating up cycle								
S.1	59.88	54.53	5.33	9.77	1.19	1.08	.10	9.25
S.2	49.22				0.98			
S.3	54.51				1.09			
Second heating up cycle								
S.1	67.91	50.94	15.30	30.03	1.35	1.01	.30	29.70
S.2	38.17				0.76			
S.3	46.76				0.93			

B.33. DSC PETG 30-GF (Endothermic Peak)

Table B.13. The average endothermic peak thermal event analysis of a set of three PETG 30-GF samples.

DSC Nitrogen	Peak (° C)	Peak ($\bar{x}$)	Peak (σ)	CV	Onset x (° C)	Onset x ($\bar{x}$)	Onset x (σ)	CV
First cooling down cycle								
S.1	233.34	233.25	.07	.03	238.95	239.27	.31	.12
S.2	233.21				239.30			
S.3	233.20				239.58			
Second cooling cycle								
S.1	233.27	233.16	.10	.04	239.11	239.16	.25	.10
S.2	233.15				238.94			
S.3	233.07				239.45			

DSC Nitrogen	Heat per mole (J/mol)	Heat per mole ($\bar{x}$)	Heat per mole (σ)	CV	Enthalpy (J/g)	Enthalpy ($\bar{x}$)	Enthalpy (σ)	CV
First cooling down cycle								
S.1	57.69	56.18	2.38	4.18	1.15	1.11	.04	3.60
S.2	53.44				1.06			
S.3	57.43				1.14			
Second cooling down cycle								
S.1	53.51	54.02	2.41	4.46	1.07	1.07	.05	4.67
S.2	51.91				1.03			
S.3	56.65				1.13			

B.34. DSC ABS 20-GF (SABIC) (Tg)

Table B.14. The average glass transition analysis of a set of three ABS 20-GF (SABIC) samples.

DSC Nitrogen	Midpoint Tg (° C)	Midpoint Tg ($\bar{x}$)	Midpoint Tg (σ)	CV	Onset x (° C)	Onset x ($\bar{x}$)	Onset x (σ)	CV
First heating up cycle								
S.1	108.98	109.28	.61	.55	105.70	106.11	.72	.67
S.2	108.89				105.68			
S.3	109.99				106.95			
Second heating up cycle								
S.1	109.63	109.45	.35	.31	106.63	106.45	.34	.31
S.2	109.04				106.05			
S.3	109.69				106.67			

DSC Nitrogen	Δ Cp (J/g·°C)	Δ Cp ($\bar{x}$)	Δ Cp (σ)	CV	Change (mW)	Change ($\bar{x}$)	Change (σ)	CV
First heating up cycle								
S.1	.212	.20	.01	5.0	.082	.084	.005	5.95
S.2	.219				.090			
S.3	.192				.080			
Second heating up cycle								
S.1	.246	.24	.007	2.91	.095	.10	.005	5.0
S.2	.258				.105			
S.3	.244				.101			

B.35. DSC ABS 20-GF (SABIC) (Endothermic Peak)

Table B.15. The average endothermic peak thermal event analysis of a set of three ABS 20-GF (SABIC) samples.

DSC Nitrogen	Peak (° C)	Peak ($\bar{x}$)	Peak (σ)	CV	Onset x (° C)	Onset x ($\bar{x}$)	Onset x (σ)	CV
First heating up cycle								
S.1	236.60	236.66	.06	.025	232.20	231.28	.81	.35
S.2	236.66				231.01			
S.3	236.72				230.64			
Second heating up cycle								
S.1	236.67	236.52	.12	.050	230.71	230.77	.06	.02
S.2	236.44				230.77			
S.3	236.46				230.83			

DSC Nitrogen	Heat per mole (J/mol)	Heat per mole ($\bar{x}$)	Heat per mole (σ)	CV	Enthalpy (J/g)	Enthalpy ($\bar{x}$)	Enthalpy (σ)	CV
First heating up cycle								
S.1	49.12	47.36	2.33	4.91	.98	.94	.04	4.25
S.2	44.71				.89			
S.3	48.25				.96			
Second heating up cycle								
S.1	52.94	48.01	5.19	10.81	1.05	.95	.10	10.52
S.2	48.52				0.97			
S.3	42.59				0.85			

B.36. DSC ABS 20-GF (SABIC) (Exothermic Peak)

Table B.16. The average exothermic peak thermal event analysis of a set of three ABS 20-GF (SABIC) samples.

DSC Nitrogen	Peak (° C)	Peak ($\bar{x}$)	Peak (σ)	CV	Onset x (° C)	Onset x ($\bar{x}$)	Onset x (σ)	CV
First cooling down cycle								
S.1	233.09	233.19	.11	.04	239.23	239.15	.07	.02
S.2	233.32				239.15			
S.3	233.18				239.08			
Second cooling down cycle								
S.1	233.14	233.15	.02	.008	238.99	238.95	.33	.13
S.2	233.18				238.60			
S.3	233.14				239.27			

DSC Nitrogen	Heat per mole (J/mol)	Heat per mole ($\bar{x}$)	Heat per mole (σ)	CV	Enthalpy (J/g)	Enthalpy ($\bar{x}$)	Enthalpy (σ)	CV
First heating up cycle								
S.1	47.40	46.30	1.78	3.84	.94	.92	.03	3.26
S.2	47.27				.94			
S.3	44.25				.88			
Second heating up cycle								
S.1	46.34	44.87	1.33	2.96	.92	.89	.02	2.24
S.2	44.56				.89			
S.3	43.72				.87			

B.37. DSC ABS 20-CF

Table B.17. The arithmetic mean values, heating up and cooling down DSC readings, for ABS 20-CF.

DSC	($\bar{x}$)
First heating up cycle	
Midpoint Tg (° C)	105.21
Onset Tg (° C)	101.63
Δ Cp (J/g·°C)	.20
Change (mW)	.08
Second heating up cycle	
Midpoint Tg (° C)	106.19
Onset Tg (° C)	102.51
Δ Cp (J/g·°C)	.24
Change (mW)	.09

DSC	($\bar{x}$)
First heating up cycle	
Endothermic peak (° C)	139.04
Onset x (° C)	129.30
Heat per mole (J/mol)	72.37
Enthalpy (J/g)	1.44
Second heating up cycle	
Endothermic peak (° C)	139.62
Onset x (° C)	130.71
Heat per mole (J/mol)	76.50
Enthalpy (J/g)	1.52

DSC	($\bar{x}$)
First cooling down cycle	
Exothermic peak (° C)	121.10
Onset x (° C)	124.63
Heat per mole (J/mol)	90.42
Enthalpy (J/g)	1.80
Second cooling down cycle	
Exothermic peak (° C)	120.46
Onset x (° C)	124.20
Heat per mole (J/mol)	84.65
Enthalpy (J/g)	1.69

B.38. DSC ABS 20-GF

Table B.18 The arithmetic mean values, heating up and cooling down DSC readings, for ABS 20-GF.

DSC	($\bar{x}$)
First heating up cycle	
Midpoint Tg (° C)	105.30
Onset Tg (° C)	102.82
Δ Cp (J/g·°C)	.31
Change (mW)	.10
Second heating up cycle	
Midpoint Tg (° C)	106.57
Onset Tg (° C)	103.02
Δ Cp (J/g·°C)	.26
Change (mW)	.80

DSC	($\bar{x}$)
First heating up cycle	
Endothermic peak (° C)	138.39
Onset x (° C)	129.76
Heat per mole (J/mol)	53.93
Enthalpy (J/g)	1.00
Second heating up cycle	
Endothermic peak (° C)	139.44
Onset x (° C)	130.90
Heat per mole (J/mol)	69.11
Enthalpy (J/g)	1.38

DSC	($\bar{x}$)
First cooling down cycle	
Exothermic peak (° C)	119.18
Onset x (° C)	123.39
Heat per mole (J/mol)	75.95
Enthalpy (J/g)	1.51
Second cooling down cycle	
Exothermic peak (° C)	118.34
Onset x (° C)	123.49
Heat per mole (J/mol)	67.20
Enthalpy (J/g)	1.34

B.39. DSC ABS 40-GF

Table B.19. The arithmetic mean values, heating up and cooling down DSC readings, for ABS 40-GF.

DSC	($\bar{x}$)
First heating up cycle	
Midpoint Tg (° C)	105.74
Onset Tg (° C)	102.09
Δ Cp (J/g·°C)	.145
Change (mW)	.05
Second heating up cycle	
Midpoint Tg (° C)	106.42
Onset Tg (° C)	102.92
Δ Cp (J/g·°C)	.191
Change (mW)	.06

DSC	($\bar{x}$)
First heating up cycle	
Endothermic peak (° C)	138.10
Onset x (° C)	128.10
Heat per mole (J/mol)	58.54
Enthalpy (J/g)	1.17
Second heating up cycle	
Endothermic peak (° C)	139.50
Onset x (° C)	129.98
Heat per mole (J/mol)	59.98
Enthalpy (J/g)	1.19

DSC	($\bar{x}$)
First cooling down cycle	
Exothermic peak (° C)	120.27
Onset x (° C)	124.71
Heat per mole (J/mol)	61.31
Enthalpy (J/g)	1.22
Second cooling down cycle	
Exothermic peak (° C)	119.80
Onset x (° C)	124.82
Heat per mole (J/mol)	56.18
Enthalpy (J/g)	1.12

B.40. DSC PETG 30-GF

Table B.20. The arithmetic mean values, heating up and cooling down DSC readings, for PETG 30-GF.

DSC	($\bar{x}$)
First heating up cycle	
Midpoint Tg (° C)	77.52
Onset Tg (° C)	75.16
Δ Cp (J/g·°C)	.246
Change (mW)	.08
Second heating up cycle	
Midpoint Tg (° C)	77.06
Onset Tg (° C)	74.31
Δ Cp (J/g·°C)	.23
Change (mW)	.08

DSC	($\bar{x}$)
First heating up cycle	
Exothermic peak (° C)	236.63
Onset x (° C)	230.76
Heat per mole (J/mol)	54.53
Enthalpy (J/g)	1.08
Second heating up cycle	
Exothermic peak (° C)	236.55
Onset x (° C)	230.84
Heat per mole (J/mol)	50.94
Enthalpy (J/g)	1.01

DSC	($\bar{x}$)
First cooling down cycle	
Endothermic peak (° C)	233.25
Onset x (° C)	239.27
Heat per mole (J/mol)	56.18
Enthalpy (J/g)	1.11
Second cooling down cycle	
Endothermic peak (° C)	233.16
Onset x (° C)	239.16
Heat per mole (J/mol)	54.02
Enthalpy (J/g)	1.07

B.41. DSC ABS 20-GF (SABIC)

Table B.21 The arithmetic mean values, heating up and cooling down DSC readings, for ABS 20-GF (SABIC).

DSC	($\bar{x}$)
First heating up cycle	
Midpoint Tg (° C)	109.28
Onset Tg (° C)	106.11
Δ Cp (J/g·°C)	.20
Change (mW)	.084
Second heating up cycle	
Midpoint Tg (° C)	109.45
Onset Tg (° C)	106.45
Δ Cp (J/g·°C)	.24
Change (mW)	.10

DSC	($\bar{x}$)
First heating up cycle	
Exothermic peak (° C)	236.66
Onset x (° C)	231.28
Heat per mole (J/mol)	47.36
Enthalpy (J/g)	.94
Second heating up cycle	
Exothermic peak (° C)	236.52
Onset x (° C)	230.77
Heat per mole (J/mol)	48.01
Enthalpy (J/g)	.95

DSC	($\bar{x}$)
Second cooling down cycle	
Endothermic peak (° C)	233.19
Onset x (° C)	239.15
Heat per mole (J/mol)	46.30
Enthalpy (J/g)	.92
Second cooling down cycle	
Endothermic peak (° C)	233.15
Onset x (° C)	238.95
Heat per mole (J/mol)	44.87
Enthalpy (J/g)	.89

B.42. DSC ABS 20-CF

Table B.22. The standard deviations, heating up and cooling down DSC readings, for ABS 20-CF.

DSC	(σ)
First heating up cycle	
Midpoint Tg (° C)	2.12
Onset Tg (° C)	1.83
Δ Cp (J/g·°C)	.02
Change (mW)	.009
Second heating up cycle	
Midpoint Tg (° C)	.11
Onset Tg (° C)	.19
Δ Cp (J/g·°C)	.005
Change (mW)	.004

DSC	(σ)
First heating up cycle	
Endothermic peak (° C)	.41
Onset x (° C)	.78
Heat per mole (J/mol)	2.85
Enthalpy (J/g)	.06
Second heating up cycle	
Endothermic peak (° C)	.06
Onset x (° C)	.32
Heat per mole (J/mol)	6.83
Enthalpy (J/g)	.13

DSC	(σ)
First cooling down cycle	
Exothermic peak (° C)	.26
Onset x (° C)	.08
Heat per mole (J/mol)	5.94
Enthalpy (J/g)	.12
Second cooling down cycle	
Exothermic peak (° C)	.39
Onset x (° C)	.08
Heat per mole (J/mol)	7.05
Enthalpy (J/g)	.14

B.43. DSC ABS 20-GF

Table B.23. The standard deviations, heating up and cooling down DSC readings, for ABS 20-GF.

DSC	(σ)
First heating up cycle	
Midpoint Tg (° C)	1.49
Onset Tg (° C)	2.06
Δ Cp (J/g·°C)	.06
Change (mW)	.02
Second heating up cycle	
Midpoint Tg (° C)	.60
Onset Tg (° C)	.90
Δ Cp (J/g·°C)	.012
Change (mW)	.006

DSC	(σ)
First heating up cycle	
Endothermic peak (° C)	.39
Onset x (° C)	1.48
Heat per mole (J/mol)	6.16
Enthalpy (J/g)	.02
Second heating up cycle	
Endothermic peak (° C)	.39
Onset x (° C)	.30
Heat per mole (J/mol)	1.50
Enthalpy (J/g)	.03

DSC	(σ)
First cooling down cycle	
Exothermic peak (° C)	.50
Onset x (° C)	.30
Heat per mole (J/mol)	14.78
Enthalpy (J/g)	.29
Second cooling down cycle	
Exothermic peak (° C)	.80
Onset x (° C)	.18
Heat per mole (J/mol)	10.4
Enthalpy (J/g)	.20

B.44. DSC ABS 40-GF

Table B.24. The standard deviations, heating up and cooling down DSC readings, for ABS 40-GF.

DSC	(σ)
First heating up cycle	
Midpoint Tg (° C)	.21
Onset Tg (° C)	.53
Δ Cp (J/g·°C)	.01
Change (mW)	.004
Second heating up cycle	
Midpoint Tg (° C)	.49
Onset Tg (° C)	.77
Δ Cp (J/g·°C)	.014
Change (mW)	.005

DSC	(σ)
First heating up cycle	
Endothermic peak (° C)	.23
Onset x (° C)	.75
Heat per mole (J/mol)	5.78
Enthalpy (J/g)	.11
Second heating up cycle	
Endothermic peak (° C)	.37
Onset x (° C)	.71
Heat per mole (J/mol)	6.49
Enthalpy (J/g)	.13

DSC	(σ)
First cooling down cycle	
Exothermic peak (° C)	.04
Onset x (° C)	.02
Heat per mole (J/mol)	8.33
Enthalpy (J/g)	.16
Second cooling down cycle	
Exothermic peak (° C)	.07
Onset x (° C)	.26
Heat per mole (J/mol)	5.60
Enthalpy (J/g)	.11

B.45. DSC PETG 30-GF

Table B.25. The standard deviations, heating up and cooling down DSC readings, for PETG 30-GF.

DSC	(σ)
First heating up cycle	
Midpoint Tg (° C)	.48
Onset Tg (° C)	.09
Δ Cp (J/g·°C)	.02
Change (mW)	.01
Second heating up cycle	
Midpoint Tg (° C)	.04
Onset Tg (° C)	.15
Δ Cp (J/g·°C)	.01
Change (mW)	.002

DSC	(σ)
First heating up cycle	
Exothermic peak (° C)	.04
Onset x (° C)	.12
Heat per mole (J/mol)	5.33
Enthalpy (J/g)	.10
Second heating up cycle	
Exothermic peak (° C)	.15
Onset x (° C)	.27
Heat per mole (J/mol)	15.30
Enthalpy (J/g)	.30

DSC	(σ)
First cooling down cycle	
Endothermic peak (° C)	.07
Onset x (° C)	.31
Heat per mole (J/mol)	2.38
Enthalpy (J/g)	.04
Second cooling down cycle	
Endothermic peak (° C)	.10
Onset x (° C)	.25
Heat per mole (J/mol)	2.41
Enthalpy (J/g)	.05

B.46. DSC ABS 20-GF (SABIC)

Table B.26. The standard deviations, heating up and cooling down DSC readings, for ABS 20-GF (SABIC).

DSC	(σ)
First heating up cycle	
Midpoint Tg (° C)	.61
Onset Tg (° C)	.72
Δ Cp (J/g·°C)	.01
Change (mW)	.005
Second heating up cycle	
Midpoint Tg (° C)	.35
Onset Tg (° C)	.34
Δ Cp (J/g·°C)	.007
Change (mW)	.005

DSC	(σ)
First heating up cycle	
Exothermic peak (° C)	.06
Onset x (° C)	.81
Heat per mole (J/mol)	2.33
Enthalpy (J/g)	.04
Second heating up cycle	
Exothermic peak (° C)	.12
Onset x (° C)	.06
Heat per mole (J/mol)	5.19
Enthalpy (J/g)	.10

DSC	(σ)
First cooling down cycle	
Endothermic peak (° C)	.11
Onset x (° C)	.07
Heat per mole (J/mol)	1.78
Enthalpy (J/g)	.03
Second cooling down cycle	
Endothermic peak (° C)	.02
Onset x (° C)	.33
Heat per mole (J/mol)	1.33
Enthalpy (J/g)	.02

B.47. DSC ABS 20-CF

Table B.27. The coefficient of variation, heating up and cooling down DSC readings, for ABS 20-CF.

DSC	CV
First heating up cycle	
Midpoint Tg (° C)	2.01
Onset Tg (° C)	1.80
Δ Cp (J/g·°C)	10
Change (mW)	11.25
Second heating up cycle	
Midpoint Tg (° C)	0.10
Onset Tg (° C)	.18
Δ Cp (J/g·°C)	2.08
Change (mW)	4.44

DSC	CV
First heating up cycle	
Endothermic peak (° C)	.29
Onset x (° C)	.60
Heat per mole (J/mol)	3.93
Enthalpy (J/g)	4.16
Second heating up cycle	
Endothermic peak (° C)	.04
Onset x (° C)	.24
Heat per mole (J/mol)	8.92
Enthalpy (J/g)	8.55

DSC	CV
First cooling down cycle	
Exothermic peak (° C)	.21
Onset x (° C)	.06
Heat per mole (J/mol)	6.56
Enthalpy (J/g)	6.66
Second cooling down cycle	
Exothermic peak (° C)	.32
Onset x (° C)	.06
Heat per mole (J/mol)	8.32
Enthalpy (J/g)	8.28

B.48. DSC ABS 20-GF

Table B.28. The coefficient of variation, heating up and cooling down DSC readings, for ABS 20-GF.

DSC	CV
First heating up cycle	
Midpoint Tg (° C)	1.41
Onset Tg (° C)	2.00
Δ Cp (J/g·°C)	19.35
Change (mW)	20
Second heating up cycle	
Midpoint Tg (° C)	.56
Onset Tg (° C)	.87
Δ Cp (J/g·°C)	4.61
Change (mW)	.75

DSC	CV
First heating up cycle	
Endothermic peak (° C)	.28
Onset x (° C)	1.14
Heat per mole (J/mol)	11.42
Enthalpy (J/g)	2.0
Second heating up cycle	
Endothermic peak (° C)	.27
Onset x (° C)	.21
Heat per mole (J/mol)	2.17
Enthalpy (J/g)	2.17

DSC	CV
First cooling down cycle	
Exothermic peak (° C)	.41
Onset x (° C)	.24
Heat per mole (J/mol)	19.46
Enthalpy (J/g)	19.20
Second cooling down cycle	
Exothermic peak (° C)	.67
Onset x (° C)	.14
Heat per mole (J/mol)	15.58
Enthalpy (J/g)	14.92

B.49. DSC ABS 40-GF

Table B.29. The coefficient of variation, heating up and cooling down DSC readings, for ABS 40-GF.

DSC	CV
First heating up cycle	
Midpoint Tg (° C)	.19
Onset Tg (° C)	.51
Δ Cp (J/g·°C)	6.89
Change (mW)	8.0
Second heating up cycle	
Midpoint Tg (° C)	.46
Onset Tg (° C)	.74
Δ Cp (J/g·°C)	7.32
Change (mW)	8.33

DSC	CV
First heating up cycle	
Endothermic peak (° C)	.16
Onset x (° C)	.58
Heat per mole (J/mol)	9.87
Enthalpy (J/g)	9.40
Second heating up cycle	
Endothermic peak (° C)	.26
Onset x (° C)	.54
Heat per mole (J/mol)	10.82
Enthalpy (J/g)	10.92

DSC	CV
First cooling down cycle	
Exothermic peak (° C)	.03
Onset x (° C)	.01
Heat per mole (J/mol)	13.58
Enthalpy (J/g)	13.11
Second cooling down cycle	
Exothermic peak (° C)	.05
Onset x (° C)	.20
Heat per mole (J/mol)	9.96
Enthalpy (J/g)	9.82

B.50. DSC PETG 30-GF

Table B.30. The coefficient of variation, heating up and cooling down DSC readings, for PETG 30-GF.

DSC	CV
First heating up cycle	
Midpoint Tg (° C)	.61
Onset Tg (° C)	.11
Δ Cp (J/g·°C)	8.13
Change (mW)	12.5
Second heating up cycle	
Midpoint Tg (° C)	.05
Onset Tg (° C)	.15
Δ Cp (J/g·°C)	4.34
Change (mW)	.002

DSC	CV
First heating up cycle	
Exothermic peak (° C)	.01
Onset x (° C)	05
Heat per mole (J/mol)	9.77
Enthalpy (J/g)	9.25
Second heating up cycle	
Exothermic peak (° C)	.06
Onset x (° C)	.11
Heat per mole (J/mol)	30.03
Enthalpy (J/g)	29.70

DSC	CV
First cooling down cycle	
Endothermic peak (° C)	.03
Onset x (° C)	.12
Heat per mole (J/mol)	4.18
Enthalpy (J/g)	3.60
Second cooling down cycle	
Endothermic peak (° C)	.04
Onset x (° C)	.10
Heat per mole (J/mol)	4.46
Enthalpy (J/g)	4.67

B.51. DSC ABS 20-GF (SABIC)

Table B.31. The coefficient of variation, heating up and cooling down DSC readings, for ABS 20-GF (SABIC).

DSC	CV
First heating up cycle	
Midpoint Tg (° C)	.55
Onset Tg (° C)	.67
Δ Cp (J/g·°C)	5.0
Change (mW)	5.95
Second heating up cycle	
Midpoint Tg (° C)	.31
Onset Tg (° C)	.31
Δ Cp (J/g·°C)	2.91
Change (mW)	5.0

DSC	CV
First heating up cycle	
Exothermic peak (° C)	.025
Onset x (° C)	.35
Heat per mole (J/mol)	4.91
Enthalpy (J/g)	4.25
Second heating up cycle	
Exothermic peak (° C)	.050
Onset x (° C)	.02
Heat per mole (J/mol)	10.81
Enthalpy (J/g)	10.52

DSC	CV
Second cooling down cycle	
Endothermic peak (° C)	.04
Onset x (° C)	.02
Heat per mole (J/mol)	3.84
Enthalpy (J/g)	3.26
Second cooling down cycle	
Endothermic peak (° C)	.008
Onset x (° C)	.13
Heat per mole (J/mol)	2.96
Enthalpy (J/g)	2.24

B.52. DSC Thermal Analysis Comparison (Summary)

Table B.32. The comparison between the initial to the secondary heating cycle for ABS 20-CF.

First heating cycle compared to the second heating cycle		
DSC (Tg)	Change	Percentage change (%)
Midpoint Tg (° C)	0.98	0.93
Onset Tg (° C)	0.88	0.85
Δ Cp (J/g·°C)	0.04	20.0
Change (mW)	0.01	12.5

First heating cycle compared to the second heating cycle		
DSC (Endothermic event)	Change	Percentage change (%)
Peak temperature (° C)	0.58	0.41
Onset x (° C)	1.41	1.09
Heat per mole (J/mol)	4.13	5.70
Enthalpy (J/g)	0.08	5.55

First heating cycle compared to the second heating cycle		
DSC (Exothermic event)	Change	Percentage change (%)
Peak temperature (° C)	-0.64	-0.53
Onset x (° C)	-0.43	-0.34
Heat per mole (J/mol)	-5.77	-6.85
Enthalpy (J/g)	-0.11	-6.50

B.53. DSC Thermal Analysis Comparison (Summary)

Table B.33. The comparison between the initial to the secondary heating cycle for ABS 20-GF.

First heating cycle compared to the second heating cycle		
DSC (Tg)	Change	Percentage change (%)
Midpoint Tg (° C)	1.27	1.20
Onset Tg (° C)	0.20	0.19
Δ Cp (J/g·°C)	-0.05	-19.23
Change (mW)	0.70	700

First heating cycle compared to the second heating cycle		
DSC (Endothermic event)	Change	Percentage change (%)
Peak temperature (° C)	1.05	0.76
Onset x (° C)	1.14	0.88
Heat per mole (J/mol)	15.18	28.15
Enthalpy (J/g)	0.38	38.0

First heating cycle compared to the second heating cycle		
DSC (Exothermic event)	Change	Percentage change (%)
Peak temperature (° C)	-0.84	-0.70
Onset x (° C)	0.10	0.08
Heat per mole (J/mol)	-8.75	-11.52
Enthalpy (J/g)	-0.17	-11.26

B.54. DSC Thermal Analysis Comparison (Summary)

Table B.34. The comparison between the initial to the secondary heating cycle for ABS 40-GF.

First heating cycle compared to the second heating cycle		
DSC (Tg)	Change	Percentage change (%)
Midpoint Tg (° C)	0.68	0.64
Onset Tg (° C)	0.83	0.81
Δ Cp (J/g·°C)	0.046	31.72
Change (mW)	0.01	20.0

First heating cycle compared to the second heating cycle		
DSC (Endothermic event)	Change	Percentage change (%)
Peak temperature (° C)	1.40	1.01
Onset x (° C)	1.88	1.47
Heat per mole (J/mol)	1.44	2.46
Enthalpy (J/g)	0.02	1.71

First heating cycle compared to the second heating cycle		
DSC (Exothermic event)	Change	Percentage change (%)
Peak temperature (° C)	-0.47	-0.39
Onset x (° C)	0.11	0.09
Heat per mole (J/mol)	-5.13	-8.37
Enthalpy (J/g)	-0.10	-8.20

B.55. DSC Thermal Analysis Comparison (Summary)

Table B.35. The comparison between the initial to the secondary heating cycle for PETG 30-GF.

First heating cycle compared to the second heating cycle		
DSC (Tg)	Change	Percentage change (%)
Midpoint Tg (° C)	-0.46	-0.59
Onset Tg (° C)	-0.85	-1.13
Δ Cp (J/g·°C)	-0.016	-6.50
Change (mW)	N/A	N/A

First heating cycle compared to the second heating cycle		
DSC (Endothermic event)	Change	Percentage change (%)
Peak temperature (° C)	-0.08	0.03
Onset x (° C)	0.08	0.03
Heat per mole (J/mol)	-3.59	-6.58
Enthalpy (J/g)	-0.07	-6.48

First heating cycle compared to the second heating cycle		
DSC (Exothermic event)	Change	Percentage change (%)
Peak temperature (° C)	-0.09	-0.04
Onset x (° C)	-0.11	-0.05
Heat per mole (J/mol)	-2.16	-3.84
Enthalpy (J/g)	-0.04	-3.60

B.56. DSC Thermal Analysis Comparison (Summary)

Table B.36. The comparison between the initial to the secondary heating cycle for ABS 20-GF (SABIC).

First heating cycle compared to the second heating cycle		
DSC (Tg)	Change	Percentage change (%)
Midpoint Tg (° C)	0.17	0.16
Onset Tg (° C)	0.34	0.32
Δ Cp (J/g·°C)	0.04	20.0
Change (mW)	0.016	19.05

First heating cycle compared to the second heating cycle		
DSC (Endothermic event)	Change	Percentage change (%)
Peak temperature (° C)	-0.14	-0.06
Onset x (° C)	-0.51	-0.22
Heat per mole (J/mol)	0.64	1.37
Enthalpy (J/g)	0.01	1.06

First heating cycle compared to the second heating cycle		
DSC (Exothermic event)	Change	Percentage change (%)
Peak temperature (° C)	-0.04	-0.02
Onset x (° C)	-0.20	-0.08
Heat per mole (J/mol)	-1.43	-3.09
Enthalpy (J/g)	-0.03	-3.26

B.57. Secondary DSC Analysis for ABS 20 (GF and CF).

Table B.37. The arithmetic mean of ABS 20-GF and ABS 20-CF for a set of three DSC replicate experiments after their secondary heating up and cooling down thermal events.

DSC	$(\bar{\mathbf{x}})$
20 wt. % GF	
Midpoint Tg (° C)	106.57
Onset Tg (° C)	103.02
Δ Cp (J/g·°C)	.26
Change (mW)	.80
20 wt. % CF	
Midpoint Tg (° C)	106.19
Onset Tg (° C)	102.51
Δ Cp (J)· $(\mathrm{g}\cdot^{\circ}\mathbf{C})^{-1}$	.24
Change (mW)	.09

DSC	$(\bar{\mathbf{x}})$
20 wt. % GF	
Endothermic peak (° C)	139.44
Onset x (° C)	130.90
Heat per mole (J/mol)	69.11
Enthalpy (J/g)	1.38
20 wt. % CF	
Endothermic peak (° C)	139.62
Onset x (° C)	130.71
Heat per mole (J/mol)	76.50
Enthalpy (J/g)	1.52

DSC	$(\bar{\mathbf{x}})$
20 wt. % GF	
Exothermic peak (° C)	118.34
Onset x (° C)	123.49
Heat per mole (J/mol)	67.20
Enthalpy (J/g)	1.34
20 wt. % CF	
Exothermic peak (° C)	120.46
Onset x (° C)	124.20
Heat per mole (J/mol)	84.65
Enthalpy (J/g)	1.69

B.58. Secondary DSC Analysis for ABS (40-GF and 20-GF).

Table B.38. The arithmetic mean of ABS 40-GF and ABS 20-GF for a set of three DSC replicate experiments after their secondary heating up and cooling down thermal events.

DSC	$(\bar{\mathbf{x}})$
40 wt. % GF	
Midpoint Tg (° C)	106.42
Onset Tg (° C)	102.92
Δ Cp (J/g·°C)	.191
Change (mW)	.06
20 wt. % GF	
Midpoint Tg (° C)	106.57
Onset Tg (° C)	103.02
Δ Cp (J)· $(\mathbf{g}\cdot^{\circ}\mathbf{C})^{-1}$	.26
Change (mW)	.80

DSC	$(\bar{\mathbf{x}})$
40 wt. % GF	
Endothermic peak (° C)	139.50
Onset x (° C)	129.98
Heat per mole (J/mol)	59.98
Enthalpy (J/g)	1.19
20 wt. % GF	
Endothermic peak (° C)	139.44
Onset x (° C)	130.90
Heat per mole (J/mol)	69.11
Enthalpy (J/g)	1.38

DSC	$(\bar{\mathbf{x}})$
40 wt. % GF	
Exothermic peak (° C)	119.80
Onset x (° C)	124.82
Heat per mole (J/mol)	56.18
Enthalpy (J/g)	1.12
20 wt. % GF	
Exothermic peak (° C)	118.34
Onset x (° C)	123.49
Heat per mole (J/mol)	67.20
Enthalpy (J/g)	1.34

B.59. Secondary DSC Analysis for ABS 20-GF (SABIC and Techmer).

Table B.39. The arithmetic mean of ABS 20-GF (SABIC) and ABS 20-GF (Techmer) for a set of three DSC replicate experiments after their secondary heating up and cooling down thermal events.

DSC	($\bar{\mathbf{x}}$)
20 wt. % GF (SABIC)	
Midpoint Tg (° C)	109.45
Onset Tg (° C)	106.45
Δ Cp (J/g·°C)	.24
Change (mW)	.10
20 wt. % GF (Techmer)	
Midpoint Tg (° C)	106.57
Onset Tg (° C)	103.02
Δ Cp (J/g·°C)	.26
Change (mW)	.80

B.60. ABS 20-GF and ABS 20-CF (Summary)

Table B.40. The summary indicating the percentage change in the secondary DSC analyses, when comparing ABS 20 wt. % GF to ABS 20 wt. % CF.

ABS 20 wt. % GF compared to ABS 20 wt. % CF (Heating up cycle)

DSC (Tg)	Change	Percentage change (%)
Midpoint Tg (° C)	0.38	0.36
Onset Tg (° C)	0.51	0.50
Δ Cp (J/g·°C)	0.02	8.33
Change (mW)	0.71	788.89

ABS 20 wt. % GF compared to ABS 20 wt. % CF (Heating up cycle)

DSC (Endothermic event)	Change	Percentage change (%)
Peak temperature (° C)	-0.18	-0.13
Onset x (° C)	0.19	0.15
Heat per mole (J/mol)	-7.39	-9.66
Enthalpy (J/g)	-0.14	-9.21

ABS 20 wt. % GF compared to ABS 20 wt. % CF (Cooling down cycle)

DSC (Exothermic event)	Change	Percentage change (%)
Peak temperature (° C)	-2.12	-1.76
Onset x (° C)	-0.71	-0.57
Heat per mole (J/mol)	-17.45	-20.61
Enthalpy (J/g)	-0.35	-20.71

B.60. ABS 40-GF and ABS 20-CF (Summary)

Table B.41. The summary indicating the percentage change in the secondary DSC analyses, when comparing ABS 40-GF to ABS 20-CF.

ABS 40 wt. % GF compared to ABS 20 wt. % GF (Heating up cycle)

DSC (Tg)	Change	Percentage change (%)
Midpoint Tg (° C)	-0.15	-0.14
Onset Tg (° C)	-0.10	-0.10
Δ Cp (J/g·°C)	-0.069	-26.54
Change (mW)	-0.74	-92.5

ABS 40 wt. % GF compared to ABS 20 wt. % GF (Heating up cycle)

DSC (Endothermic event)	Change	Percentage change (%)
Peak temperature (° C)	0.06	0.04
Onset x (° C)	-0.92	-0.70
Heat per mole (J/mol)	-9.13	-13.21
Enthalpy (J/g)	-0.19	-13.77

ABS 40 wt. % GF compared to ABS 20 wt. % GF (Cooling down cycle)

DSC (Exothermic event)	Change	Percentage change (%)
Peak temperature (° C)	1.46	1.23
Onset x (° C)	1.33	1.08
Heat per mole (J/mol)	-11.02	-16.40
Enthalpy (J/g)	-0.22	-16.42

B.61. ABS 20-GF (SABIC) and ABS 20-GF (Techmer) (Summary)

Table B.42. The summary indicating the percentage change in the second DSC analyses, when comparing ABS 20-GF (SABIC) to ABS 20-GF (Techmer).

ABS 20 wt. % GF (SABIC) compared to ABS 20 wt. % GF (Techmer) (Heating up cycle)

DSC (Tg)	Change	Percentage change (%)
Midpoint Tg (° C)	2.88	2.77
Onset Tg (° C)	3.43	3.33
Δ Cp (J/g·°C)	-0.02	-7.69
Change (mW)	-0.70	-87.5

Vita

Fernando A. Rodriguez Lorenzana was born in Cd. Juarez, Chihuahua and graduated from Colegio de Bachilleres del Estado de Chihuahua, Plantel 5, in 2012. In May 2017, He earned his Bachelor of Science in Mechanical Engineering with Cum Laude honors from The University of Texas at El Paso. In September 2017, he was awarded a graduate teaching assistantship by Mechanical Engineering Department to pursue his graduate studies. While pursuing his master's degree, in May 2018, he joined the W.M. Keck Center for 3D Innovation at The University of Texas at El Paso as graduate research assistant under the guidance of Dr. David Espalin. In March 2019, he presented his research findings at the Southwest Emerging Technology Symposium.

Contact Information: farodriguezlorenzana@miners.utep.edu